Development of techniques for high-resolution spatially-resolved elemental analysis in materials of interest in luminescence dating.

By

Scott Grainger

Thesis submitted in fulfilment of the degree Master of Science by Research

Department of Archaeology
Durham University
2009

DECLARATION

No part of this thesis has been submitted for a previous degree and no part has been previously published.

Abstract

A series of analytical techniques have been developed to characterise the surface distribution of elements in a number of materials of archaeological interest, in support of current and future research in luminescence dating techniques.

Under certain circumstances, sample heterogeneity, with respect to naturally occurring radionuclides, may significantly reduce the levels of accuracy associated with experimentally determined luminescence dates.

The aim of this thesis is to develop a series of high-resolution, spatially resolved techniques to assess and quantify the degree of matrix (material fabric) radionuclide heterogeneity present in a number of archaeological materials.

Digital analysis and mineralogical staining techniques were combined to provide initial data regarding matrix heterogeneity and the distribution patterns of potassium-bearing minerals and in some cases, provided data that were comparable to those derived from SEM-EDX analyses.

Alpha autoradiographic techniques using solid state nuclear track detectors (CR-39) were applied initially to map localised differences in surface alpha activity, and were subsequently developed to provide semi-quantitative data about the concentration of alpha emitters present, and by association, the likely concentrations of uranium and thorium.

Micro-sampling techniques were developed to produce material for instrumental analysis (ICP-MS and AAS), to provide quantitative information about the

concentrations of uranium, thorium and potassium in the areas of interest, highlighted by the application of the aforementioned techniques.

The techniques were successfully applied in a number of case studies, providing both quantitative and qualitative information relating to material characteristics with respect to luminescence dating techniques.

Table of Contents

Volume 1

Acknowledgements

I would like to thank Prof. Ian Bailiff and Dr. Andrew Millard for supervision, advice and continued support throughout the production of this thesis.

I thank Sophie Blain for her assistance in organising SEM analyses at the University of Bordeaux.

I would also like to thank the technical staff of the Department of Geography, Durham University for the provision of analytical facilities, with very special thanks in particular to Martin West, for specialist scientific support (ICP-MS).

Finally, I thank my parents Pat and John Grainger for the encouragement and support they have given constantly, and to whom this work is dedicated.

Chapter 1 Introduction

Absolute dating techniques based on the measurement of luminescence have been developed over the last fifty years and now form a series of established methods used to determine the age of a number of archaeological materials including fired ceramics and sediments (Wintle, 2008). The measurement and characterisation of the luminescence properties of a number of mineral species, particularly quartz and feldspars, forms the basis of current techniques; these minerals may be present as included or minor composite materials in the case of brick and archaeological ceramics, or represent a major compositional component in the case of sediments. In either case, the build up of luminescence signal following a zeroing event (firing in the case of ceramics, optical bleaching in the case of sediments) is directly proportional to the amount of radiation absorbed by the phosphor grain (naturally occurring crystalline material).

The presence of naturally occurring radionuclides in the burial environment, within the materials of interest, and potentially within the actual crystalline materials, together with radiation that originates from the wider environment (e.g. gamma and cosmic) contributes to the total radiation dose absorbed by the luminescent materials which are used in dating techniques.

Routinely, disaggregated mineral grains are selected within the grain size range of 90 -355 μm for use in luminescence dating techniques, where, depending on grain size and environmental factors, a substantial contribution to total absorbed dose may be derived from the immediate grain environment (Mejdahl, 1979). Hydrofluoric acid etching techniques are used to remove outer grain material, and hence any contribution to total absorbed dose due to externally derived

alpha particle absorption; the applicable environmental dose rate for etched grains now consists of two major components – the gamma and cosmic contributions which originate from the wider environment, and the beta dose rate which is primarily derived from the matrix material in which the mineral grains are included.

Current techniques used to quantify the applicable beta dose component (essential to the calculation of luminescence age) are based on the analysis of bulk matrix material and this approach is valid providing the following assumptions are correct;

1. Phosphor grains are distributed uniformly throughout the matrix.
2. The matrix is homogeneous with regard to radionuclide concentration.

Deviation from these assumptions may increase the levels of uncertainty associated with the use of the bulk matrix beta dose rate value in the age calculation equation, where combined annual dose rate is composed of beta, gamma and cosmic radiation components.

$$\text{Age (ka)} = \frac{\text{Equivalent Dose (Gy)}}{\text{Dose Rate (Gy/ka)}}$$

Recent developments that involve the use of luminescence scanning techniques (Bailiff and Mikhailik, 2003 - described in Chapter 8) and single grain luminescence measurements (Duller and Murray, 2000) have highlighted the potential for significant variability in phosphor grain luminescence sensitivity;

indeed, the total measured luminescence intensity from a typical aliquot of disaggregated grains is found routinely, to originate predominantly from a very small number of "bright" grains (McCoy et al., 2000). In this case, the use of the bulk matrix beta radiation derived dose rate value in dating calculations may not be appropriate where dose rate heterogeneity is apparent; hence, the ability to identify and characterise the extent of matrix heterogeneity may provide useful information in the assessment of the degree of uncertainty associated with disaggregated grain techniques and the suitability of such materials for luminescence dating.

This thesis concerns the development of a series of analytical techniques that can be used to provide information about the concentration and distribution patterns of the naturally occurring radionuclides present in the archaeological matrices of interest, which are the sources of localised sample radioactivity and from which the absorbed dose is ultimately derived. Also considered are the geochemical and mineralogical aspects relevant to the materials of interest, and the mechanisms by which the radionuclides of interest may be present.

The application of several analytical techniques is explored to provide both qualitative and quantitative information about the dispersion characteristics (i.e. how the radionuclides are distributed) and concentrations of the naturally occurring radionuclides, ^{238}U, ^{232}Th and ^{40}K. In the case of uranium and thorium it is important to remember that the techniques used provide information about parent concentration only, and do not enable characterisation of daughter activity or provide information on disruption to secular equilibrium.

The methods developed for the determination of ^{40}K are not isotope-specific and hence determined concentrations refer to all naturally occurring isotopes of potassium (predominantly ^{39}K); the presence of ^{40}K is assumed to correlate directly with the mean natural isotopic abundance value (0.0117% - International Union of Pure and Applied Chemistry, IUPAC).

A series of archaeological materials have been chosen to validate the methods developed within the project and are representative of a number of differing sample matrix types encountered routinely in luminescence dating, including several types of brick and a clay based sediment.

Chapter 2 Introduction to compositional and chemical aspects

Introduction

The main focus of this research project is to develop a series of analytical methodologies to investigate the micro-distribution patterns of radionuclides within archaeological materials; an initial study of the chemical and physical properties of these materials, including factors that may influence radionuclide distribution is appropriate. An understanding of these factors is also relevant to later stages of research where the assessment of potential analytical techniques for the determination of trace and ultra trace radionuclide concentrations will require an understanding of the chemical and mineralogical characteristics of the materials in question.

In the context of this research, the general assumption is made that for the materials of interest, ^{238}U and ^{232}Th are naturally present in trace concentrations, the abundance and distributions of which are likely to vary, depending upon the source, geochemical nature and history of the component materials. The presence of potassium and hence ^{40}K, as both a trace element and major elemental constituent of several common minerals provides the opportunity to discuss the distribution of this isotope partly as a function of mineralogical composition.

2.1 Bricks and sediments – material and compositional aspects

From the perspective of general geochemical composition, both sediments and bricks may be described primarily as a potentially complex mixture of silicates and aluminosilicates, combined with a highly variable proportion of other inorganic and organic materials. The numerous factors involved in the formation of sedimentary materials, such as composition of parent material, weathering processes, deposition modes and geochemical environment, are responsible for the highly variable nature of the sediment samples encountered routinely in archaeological investigations and indeed for the heterogeneity of the secondary clay deposits used widely in brick manufacture (Keeling, 1963).
Although the natural composition and mixing ratios of the raw and composite materials used in brick production have the potential to vary significantly, the final chemical and physical composition of all bricks must produce a product that can be fired at high temperature to produce a usable structural material.

The majority of clays used in brick making (both historic and contemporary) are secondary, sedimentary materials generally assumed to be composed of the following major components –

Clay minerals, quartz, mica, heavy minerals which are resistant to chemical weathering, and other minerals such as carbonates, phosphates, sulphates and metal oxides, the presence and concentration of which, again, is dependent upon environmental and geological factors. Organic matter and of course water are also likely to be present in variable concentrations (Keeling, 1963).

The chemical composition of archaeological sediments, as with many common soils (Fitzpatrick, 1986), is also likely to be based around this mixture of

materials, although the potential exists for extreme variation in the concentrations of each individual component.

Sediments may also contain variable quantities and sizes of included parent or local rock material; larger inclusions would usually have been removed mechanically for brick making purposes to avoid structural and firing problems.

Before discussing the geochemistry of the potential composite materials of archaeological bricks and sediments, it is useful to consider some of the factors that may contribute to the distribution patterns of naturally occurring radionuclides within these materials. In the case of sediments and clays, the obvious primary mechanisms by which homogeneity may be disrupted are the sedimentation processes by which they were formed. Variability in parent material composition, the combination of different weathering process (both chemical and physical), and the variability of deposition modes and deposition environments (including disturbance due to animal and insect activity) provide the potential for sample heterogeneity on both the macro and micro scale. That said, certain types of sedimentary deposit do have the potential to be relatively homogeneous in nature, and archaeological sediments consisting primarily of sandy materials, probably aeolian in origin, with characteristic narrow particle size ranges and material uniformity are not unusual (Donghuai et al., 2002).

Anthropogenic causes of heterogeneity, particularly in terms of historic brick manufacture, include the addition of tempering materials, particularly sand, and the combination of different clay types. The mixing techniques used were labour intensive and the earliest manufacturing methods used crude mixing techniques, including trampling under foot to facilitate mixing and the removal of larger inclusions. The introduction of the labour saving but comparatively primitive pug milling technique for mixing raw materials still could not produce the levels

of efficiency achieved when true mechanisation was introduced during the industrial revolution (Clifton-Taylor, 1962).

In terms of radionuclide content, the degree to which compositional heterogeneity may affect the macro and micro (sub mm) distribution of these elements depends entirely upon the geochemistry of the composite minerals. In the case of uranium and thorium, it is difficult to predict the likely variation in concentration unless we consider the inclusion of minerals such as zircon or other uraniferous minerals for example in the case of increased uranium, and potentially thorium concentrations (Katz et al., 1986). It is also important to remember that the homogeneity of radionuclide distributions can also be disrupted by the inclusion of minerals that tend to have naturally low radionuclide concentrations, for example quartz (mechanisms for mineral / radionuclide associations are discussed later in this chapter).

^{40}K may be present in relatively high concentrations in common potassium rich clay minerals and inclusions such as feldspathic minerals, and the characterisation of the size and distribution characteristics of these components is important.

2.2 Constituent Minerals

Introduction

An overview of the physical and geochemical characteristics of the common composite materials that are likely to be present in both brick and sediment samples is useful not only in the prediction of the likely concentrations of

radionuclides, but also in the investigation of the potential geochemical mechanisms that influence the presence and concentration of these elements. This information is also important for later work when the assessment of the appropriate analytical techniques for the determination of these elements will be necessary.

2.2.1 Clay minerals and potassium geochemistry

2.2.1.1 Kaolinite clays

The sub-group of phyllosilicates (that demonstrate a sheet like macro-molecular structure) known as clay minerals form the major component of natural clays and soils (Fitzpatrick, 1986) and it is important to consider some of the physical and chemical properties of these minerals. Primary classification is based upon molecular structure, with the clay minerals being divided into the four basic groups detailed below. The molecular structure of all clay minerals is based on the layering of the two dimensional sheets produced by the linkages between the basic tetrahedral SiO_4 units or the octahedral AlO_6 units (Fig 2.1).

Planar Si-O-Si and Al-O-Al linkages are also demonstrated. Charge compensation (to induce electrical neutrality, and hence stability) for the octahedral aluminium configuration is achieved by the protonation of the negatively charged apical oxygen ions - this structural unit forms the basis of the mineral Gibbsite.

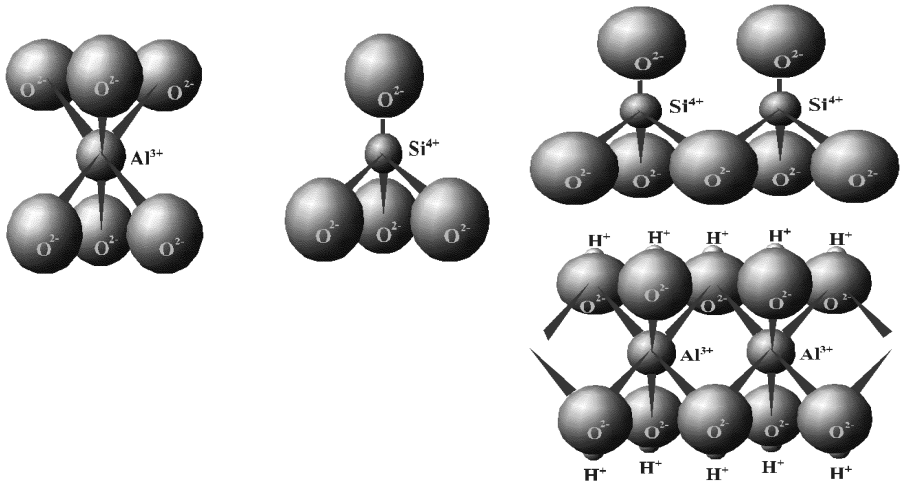

Figure 2.1 Tetrahedral and octahedral units.

Partial charge compensation may also be achieved by the "sharing" of apical oxygen atoms from both species and hence forming the Al-O-Si linkages (Fig.2.2) that when continued in two dimensions form the basic, structural sheets of which the clay minerals are composed. These basic sheets/units are also known as micelles. Here charge compensation in the Gibbsite layer is achieved by protonation of the upper apical oxygen ions and by "sharing" of the lower oxygen ions that simultaneously provides charge compensation for the tetrahedral silicate layer.

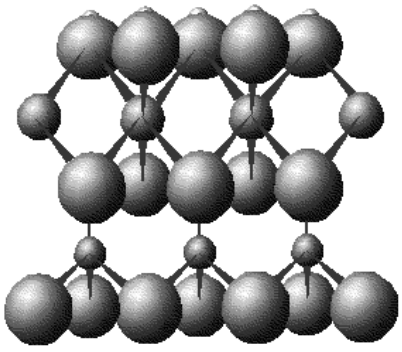

- Octahedral layer

- Tetrahedral layer

Figure 2.2 The 1:1 O-T Kaolinite structure

The basic arrangement of one tetrahedral layer bonded to one octahedral layer is the simplest example of the first basic group into which the clay minerals are divided, the Kaolinite group, which is described in mineralogical terms as having a 1:1, or O-T layer structure. The general empirical formula for kaolinite is $Al_2Si_2O_5(OH)_4$. The macro-molecular structure of the clay minerals consists of numerous layered micelles, which in the case of the kaolinite minerals are electronically neutral and held together by hydrogen bonding. The layers are difficult to separate and do not absorb water, or expand in contact with water – hence the kaolinite group members are known as non-expanding clays and this physical feature is of great importance when considering the firing property of clays; those containing a high proportion of kaolinite are deemed generally to be very useful in the manufacture of brick (Keeling, 1963; Bloodworth and Highley, 2005).

Several other less abundant members of this group exist, with structures based upon the 1:1 (O-T) arrangement.

2.2.1.2 Smectite clays, compositional potassium and isomorphous substitution

In the case of kaolinite minerals, electronic neutrality is achieved by the protonation of the upper apical oxygen ions, and the "sharing" of the lower oxygen ions with the tetrahedral silicon layer. A second means by which neutrality may be achieved is by the sharing of both upper and lower apical oxygen ions (Fig 2.3). This arrangement is known as the 2:1 or T-O-T structure and forms the basis for a further classification of clay minerals, the Smectite group, of which Pyrophyllite –empirical formula $Al_2SiO_4O_{10}(OH)_2$ is the simplest member.

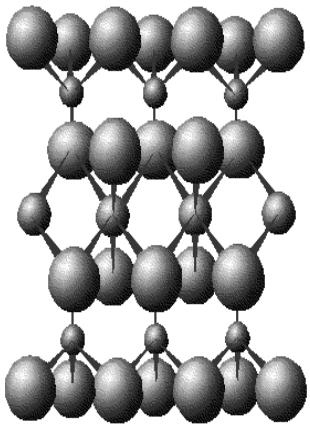

_ Tetrahedral layer

_ Octahedral layer

_ Tetrahedral layer

Figure 2.3 The 2:1 T-O-T Smectite structure.

Before discussing the characteristics of the other smectite clay minerals it is important to introduce the concept of isomorphous substitution that is common to all clay minerals, and involves the substitution of one chemical species for another during the initial crystallisation of the material. This process can occur only between species with similar ionic radii and examples are the substitution of Al^{3+} for Si^{4+} in tetrahedral coordination, and the substitution of Mg^{2+} and Fe^{2+} in octahedral coordination. The substitution of such species with differing ionic charges results in localised charge imbalance and compensation may be achieved by the association of balancing species, typically but not exclusively the M^{I} and M^{II} metals. This is of particular interest when considering the incorporation and distribution of potassium and hence ^{40}K in clay minerals, which in this case is likely to occur repeatedly throughout the crystalline structure, i.e. potential homogeneity of distribution on this scale.

Significant substitution of both Mg and Fe into the octahedral sites of the smectite mineral structure is common and the most abundant example of this

process is the mineral montmorillonite, which has partial substitution of Mg^{2+} for the octahedral Al^{3+} ions. The resultant negative charge per unit micelle results in the incorporation of interlayer hydrated cations (M^{I} and M^{II}). An idealised formula for a sodium rich montmorillonite might be $Na_{0.33}[Mg_{0.33}Al_{2.67}(OH)_2(Si_4O_{10})].nH20$. The incorporation of M^{I} and M^{II} species gives rise to the high cation exchange capacity of these minerals, which will be discussed later.

A further property of the smectite clays is the ability to absorb water, again between the micelle layers. This results in the expansion of these clays in contact with moisture and reduces the usefulness of these materials in the ceramics industry, probably due to high shrinkage on firing. Although not so relevant to the study of radionuclide distributions in either brick or sediment samples, it is interesting to consider, from a dosimetric point of view, that sediments rich in the smectite clays such as montmorillonite may have a higher capacity to vary in water content than those from non-expanding groups. Water content is one of the major sources of potential error in the luminescence dating of sediments, due to dose attenuation factors, and the use of XRD to determine clay types might be useful.

2.2.1.3 Illite clays and compositional potassium

Al^{3+} ions may also substitute in the tetrahedral Si^{4+} sites, again leading to the formation of negatively charged layers. When subsequent charge compensation is achieved by the inclusion of interlayer M^{I} and M^{II} cations (note – not the hydrated cations as found in the Smectites) an additional series of minerals known as the Illite group is formed. Based on the 2:1 layer structure, this series of

minerals contains the natural Micas, based on the substituted Pyrophyllite structure in the case of Muscovite (white mica) and in which the interlayer cations are predominantly potassium. The idealised formula for Muscovite is $[KAl_2(OH)_2SiO_3AlO_{10}]$ and the structure of the Illite clays are typically similar, but with variable, generally lower substitution of Al leading to a reduced number of interlayer potassium ions. It should also be noted that the other M^{I} and M^{II} cations may substitute for potassium, however in respect to the context of this research, Illite clays including Micas must be regarded as a fundamental source of potassium, and hence ^{40}K.

The presence of non-hydrated interlayer cations makes these minerals harder than the other 2:1 structured minerals, and prevents the absorption of water, resulting in the non-expanding nature of these types of clay. The use of Illite clays, together with Kaolinites is favoured in the production of modern bricks due to the resultant structural and physical properties (Bloodworth and Highley, 2005).

In the combination of Illite and Kaolinite clays, it is useful to reintroduce the subject of mixing efficiency as these species represent examples of relatively low and high potassium bearing minerals. The homogeneity of the matrix derived potassium (^{40}K) distributions for mixtures of these clays is likely to be a function of how well the individual phases are mixed. When examining the fabric of historic bricks, it is not uncommon to find discoloration and other patterns within the matrix that appear visually to be the result of poor mixing. One interesting aspect to consider during the main body of this research will be to investigate the correlation between visual heterogeneity and radionuclide distribution.

2.2.1.4 Chlorite clays

The final group of silicate clay minerals, the Chlorites, are sometimes excluded from general descriptions and instead discussed as an individual group within the phyllosilicates. This is primarily because some of the physical and chemical attributes of these minerals do not conform to those used generally to define clays, but as clay deposits are rarely composed of single varieties of clay mineral, a brief description of this group, on the assumption that they may be present naturally in some sediments, and in smaller amounts in other clays useful to ceramic production, is worthwhile.

The structure of the Chlorite minerals is based on the 2:1:1 structural unit (Fig.2.4) and can be understood partially in terms of the charge compensation mechanisms common to other minerals. With the Chlorite minerals however, charge compensation is effected not by the interleaving of hydrated or non-hydrated M^{I} and M^{II} species, but by the interleaving of positively charged layers, based around the Gibbsite structure described earlier, with partial or complete substitution of Mg^{2+} for Al^{3+}.

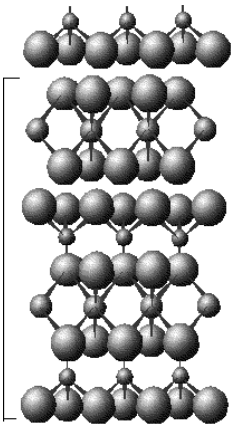

- Additional Octahedral layer (Al/Mg based)

- Tetrahedral layer

- Octahedral layer

- Tetrahedral layer

Figure 2.4 The 2:1:1:1 Chlorite structure.

The resulting micelle structures are held together very strongly and this feature accounts for the physical properties displayed by these minerals that are often used to differentiate this species from the other clays.

2.2.2 Quartz

Although this project is concerned with the distribution and quantification of radionuclides in archaeological materials, it is important to mention the use of quartz as the primary phosphor used in luminescence dating.

Quartz is an igneous mineral that belongs to the group of silicaceous minerals known as the tectosilicates, where the 2 dimensional sheet structure displayed by the phyllosilicate minerals is effectively extended to three dimensions. This group of minerals are also known as structural or framework silicates due to the three dimensional crystal lattices that form the macromolecular structures common to this species.

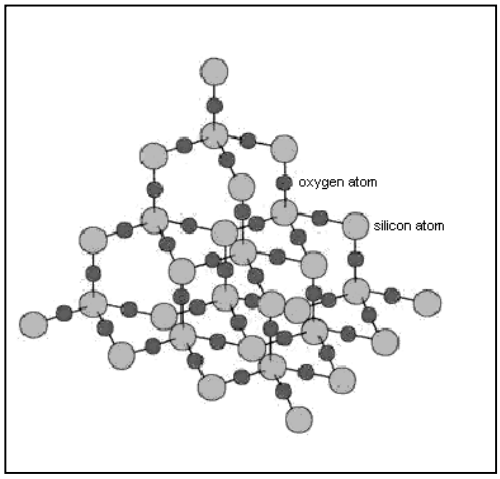

Figure 2.5 Three dimensional structure of quartz

Quartz is one of the more chemically stable surface minerals, and as such is resistant to chemical weathering processes. This feature explains why quartz is present in other sedimentary material, together with clay minerals that are formed primarily by the weathering of less stable parent rock constituents. As mentioned previously, quartz may be present to a highly variable degree in sedimentary materials and natural clay deposits, but is also added as a tempering agent in the manufacture of brick.

The luminescence properties of quartz and its use in dating have been investigated for more than 50 years (Wintle, 2008) and continuing research into the properties of this material forms the basis for much of the current activity in the field of luminescence dating. The use of quartz is often preferred to that of other naturally occurring crystalline minerals such as feldspars, which are prone to anomalous fading effects, whereby the potential loss of trapped charge (and hence subsequent luminescence signal) over time, results in a potential underestimation in evaluated absorbed dose. With the empirical chemical formula SiO_2 , naturally occurring quartz, in common with all naturally occurring (and indeed synthetic) crystalline materials, contains varying concentrations of trace element contaminants; it is in fact, the presence of these contaminants, in the form of extrinsic lattice defects, together with intrinsic defects that effect the charge trapping and luminescence mechanisms exhibited by such minerals.

Uranium, thorium and potassium are typically present in quartz at concentrations that are significantly lower than mean natural abundance values (Aitken, 1985) however the presence of these elements in trace concentrations

may contribute to the internal dose rate and should not be disregarded. Potassium may be present in quartz as a charge compensator for substitutional Al^{3+} cations; the presence of Al impurity in quartz is common, and the concentration and dispersion of this element, within even a single quartz grain, can vary by several orders of magnitude at the μm level, with subsequent potential for any charge compensation species to display similar distribution patterns (Pankrath et al., 1992).

Depending upon the geochemical environment during initial crystallisation, quartz may also contain micro-inclusions of other minerals (Huntley et al., 1993), including feldspar (with associated potential to contain high levels of potassium) and heavier minerals such as zircon; the latter may be present as a seeding component around which quartz may crystallise and depending upon the size of the internal inclusion, contribute, internally, to the dose rate received by an individual grain. Although an extensive analytical protocol to determine the presence and nature of internal dose contributors to single grains is not appropriate to this project, an initial study of the feasibility of such techniques will be useful.

2.2.3 Feldspars and compositional potassium

The feldspar group is the most abundant class of minerals compromising around 60% of the Earth's crust. Feldspars are actually analogous to quartz in terms of composition and structure, however in feldspars, up to 50% of the Si atoms are substituted by aluminium. The resultant charge imbalance requires the incorporation of further cations, predominantly Na^{+}, K^{+} and Ca^{2+}.

The majority of feldspars can be classified in terms of a ternary system based upon the three end members below -

$NaAlSi_3O_8$ – $KAlSi_3O_8$ – $CaAl_2Si_2O_8$

Albite Orthoclase Anorthite

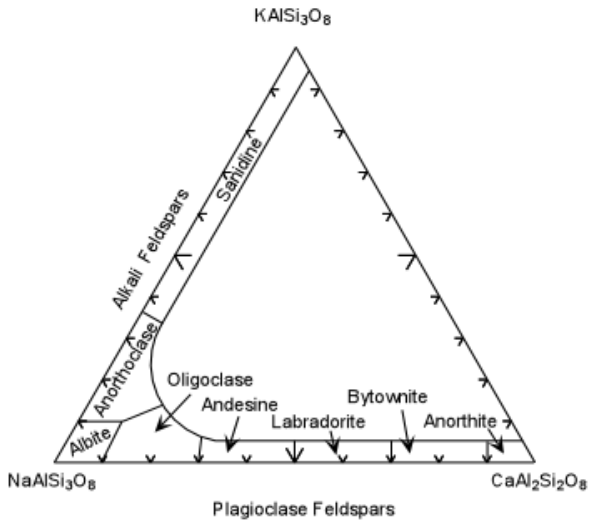

Figure 2.6 Ternary diagram of feldspar members

Isomorphous substitution is common between Na^+ and Ca^{2+} ions, however the K^+ ion is too large to substitute for Ca^{2+}. Feldspars tend not to be homogeneous in nature, and can be described in terms of solid solutions of parent components with differing degrees of isomorphous substitution. Because the K^+ ion cannot substitute for the Ca^{2+} ion, there is a tendency for two phase mixtures to result.

Feldspars containing variable proportions of Na and K content are known as the Alkali or K-feldspars, with the general formula $Na_xK_{(1-x)}AlSiO_3$.

As included materials in clay or sediments, alkali feldspar grains have the potential to be considerably richer in potassium (^{40}K) than the surrounding

medium and hence, affect the uniformity of the distribution of this isotope. Whilst feldspars are similar to quartz in structure, the geochemical stability of these minerals is significantly lower than that of quartz; feldspars weather readily, both chemically and physically and in fact, the chemical weathering of feldspars is responsible for the formation of many clay minerals and indeed quartz (as demonstrated below).

$$4KAlSi_3O_8 + H^+ + 2H_2O \rightarrow 4K^+ + Al_4Si_4O_{10}(OH) + 8\ SiO_2$$

Orthoclase + Hydrogen ion + water → Potassium + Kaolinite + Quartz

As with all included materials in natural clays and sediments, abundance, distribution and size are likely to be directly related to the composition of the parent materials, the sedimentation processes involved and the geochemical environment during burial.

2.3 Uranium and thorium

2.3.1 Abundance and distribution

The abundance of thorium (^{232}Th) in the Earth's crust is around 8 ppm, whilst uranium (^{238}U +^{235}U) is present at around 2.3 ppm; apart from selected ores and actinide rich mineral deposits (e.g. pitchblend, uranite, and certain uraniferous granites for uranium, monazites for thorium and zircons, potentially for both

species) these elements are widely dispersed (Greenwood and Earnshaw, 1997). In relation to this study, consideration is given to the potential by which these elements may be distributed heterogeneously within archaeological samples. The only stable oxidation state of thorium is ThIV and the relatively low solubility of this species in the natural, aqueous environment limits the number of mechanisms by which the incorporation of this element into natural sediments and clays may occur; the thorium content is likely to be predominantly associated with particulate and sedimentary processes (Cochran et al., 1986) both inorganic and organic (thorium has a strong tendency to form stable complexes with the latter). The assumption is made at this point that the thorium content of the matrices of interest (brick and sediment) is primarily fixed (due to the insolubility of thorium compounds) at the time of deposition and the heterogeneity of the distribution of this element is derived primarily from the thorium content and sedimentation patterns of the composite materials. Whilst this may also be relevant to the distribution patterns of uranium, the aqueous chemistry of uranium is interesting and provides the mechanisms by which both the concentration and leaching of this element in the natural environment are possible.

2.3.2 Oxidation states and stability

In the solid state, numerous oxidation states are possible for uranium, with a predominance of the IV and VI species. In the aqueous environment, the uranyl cation UO_2^{2+} represents the most stable form of uranium (i.e. U^{VI}), and although compounds of uranium in different oxidation states may exist in solution, there is a tendency to disproportionation and oxidation to the stable uranyl ion. The

chemical nature of the uranyl ion in the natural aqueous environment is dependent upon several factors, including pH and CO_2 concentration. At pH <5 the free uranyl ion is the dominant species whilst at pH >5 several hydrolysed species are present including UO_2OH^+, $(UO_2)_3(OH)^{5+}$, $UO_2(OH)_3^-$, $UO_2(OH)_2$, and $(UO_2)_3(OH)_7^-$ (Krepelova et al. , 2006). These species may occur due to the loss of H^+ from a coordinated water molecule, and subsequent –OH– bridging (Greenwood and Earnshaw, 1997).

The uranyl anion is linear, and as with analogous actinyl ions, including thorium, coordination with 4, 5 or 6 ligands is possible leading to the formation of complexes with octahedral, pentagonal bipyramidal, and hexagonal bipyramidal geometry. In the case of the uranyl ion, the ready formation of stable carbonato complexes explains the tendency of uranium to concentrate in carbonate rich materials, a property which is exploited in uranium series dating, together with the insolubility of the Th and Pa progeny. The formation and abundance of the uranyl-carbonato complexes are again dependent upon pH and of course the concentration of CO_2 present. At pH<7, in the presence of sufficient CO_2, the carbonato complexes dominate the aqueous uranyl speciation equilibrium with species such as $(UO_2)_2CO_3(OH)_3^-$, - $UO_2(CO_3)_2^{2-}$ and $UO_2(CO_3)_3^{4-}$, the latter being the tricarbonato complex associated with the carbonate leaching of uranium from mineral ores.

2.3.3 Mobility and mechanisms

If consideration is now given to the possible mechanisms by which uranium may be incorporated into sediments and natural clays, the importance of the behaviour of the uranyl anion in the natural aqueous environment becomes apparent. The idealised structure of the clay minerals, as discussed previously,

refers to repeating units of sheet layers, based upon the O-Si-O and Al-O-Si linkages and other factors relating to charge compensation. One important aspect to consider is that these structures are not infinite in nature, and that the natural termination or breakage of these sheets will result in edge charge imbalance, for example $–O^-$ end groups, similar to those found on the basic Kaolinite structure where protonation of the apical oxygen ion effects charge compensation.

Cation exchange occurs readily at these sites and this factor is of great relevance when considering the mechanisms by which uranium may be incorporated into minerals. The incorporation of thorium into clay minerals by ion exchange is also possible, but as previously stated, the abundance of thorium in solution reduces the relevance of this process within the context of this research.

The extent to which cation exchange can occur in different clay minerals is important when considering the factors affecting uranium uptake; the cation exchange capacity (CEC) of different clay minerals is widely understood and in practice easily determined (Borden and Giese, 2001). Several studies have been carried out to examine the factors affecting the uptake of uranium and as expected, these include not only the CEC of the clay minerals, but also the REDOX potential, pH and CO_2 concentration of the aqueous environment (Krepelova et al., 2006).

In the presence of CO_2, the rate at which uranium is adsorbed onto Kaolinite for example, reaches a maximum at around neutral pH, and declines dramatically at pH<4 and pH>9. At neutral pH, in the presence of CO_2, the $(UO_2)_2CO_3(OH)^{3-}$ ion represents the major species in solution. In the absence of CO_2, the rate of adsorption is lowest at pH values below pH4, when the free uranyl ion UO_2^{2+}

dominates. Therefore maximum adsorption occurs in this system when speciation is dominated by the hydrolysed species.

A further complicating factor in the adsorption of uranium by clay minerals is the presence of organic matter, in particular humic acids (HA). In the presence of HA and the absence of CO_2, the uranyl ion is the dominant species only at low pH values; at neutral pH the formation of uranyl/HA complexes dominate. It is interesting to note at this point that the presence of intermediate concentrations of HA (10mg/l) may serve to increase the rate at which uranium uptake occurs, probably by the interaction of the UVI/HA complex with Kaolinite. At higher concentrations (50 mg/l HA) the uptake of uranium is impeded (Krepelova et al., 2006).

It is suggested that the interaction of the uranyl ion, and related species, with clay minerals may be predominantly by the relatively simple cation exchange process, however recent EXAFS investigations have revealed that there may be inner sphere coordination between the uranium ion and SiO_4 tetrahedra (Catalano and Brown, 2005). It is clear that the behaviour, and subsequent incorporation of uranium into natural clays, is extremely complex, and dependent upon several environmental factors.

The potential for mobility of uranium species in the natural environment is dominated primarily by oxidation state; in reducing environments (comparable to those in which the $Fe^{3+} \rightarrow Fe^{2+}$ redox reaction takes place) the tetra-valent oxidation state, UIV predominates, and here, the geochemistry of uranium becomes very similar to that of thorium. This behaviour is further reinforced by the similarity in the sizes of the ionic radii of the two species (see Table 2.1);

thorium has the potential to demonstrate similar substitution patterns as uranium and evidence of this feature can be seen in minerals such as zircon, where both species substitute freely due to the ionic radius of Zr^{4+}

2.3.4 Mineral associations

The relatively large atomic radii of uranium and thorium (see Table 2.1) result in the association of these elements with certain igneous materials, probably due to the geological processes and timescales at which these minerals were formed in addition to simple size effects. In the case of quartz however, the large ionic radii of these radionuclides serves to hinder their inclusion into the crystalline structure by any mechanisms other than the entropic processes by which other trace elements are incorporated; uranium and thorium display a stronger association with "heavier", chemically resistant minerals such as the zircons and other placer deposits such as the phosphate rich monazites.

Ion (Oxidation state)	Coordination No.	Ionic Radius Å
Al (3+)	4	0.39
	6	0.54
Ca (+2)	6	2.00
	8	2.12
Na (+1)	6	2.02
	9	2.24
K(+1)	8	2.51
	12	2.64
Si (+4)	4	0.26
U (+4)	6	0.89
U (+6)	2	0.45
	7	0.81
Th (+4)	8	2.05
Zr (+4)	8	0.84

Table 2.1 Effective Ionic Radii in Crystals
Source CRC Handbook of Chemistry and Physics 77th edition.

2.4 Uranium, thorium and potassium – summary of relevant factors

Uranium

Present in trace (mg/kg or μg/g) concentrations in material matrix and to a lesser extent in quartz. Concentrated in heavy, resistant minerals such as zircon which may be present as inclusions within the matrix or micro-inclusions within quartz. May be present in carbonate or phosphate rich inclusions (such as monazite).

In bricks, concentration is primarily fixed at the time of manufacture although emanation of radon may affect secular equilibrium.

In sediments, uranium demonstrates the potential to accumulate in both organic and clay based phases; stability is dependent upon environmental factors and redox potential.

Thorium

Present in trace concentrations in material matrix and to a lesser extent in quartz. Concentrated in heavy, resistant minerals such as zircon which may be present as inclusions within the matrix or micro-inclusions within quartz.

Concentration is primarily fixed at the time of manufacture. In sediments, mobility is likely to be due to physical rather than chemical factors.

Present in monazite inclusions.

Potassium

Present in both trace and macro concentrations in clay minerals.

Present to a lesser extent in quartz as a charge compensator or other defect.

Present in high concentrations in feldspathic phases and included grains.

The relatively brief introduction to some of the factors concerning the macro and micro distribution of radionuclides in archaeological bricks and sediments, given above, has demonstrated that the mechanisms which may be responsible for these patterns are both numerous, complex and difficult to predict. The overall purpose of this initial work is to introduce and explain some of the compositional and geochemical elements that are relevant within the context of this research and to provide a basis from which further study may progress. It has also been demonstrated that the potential for heterogeneity in the distribution of these radionuclides is a fundamental consequence of the origin and production of these materials. It should also be made clear at this point that the assessment of the distribution patterns of the radionuclides in question are important because of the direct link between radionuclide concentration and dose rate, and hence dose rate distribution within the sample material. The extent to which dose rate distribution varies spatially is of course dependent upon the type of radiation being emitted; the next stage of this research will in part assess the level of spatial resolution required in the analytical determination of ^{238}U, ^{232}Th and ^{40}K to provide useful information with respect to single grain dating applications.

Chapter 3 Initial analytical considerations

3.1 Introduction to dosimetry

Before full consideration can be given to the analytical and detection capabilities required to determine the micro–distribution characteristics of natural radionuclides in archaeological materials, an appropriate sampling rationale must be devised. This rationale must include, the assessment of the degree of spatial resolution that will be required to produce analytical data that can be used to provide information which will be relevant to the support of current luminescence dating research. Hence, a strategy should be devised that can be adapted to provide information regarding the macro radionuclide distribution characteristics of a material, together with the ability to focus on a specific area of interest on the mm or sub-mm scale, an example of which could be the material directly surrounding a single "bright" phosphor grain in situ or indeed, an investigation of the internal radionuclide concentrations of the grain in question.

3.1.1 Contribution to absorbed dose

In order to realise an effective sampling rationale, consideration must first be given to the factors which affect the radiation dose received by the crystalline inclusions used in single and disaggregated grain dating techniques. Primarily, but not exhaustively, and in respect particularly to individual phosphor grains, these factors include the distribution, nature and activity of the sources of radiation located external to, and within, the phosphor grain from which absorbed dose is derived, and also the size and mineralogy of the phosphor grains.

3.1.2 Gamma radiation

A large contribution to the absorbed dose in single grains may be potentially derived from the environmental gamma dose contribution, and whilst quantification of this component is essential to subsequent dating calculations, further consideration is not required within the scope of this research; the maximum range of gamma rays in the materials of interest is in excess of 25 cm and as such, on the mm and sub-mm scales associated with this research, the gamma flux may be regarded as uniform. Absorbed dose due to exposure to cosmic rays may also be regarded as uniform and hence, attention at this stage is concentrated only on the alpha- and beta- derived contributions to absorbed dose.

Consideration must be given initially, to the volume of matrix material which immediately surrounds a single phosphor grain and from which contributions to absorbed dose originate.

3.1.3 Alpha particles

The alpha particles emitted by members of the uranium and thorium decay series have a very limited range in quartz and siliceous ceramic matrices (average range value 25 μm – Aitken, 1985), and this presents certain difficulties in the formulation of an appropriate sampling regime, if a spatially resolved investigation were required.

The quantitative assessment of the alpha contribution to absorbed dose from the immediate grain environment has been attempted using NAA methods (Wagner et al., 2005) although this level of investigation is not practical within the scope of this research.

The effective attenuation of alpha radiation within the outer surface layer of quartz grains (>90 μm in diameter) reduces the significance of this external contribution to total absorbed dose as grain size increases. For practical purposes the general characterisation of alpha emitter distributions may suffice, although the potential to produce a semi-quantitative method of surface activity determination was explored, as discussed further below.

A technique for the partial characterisation of the localised heterogeneity in the distribution of alpha emitting radionuclides, with sub-mm resolution, has been introduced previously, based on the use of Solid State Nuclear Track Detector (SSNTD) materials (Haustein et al., 2003); Taking into account the practical and financial constraints of this research project, the use of these detectors, at this level of resolution represents the most appropriate methodology for characterisations of this type. It is also feasible that the assessment of alpha emitter micro-distribution patterns at this level of resolution could be used to provide information about the heterogeneity of the beta dose-rate distributions arising from members of the U and Th decay series.

3.1.4 Beta radiation

Beta particles have a much longer range in comparison to alpha particles (for equivalent particle energies). The range of beta particles is dependent upon numerous factors including the initial or incident energy of the beta particle and material characteristics such as density and elemental composition. Within the scope of this work, the beta particle range from which significant dose is delivered to a point of interest is more perhaps more appropriate. Recent work by Mayya et al. (2006) investigates the effect of dose rate variations to single phosphor grains that result from the presence of individual beta point source emitters or "hot spots" within a sample matrix. Calculations were based on a modified Dose point kernel approach and utilised a maximum dose-contributing distance of 2.28 mm, based on the calculated range of ^{40}K beta particles in a typical sediment matrix.

A greater potential for non-uniformity in beta dose rate due to heterogeneity in the distribution of sources is likely to be associated with fluctuations in local potassium concentration (see Chapter 2), a minimum sampling resolution of 2 mm should be acceptable in the production of useful information relating to the characterisation of the macro distribution patterns of component radionuclides.

3.2 Matrix characterisation

3.2.1 Initial tests

The development of a single, generalised sampling strategy is not appropriate due to the expected variability in matrix compositions; instead, a number of

optimised strategies, based on matrix specific characteristics need to be developed.

3.2.1.1 Analysis of digital images

An initial assessment based on the use of microscopic techniques may provide useful information on the macro and sub-mm material characteristics of a particular sample. Mineral grain abundance and distribution, material heterogeneity with respect to colour and texture and the presence of voids or other anomalous features may be identified using these means. The use of digital photography and the subsequent application of image processing techniques were applied to reveal areas of visual heterogeneity which may not be immediately obvious to the naked eye. The development of a suitable algorithm to optimise the identification of subtle colour differences in fired ceramics and sedimentary materials also formed part of the initial methodology.

3.2.1.2 Staining techniques

The use of geological staining techniques (Hayes and Klugman, 1959) may be used to identify K-rich mineral inclusions and, with the use of conventional microscopy, offers potential insight into the distribution patterns of these

minerals on a mm and sub-mm scale. Again, the use of digital imaging techniques may be used to estimate the surface abundance of potassium bearing mineral phases, although most staining techniques provide qualitative data only. Surface chemical treatments may also be used to differentiate between mineral phases, particularly the non-potassium feldspar minerals and quartz which are difficult to assess without the use of specialised petrographic techniques.

In comparison, the application of qualitative Scanning Electron Microscopy – Energy Dispersive X-ray detection (SEM-EDX) based techniques may offer some advantages, but is prohibitively expensive for routine initial assessments. SEM techniques are not suitable for the qualitative or quantitative determination of uranium and thorium at the levels associated with most common clay minerals. However they can be used to detect zircon inclusions which usually have a high uranium content and the use of this approach is discussed later.

3.2.1.3 Solid State Nuclear Track Detectors

The use of solid state nuclear track detector (SSNTD) materials has been introduced briefly as a qualitative method to indicate the homogeneity of surface alpha emitter distributions in archaeological materials (Haustein et al., 2003). These materials form the basis of alpha auto-radiographic techniques whereby the emission of alpha particles can be detected by the development of latent tracks within the detector material. CR-39 is a commercially available SSNTD which is suitable for the detection of the alpha particles emitted from the members of the U and Th decay series. The material is inexpensive (Tastrack) and readily available; initial calculations indicate that this detector will provide useful results within the timescales associated with sample throughput in a

commercial luminescence dating laboratory (Durham, 3-6 months). Alpha autoradiographs were used to provide semi-quantitative information about the uniformity of the surface alpha activity, with a potential detection resolution based on both the alpha particle range, angle of incidence subsequent diameter and length of the developed tracks – these quantities will be discussed at a later stage but the resolution is likely to be less than 100 microns.

Further factors of particular relevance are the distribution characteristics, and the variability in luminescence sensitivity (as a function of absorbed dose) of the quartz grains that may ultimately be used in dating. Whilst the distribution of quartz grains may be assessed visually, the sensitivity of individual grains may only be determined using luminescence techniques, either by the analysis of single disaggregated grains or *in situ* using spatially resolved techniques.

A practicable consideration of the available matrix information and grain luminescence characteristics, combined with an appreciation of the rationale for analysis will be used to develop a sampling rationale – this may be applicable to a single quartz grain, or a general characterisation of the macro and micro-isotopic distribution patterns of a chosen material to provide useful information for disaggregated grain techniques.

3.2.2 Sampling strategies for quantitative analysis

There are many different analytical techniques that can be used to provide quantitative information, and the suitability of the most widely used of these techniques for this work will be assessed.

In contrast to the qualitative techniques described earlier, they require the removal of material from the sample matrix. The amount of material removed for each aliquot together with the resolution and frequency of sampling are key factors affecting the levels of detection.

3.2.2.1 Sampling considerations

Probabilistic approaches to sampling strategy, similar to those used in basic archaeological prospection (Renfrew and Bahn, 2000), are based upon the selection of sampling sites using either a random and /or stratified approach. These types of rationale are used primarily when there are no available data on which to base a definitive sampling rationale and may be useful in this research if the determination of the mean matrix elemental concentrations is in a sample that is effectively homogeneous.

In the simplest case, a pre-defined number of sample aliquots are taken randomly across the surface of a defined area of interest (simple random sampling). If a square grid is produced to represent this area, sampling points can be identified by assigning an appropriate number of randomly generated x ,y coordinates. The optimum size of each grid-square and sampling volume may be defined in this case as a function of the volume within which the majority of the absorbed dose is deposited, although sampling within this area on a smaller scale

may be appropriate for other samples. One disadvantage with this sampling strategy is that if random clustering occurs during the generation of sampling sites, there is a potential that the effective area being sampled will not be representative of the total area – clustered or localised areas of increased radionuclide concentration may be excluded from the sample set.

A more useful approach with this type of sample matrix is the use of a systematic approach, where an appropriate number of samples are taken uniformly across the area of interest (Fig 3.1). In this case, the probability of detecting discrete areas of increased radionuclide concentration should potentially be increased, depending on the size, distribution and relative concentration of the composite isotopes.

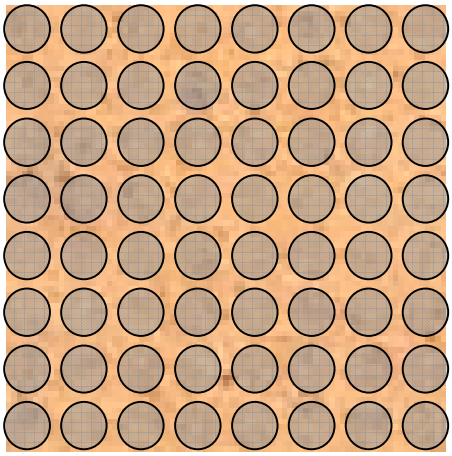

Figure 3.1 Systematic sampling rationale, in which 64 x 1 mm aliquots are taken across the entire surface of the section.

On a routine basis, due to time and instrumental constraints, it is unlikely that the number of aliquots shown in Fig 3.1 could be processed or indeed required. A modified version of the systematic rationale, where fewer aliquots are taken may provide acceptable levels of resolution across the entire surface (Fig 3.2),

although the selection of a smaller area of interest, with no compromise in spatial resolution may be preferred (Fig. 3.3).

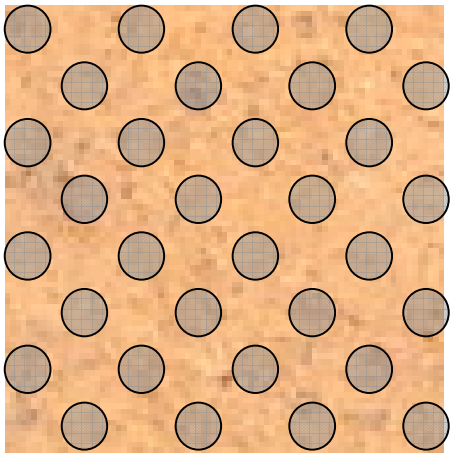

Figure 3.2.
Systematic sampling rationale with reduced sampling frequency.

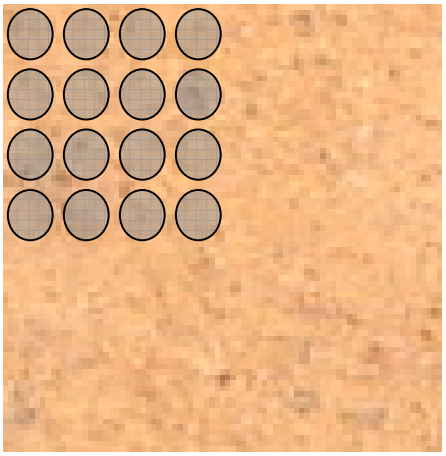

Figure 3.3.
Systematic sampling rationale in which the area of interest has been reduced (4 mm x 4 mm) to provide high resolution sampling.

The major advantage of using the qualitative procedures highlighted earlier is the decreased reliance on probabilistic sampling strategies. The identification of areas of increased K concentration, the distribution patterns of alpha emitters and the visual identification of differing mineral species will facilitate the development of an intelligent, non-probabilistic approach to sampling.

Examples of non-probabilistic sampling strategies based on initial qualitative data are depicted below.

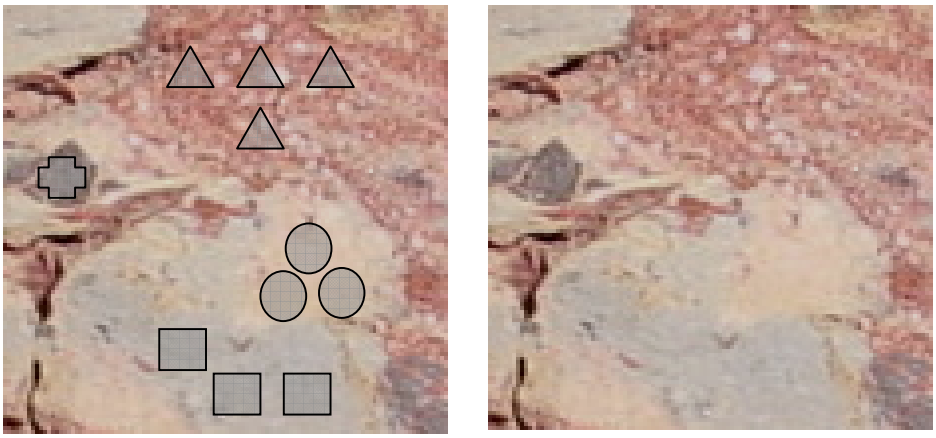

Figure 3.4**.** Sample 295-7-1 (10 mm slice – coarse textured brick).

Samples may be taken from four discrete regions of interest which have differing visual and textural properties.

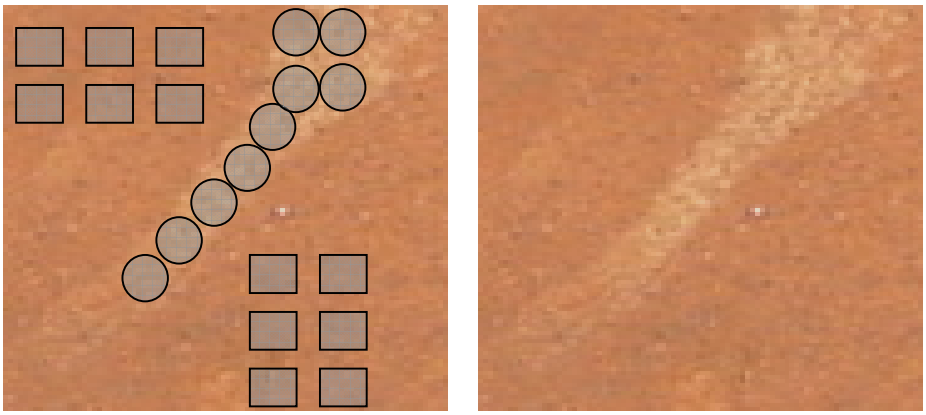

Figure 3.5 Sample 295-8 (10 mm slice – fine textured brick).

Samples may be taken to identify compositional variations between apparently different clay types.

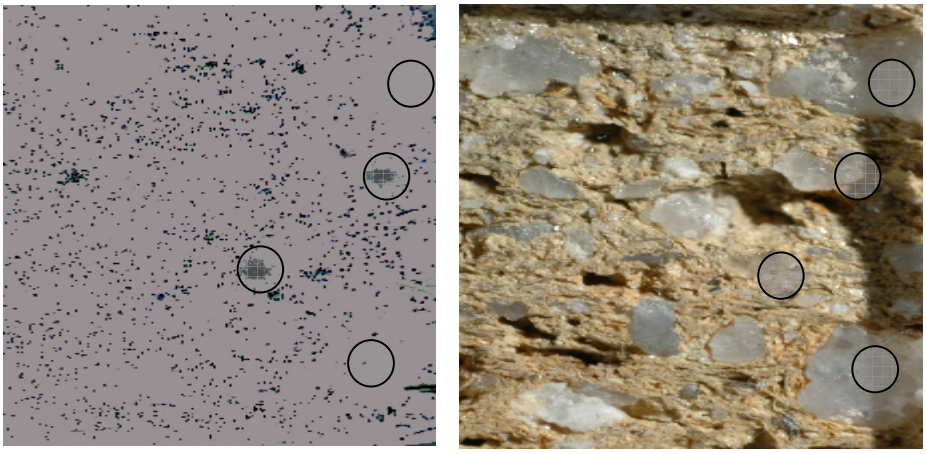

Figure 3.6 Sample 321-1 (10 mm slice – coarse textured brick) – Alpha autoradiograph (left) produced using CR-39. Areas of high and low alpha activity have been highlighted as regions of sampling interest. In this case, the precise visual correlation of autoradiograph and sample image enables micro-sampling to be carried out at strategic points.

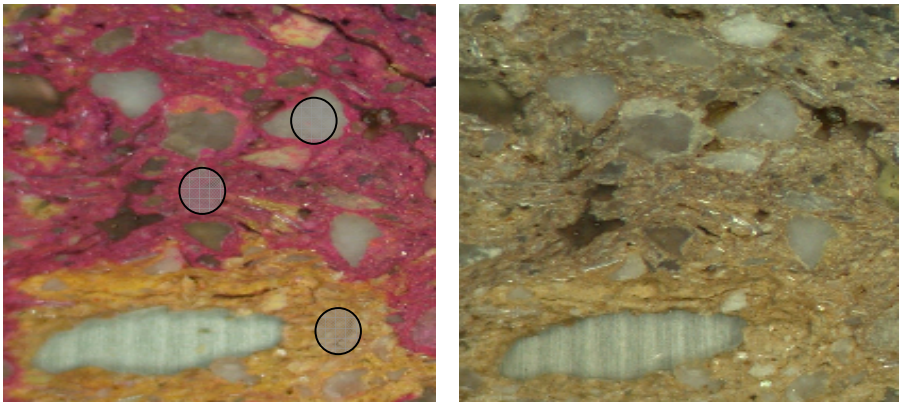

Figure 3.7 Sample 321-1 (10 mm slice) – Surface etching with hydrofluoric acid vapour followed by subsequent treatment with sodium hexanitrocobaltate (III) staining with eosin solution (left).

Areas of increased K concentration are stained yellow, quartz grains remain effectively unchanged, whilst non-quartz phases develop a red-pink stain. The highlighted sampling sites represent areas of interest, namely, quartz, K-rich phase and general non-quartz matrix phase.

3.2.2.2 Sampling techniques

The sampling rationales detailed in the captions are based on the assumption that it will be possible to remove aliquots of matrix material at this level of resolution. Initial trials using a hand held micro-drill fitted with a 1 mm diameter dental burr, used in conjunction with a standard laboratory microscope were successful in removing micro-aliquots of material from archaeological brick slices (321-1), with excavated material being collected by either pipette (as a slurry with deionised water) by micro–vacuum, or if the sample matrix is physically stable, by tapping off excavated material into a suitable collection vessel. If sample drilling is carried out to a depth of 1 mm, the total excavated material weight (assuming density of 2.6 $g.cm^{-3}$) will be approximately 20 mg. However this calculation does not take into account the porous nature of many archaeological materials, or mechanical loss; in reality the amount of sample retrieved per aliquot is likely to be significantly less.

Care must be taken with the use of encapsulation materials as material excavated from porous samples which have been previously encapsulated using standard laboratory means, are likely to contain substantial quantities of the encapsulation material (Epothin™ cold setting epoxy resin)

One option to permit the removal of material from sediments, without the requirement for encapsulation, is the use of a micro-auger, with a diameter of ~2-5 mm which may be inserted into the sediment to a suitable depth, without disrupting the spatial structure of the sample. Sub-aliquots may be subsequently removed by extrusion of the material.

Consideration must also be given to chemical digestion and preparation techniques appropriate to aliquots of this size, together with the subsequent instrumental detection limits. These considerations are discussed in the following chapters.

Chapter 4 Review of analytical techniques

The determination and quantification of the three important radionuclides, ^{238}U, ^{232}Th and ^{40}K, and the development of analytical methods by which this may be accomplished form the basis of the experimental aspects of this research. The potential instrumental, chemical and indirect methodologies outlined in previous chapters, are discussed in more detail in this chapter.

4.1 Limits of detection and sample size

Focussing initially on the determination of the most abundant isotopes of U and Th (i.e., ^{238}U and ^{232}Th) it is important to assess the likely concentrations in the sample to be examined, before deciding on an appropriate analytical technique.

When determining the suitability of an instrumental technique, including the associated limits of detection, it is necessary to consider any dilution factors that may result from sample pre-treatments, and the physical volume and form of material required for analysis.

Taken to achieve appropriate spatial resolution, the typical sample aliquots generated by the micro-drilling techniques detailed in chapter two, are likely to provide less than 30 mg of material for each analysis. If this material is digested and subsequently diluted (to 10 ml, as is appropriate for (Inductively Coupled Mass Spectrometry (ICPMS) or Atomic Absorption Spectrometry (AAS), for example), the resultant concentrations of uranium and thorium may fall within a likely concentration range of 1 to 50 μg/l (ppb) and it is this instrumental level of detection that would be required. If a method is chosen where no sample pre-

treatment is required, and it is possible to analyse the small sample aliquots directly (e.g., Neutron Activation Analysis (NAA) based techniques), then the limits of detection may be based on the quantity of analyte present. In the case of ^{238}U for example, assuming a concentration of ~3 μg/kg, a 30 mg aliquot would contain approximately 0.09 μg or 90 ng of ^{238}U.

When considering indirect methods of analysis, such as alpha autoradiography, the surface alpha activity of uranium and thorium progeny is of primary concern. Here, one of the major issues is the required sample/detector contact time; clearly, this needs to be practical within a laboratory timescale.

Potassium, and hence ^{40}K, is likely to be considerably more abundant in archaeological materials than either uranium or thorium, although the potential for variability in concentration is more substantial, depending upon the mineralogy. For the instrumental determination of potassium, it is important that any method selected provides a practical compromise between both suitable detection limits for samples with low potassium content, and a potential calibration range which can accommodate potassium rich samples. A 30 mg aliquot of material with a typical concentration of 0.1% K, would, when diluted to a final volume of 10 ml, produce a solution concentration of 30 mg/l K; this concentration could easily vary by up to two orders of magnitude, depending upon sample characteristics, and this would result in the need for further sample dilution. Although the dilution of samples to bring analyte concentrations into ranges appropriate to instrumental calibration parameters is commonplace in analytical chemistry, dilution errors and matrix effects must be considered.

It is also important to remember at this stage, that if different methods are used for the determination of uranium, thorium and potassium, sample material may need to be divided.

4.2 Introduction of analytical methods

The purpose of the following introduction to several potentially useful analytical techniques is to provide a brief overview of the underlying principles, limits of detection and associated analytical problems; this will provide enough information from which an appropriate analytical rationale may be developed. Detailed descriptions of theory, instrumentation and analytical parameters will be reserved for the individual methods selected for use during the experimental phase of the research and will be included in later chapters. Bulk methods such as high resolution gamma spectrometry have not been included at this stage as they are not appropriate to the sample quantities associated with this research and do not offer spatial resolution capability. Other methods such as fluorimetric (uranyl ion) and colorimetric determinations (e.g. the arzsenazo method) have not been included as they offer little or no advantage over established, instrumental techniques and may be more prone to matrix interferences. Pre-concentration techniques such as solvent extraction or ion-specific resin exchange mechanisms have not been mentioned in detail due to the labour intensive nature of these procedures.

4.2.1 Atomic spectrometric methods.

4.2.1.1 Atomic Emission Spectrometry (AES)

This technique is based on the measurement of radiation emitted due to the de-excitation of electrons that are undergoing transition from higher excited to lower or ground energy states. Such transitions are quantized; the wavelength of the emitted radiation is specific to a particular element and type of transition and the intensity of emission is proportional to the number of emitting species, i.e., the analyte concentration. As emissions originate from free atomic species, AES determinations require the use of an energy source that is capable of simultaneous atomization and excitation of analyte atoms, introduced in either liquid or solid form, depending upon instrument type. Several energy sources are suitable for this purpose, including those based on the employment of flame, plasma and electrical discharge effects; Inductively Coupled Plasma Atomic Emission Spectrometry (ICP-AES) is now used routinely in trace analysis and offers a limit of detection of around 5µg/kg for potassium and displays potentially greater sensitivity for uranium and thorium (Rubinson and Rubinson, 2000; Fujino et al., 2000) although matrix and other elemental / spectral interferences may be problematic. Digestion, extraction and pre-concentration techniques (e.g., acid digestion followed by separation and extraction in diisobutyl ketone) may be used to minimize interference effects and reduce limits of detection, whilst the addition of other chemical species may be used to eliminate chemical interferences (such as the addition of caesium in relatively high concentrations to reduce ionisation effects).

ICP-AES samples are aspirated in liquid form, typically in aqueous solution containing 2-3 % nitric acid or in an appropriate solvent if organic extraction techniques have been used. Spectral data relating to emission wavelengths and

potential spectral interferences are widely available (Daskalova and Boevski, 1999).

4.2.1.2 Atomic Absorption Spectrometry (AAS)

As the name of this technique implies, the underlying principle is analogous to AES, but is based on the measurement of absorbed rather than emitted radiation. In AES, atomization and excitation are simultaneous whilst AAS techniques rely upon the absorption of externally applied radiation of a specific wavelength to produce excitation. The amount of radiation absorbed is proportional to the number of absorbing species and hence to analyte concentration. Atomization is generally effected thermally, by either flame techniques (Flame Atomic Absorption Spectrometry) or by electro-thermal means (e.g. Graphite Furnace – GF-AAS). Although simultaneous relaxation, (and hence emission) does occur, flame and temperature conditions are carefully controlled to minimize this effect. Similarly, self- absorption may also be problematic in AES determinations, but this is generally noticeable only at high analyte concentrations. FAAS techniques use liquid aspiration sample introduction and typically provide sufficient sensitivity to be useful in the determination of trace concentrations of potassium, with a limit of detection of around 20 μg/kg. The use of electro-thermal sample atomization can effectively reduce both the limits of detection and the quantity of sample that is introduced to the instrument (typically 50 μl) and this form of sample introduction is appropriate in the trace determination of uranium and thorium, particularly as both species are prone to the formation of refractory oxides in flame techniques (Rao et al., 2006).

4.2.1.3 Neutron Activation Analysis (NAA)

When a material is exposed to a flux of low energy neutrons (<0.5 eV), the majority of atomic nuclei present exhibit neutron capture, a process by which at least one neutron is incorporated into the nucleus of the target atom. The radioactive decay of the resulting unstable nuclides is accompanied by the emission of characteristic gamma photons, and the quantification of these emissions forms the basis of neutron activation analysis.

This type of analysis requires initial activation (i.e., exposure to a moderated neutron flux of suitable intensity for which access to a nuclear reactor facility is generally required), followed by subsequent high-resolution gamma spectrometry. NAA is available commercially and has been used successfully to determine U, Th and K in the materials and concentrations appropriate to this research (Jagam and Simpson 1993).

Analyte	**Reaction product**	**Half-life**	**Gamma energy (eV)**
Th	^{233}Pa	27.0 days	311.90
U	^{239}Np	2.35 days	277.60
K	^{42}K	12.4 hr	1524

Table 4.1 NAA data for U, Th and K

Sample activity is dependent upon the number of emitting species present, the rate at which neutron capture occurs (neutron capture cross section), the neutron flux to which the sample has been exposed and the radioactive half-life of the emitting species. Spectral and matrix interferences for these elements are relatively low and one advantage of NAA based techniques is that as no sample pre-treatment is required, measurements can be made on small solid aliquots. Activation techniques based on the use of higher energy neutrons are also available; the selection of this type of activation may be useful in other areas of U and Th determination, such as neutron activation induced fission track analysis, which will be discussed later.

4.2.1.4 X-Ray Fluorescence Spectrometry (XRF)

X-ray fluorescence techniques are based on the determination of the characteristic x-ray emissions that result from the transition of electrons from higher atomic energy levels to vacancies within lower atomic energy levels. Such vacancies are created initially by irradiation with x-rays that have sufficient energy to remove an electron from an inner shell (i.e., photoelectric absorption of an x-ray, followed by ejection of a photoelectron). As expected, the nature of the resultant spectrum is dependant upon several factors including atomic species, analyte concentration, the energy of the incident x-rays, the type of transition that is occurring (e.g., from L energy level to K energy level), transition type and probability, and the simultaneous scattering processes (elastic and inelastic) that result from the interaction of x-rays with matter (Attix, 1986). XRF

instrumentation is further characterised by the type of detection system used and can be described as either wavelength dispersive (WD-XRF or WDS) or energy dispersive (ED-XRF). Limits of detection for uranium and thorium have been quoted in the region of 100 μg/kg (Rubinson and Rubinson, 2000) although in practice, this level of sensitivity is difficult to achieve, particularly with the small aliquots associated with micro-sampling techniques used in this research. XRF may prove to be a useful tool in the semi-quantitative determination of potassium, at the levels encountered in archaeological materials, however, the small aliquot sizes may still prove to be problematic. XRF is most useful in the determination of bulk sample (>1 g) characteristics and so may provide important information when looking at factors such as analyte concentration in different particle size distributions; this is likely to be of particular interest when looking at matrix heterogeneity in sediments (Mayya et al., 2006).

4.2.1.5 Scanning Electron Microscopy (SEM), Electron Microprobe (EMP) and Proton Induced X-ray Emission (PIXE) techniques

Scanning electron microscopy has become an established technique in the field of materials analysis and when coupled with quantitative x-ray analysis is able to provide high-resolution, spatially resolved elemental information. The technique is based on the detection of the secondary (including auger) and backscattered electrons emanating from a material that has been bombarded with an accelerated stream of incident electrons. Scattered or emitted electrons can be distinguished by energy; backscattering (inelastic or Rutherford scattering) will result in electrons which have a similar energy value to those of the incident beam, whilst secondary electrons arising from the sample surface (with beam penetration depth depending partly upon incident energy) result from inelastic

scattering processes and have typically lower energies (<50 eV). The detection of backscattered electrons can provide useful information regarding surface elemental composition (based on contrasting Z values), whilst secondary electrons may be more useful in the determination of topographic and morphological features. The qualitative detection of heavier elements such as uranium by the detection of backscattered electrons is possible, but only if the sample matrix and concentration of analyte are appropriate (Merroun et al., 2005). Even with the use of x-ray analysis techniques, the detection of uranium and thorium is not possible at the routine concentrations at which these elements are likely to be present in the archaeological matrices of interest although it is possible that detection of relatively high localised concentrations may be possible (e.g., zircon grains). Due to the abundant nature of potassium, SEM coupled with EDX or WDS detection facilities is capable of providing useful information about the surface distribution of this element. The generation of a high-resolution "elemental map", showing the distribution of lighter elements is now a relatively routine procedure and although qualitative in nature provides very useful information about the nature, presence and indeed absence of potassium bearing minerals. These techniques may also be used to provide quantitative information on the elemental composition of small areas of interest, with resolution depending on electron beam diameter and sample positioning capability; this is a lengthy process, and hence this technique may be suitable only for the investigation of smaller areas (e.g., single grains).

Based on a similar principle to the SEM, the electron microprobe (EMP) uses a micro beam of electrons that is moved across the sample surface. The characteristic x-rays that are produced are quantified by either energy or wavelength dispersive detection. As with SEM, the levels of detection available

for uranium and thorium may mean that this technique could be useful in the identification of relatively high, localised concentrations.

Proton induced x-ray emission (PIXE) techniques are analogous to electron micro-probe XRD as the measurement of characteristic x-ray emissions forms the basis of the technique; as the name implies however, PIXE techniques are based around the use of an accelerated beam of protons to effect inner-shell ionisation, with subsequent x-ray emission resulting from auger transitions. There are several instrumental advantages to the use of proton rather than electron based incident beams including the minimisation of Bremsstrahlung and lower levels of backscattering. Limits of detection for uranium and thorium have been quoted at μg/g levels (Cohen et al., 1980); however, in the complex matrices of the archaeological materials of interest, the limits are likely to be higher and comparable to those of SEM and XRF based techniques.

4.2.2 Mass spectrometric techniques

4.2.2.1 Inductively Coupled Plasma Mass Spectrometry (ICP-MS)

Inductively coupled plasma mass spectrometry (ICP-MS) is an established method in trace and ultra-trace analysis and has been cited in numerous publications as the most appropriate method for the analysis of thorium and uranium at the levels of concentration associated with this research (Kazunori and Mitsuru, 1997; Preusser and Kasper, 2001; Bailey et al., 2003; Hou and Roos, 2008). ICP-MS is also a suitable technique for the determination of trace levels of potassium (^{39}K) when used with Dynamic Reaction Cell (DRC) plasma production to eliminate elemental interference due to the presence of Ar^{+} which

is abundant in routine Ar based plasma production. Mass spectrometric methods are based on the production of ionised species, which are differentially detected according to their mass charge ratio. A plasma provides suitable conditions for atomisation and ionisation to occur and is created by passing argon gas though a conduction coil through which RF frequency current is applied; a primary spark provides sufficient energy to initiate plasma production that is sustained by continuous argon flow and electrical current through the coil and exists at temperatures around 3000 K.

Ionic species are introduced to the separation and detection phases of the instrumentation via a number of skimmer cones, operating under increasing levels of vacuum, that act to reduce the total number of species entering the system and to focus the ion beam. The beam is focussed further by the use of an electrostatic lens before introduction to the quadrupole mass filtration stage that is present in modern ICP-MS equipment. The trajectory of ionic species passing centrally through the quadrupole, (which consists of 2 positively charged and 2 negatively charged rods with AC current superimposed onto a base DC voltage), is dependent upon the ionic M/Z ratio; hence it is possible to allow only ions of a particular M/Z ratio to reach the detector at any given time (M= Atomic Mass , Z=Atomic Number).

The sample is primarily introduced in liquid form by spray-chamber aspiration, although other sample introduction techniques exist, including direct sample introduction subsequent to laser ablation (LA).

Laser ablation ICP-MS (LA-ICP-MS) is potentially useful in this research and involves the use of a high power UV laser to achieve direct atomisation of a solid sample; the amount of sample that is atomised, and introduced to the plasma is dependant upon the energy and beam diameter of the sampling laser and the

material and surface characteristics of the sample. High sampling resolution is achievable by altering either the beam or sample position (using an X,Y,Z micro-stage controller for example). Due to the variable nature of archaeological materials, sampling reproducibility is compromised and as such, this technique, although potentially useful, should be regarded as semi-quantitative. In matrices such as bone, where the macro-elemental (e.g. Ca) composition can be regarded as quasi-uniform and it is possible to negate the introduction of errors associated with sample mass variability by comparing elemental or isotopic ratios. In a ceramic matrix such as brick, this is not possible due the variation in mineralogical composition; the mixture of silicates, aluminosilicates and other minerals

does not provide a single element base line against which other species can be measured. LA sampling also introduces the possibility that interfering species may be created as a result of the ablation process.

Although uranium and thorium determinations by ICP-MS are relatively free from elemental or molecular interference, the direct measurement of ^{40}K is problematic due to the high abundance of the Ar^+ ion; as with other techniques, ^{39}K is measured and the concentration of ^{40}K is calculated based on published isotopic abundance values.

Other routes to ionisation exist including thermal ionisation which forms the basis of the well-known TIMS based methods of analysis (Hou and Roos , 2008) and may offer superior analytical performance than ICP based ionisation for small samples. Plasma Ionisation Multi-collector Mass Spectrometry (PIMMS) is also available; here plasma ionisation is coupled with multi-channel mass

detection, which is more stable than quadrupole based mass discrimination when used with ICP ionisation.

The detection limits for U and Th are <0.01 μg/kg and for K is <1 μg/kg (in solution) the use of ICP-MS can provide analytical performance and this is more than adequate for the determinations required for this research.

4.2.3 Staining techniques and visual analysis

The use of established geo-chemical staining techniques can provide useful, qualitative initial information from which decisions about further analytical requirements can be made. Two potential sources of heterogeneity within archaeological matrices are poor mixing (different clay types and temper in ceramics) and the presence of potassium bearing minerals; the ability to detect and assess these features quickly and cost effectively would provide a useful initial screening process.

Digital enhancement of photomicrographs using a proprietary software package (e.g., Photoshop) offers the opportunity to highlight material compositional differences based on small variations in colour and surface properties. By employing a suitable algorithm, whereby effects such as contrast, brightness, hue and colour saturation are optimally adjusted, it is possible to reveal the presence of dissimilar material phases within a sample matrix that would not have been obvious to the naked eye. This is interesting if such phases are found to contain differing radionuclide concentrations or distribution patterns (i.e., correlation between visual and radionuclide heterogeneity).

Surface distribution patterns of potassium rich minerals can be identified by the application of a suitable staining medium; an aqueous solution of sodium cobaltinitrite (sodium hexanitrocobaltate (III)) produces an extremely vivid yellow colouration / precipitation when applied to potassium rich materials and, if used in conjunction with other established staining techniques (Hayes and Klugman, 1959; Berger et al., 1996), may provide qualitative information about the presence and distribution of quartz, potassium bearing clay minerals and K-feldspars. The subsequent use of microscopy coupled with digital analysis can provide further information about the size and morphology of potassium rich inclusions present; although qualitative in nature, this information is still extremely useful when considering the dosimetric aspects appropriate to luminescence dating.

4.2.4 Alpha autoradiography and solid state nuclear track detectors (SSNTD)

The decay mode of six members of the ^{232}Th series and eight members of the ^{238}U series decay is by alpha particle emission. The detection of these alpha particles, particularly if series members are in secular equilibrium, provides an indirect means by which the presence and concentration of the parent species can be determined. Standard spectrometric techniques provide information about the rate and energy of alpha emissions (Pollanen et al. 2005), but do not offer the spatial information. A number of different SSNTDs are available, and have been used extensively to measure alpha emissions in air due to the presence of radon (Chambauadet et al., 1995), and the determination of surface alpha activity in other materials (Haustein et al., 2003), known as autoradiography. Alpha

particles are highly ionising and, although they have a very limited range in most materials, leave behind a latent trail of ionisation damage. Certain polymeric materials such as CR-39 (polyallydiglycol carbonate) can be etched chemically (alkaline hydrolysis); higher etch rates are observed along the trajectory of an incident alpha particle due to radiation damage, and this results in the development of a visible "track" within the material. The number of tracks observed is proportional to the number of alpha particles striking the material at an appropriate angle and having sufficient energy to produce a latent track. In certain cases, alpha autoradiography can be used to provide semi-quantitative data about uranium or thorium concentration (assuming equal activity and secular equilibrium in a homogeneous medium), but in this context is used to provide information about the spatial distribution of non-specific alpha emitters. Etching times of around six hours produce tracks that are easily visible under slight (10X) magnification (determined by laboratory based experimentation) and the transparent nature of CR-39 facilitates the use of digital imaging techniques in the comparison of track density and distribution with sample surface morphology and other visual characteristics.

LR115 (Kodak) is another commercially available SSNTD which may also be useful in auto radiographic experiments (Sanzelle et al., 1986); a thin, coloured nitrocellulose layer forms the etchable substrate which after prolonged contact with the sample can be processed to reveal small perforations in the coloured substrate that result from increased localised etch rate due to alpha particle induced ionisation damage. LR115 is less robust than CR39 and requires greater magnification for track analysis. Contact times for both detectors range from 3-6 months, depending upon activity; this is a disadvantage, but they are cost effective, non-destructive and effectively non-labour intensive.

4.3 Analytical rationale

Based on information relating to analytical performance, the accessibility of facilities and the likely costs incurred, the suggested combination of analytical techniques to appropriately characterise the archaeological samples studied within this research are as follows –

Stage	Technique	Purpose
1.	Initial visual, digital and microscopic analysis.	Assessment of visual heterogeneity.
2.	Mineralogical staining.	Assessment of the distribution and mineralogy of K bearing minerals and to identify the presence of quartz inclusions
3.	SEM analysis (optional)	The use of SEM may provide detailed information on other elemental distributions (e.g. zircon) if required.
4.	Alpha autoradiography	Assessment of U and Th distribution.
5.	Micro sampling and quantitative ICP-MS / AAS	To quantify U, Th and K concentrations within identified areas of interest.

Chapter 5 Alpha autoradiography using CR-39

5.1 Introduction

The use of CR-39 in autoradiography was introduced in Chapter 4. This chapter provides a more detailed description of how this SSNTD is used, and the factors relevant to the scope of this work.

5.2 Factors effecting detection

The primary considerations in the use of CR-39 in the detection of incident alpha particles are the factors affecting the number of alpha particles reaching the detector from a particular sample geometry, together with those concerning the subsequent development of detectable tracks.

Aitken (1985) derived the following formula to describe the number of alpha particles, α· striking a scintillation screen from an alpha thick matrix directly situated above the detector screen.

$$\alpha\cdot = ¼\ A R\ \varrho\ n\ c \qquad \text{Eqn. 5.1}$$

A is the surface area of the scintillation screen

R is the average range of alpha particles in a particular decay series in the sample material

ϱ is the density of the sample material

n is the number of alpha emitters (assuming secular equilibrium)

c is the specific parent activity ($BqKg^{-1}$)

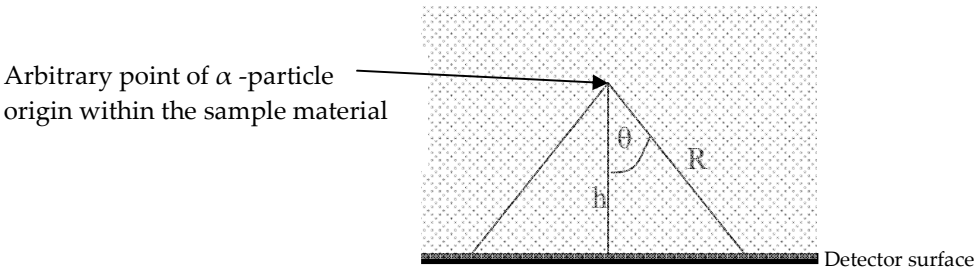

Figure 5.1 Diagram showing geometric factors used in the derivation of Eqn. 5.1, where h=R when θ=0, i.e. when an alpha particle strikes the detector perpendicularly the thickness of the contributing material (h) is equal to the range of the alpha particle. The shaded area represents sample volume.

Alpha particles originating from a depth between h=0 and h<R have the potential to reach the screen (within the confines of the solid angle Ω, where $\Omega = 2\pi(1 - \cos\theta)$ and $\cos\theta = h/R$). In reality this amounts to ¼ of the total emissions, as defined by equation 5.2, where q = the proportion of disintegrations from the material of depth h<R

$$q = \int_o^R [\frac{\Omega(h)}{4\pi(R)}]dh = 1/4 \qquad \text{Eqn. 5.2}$$

Equation 5.1 can also be used to determine the number of alpha particles striking the surface of a SSNTD detector with an equivalent geometry. However to predict the number of alpha particles that will produce a track suitable for development by etching requires the consideration of two more factors; a) the energy of the incident alpha particle, and b) the angle of incidence, specifically,

the critical angle, θ^E, which is defined as the maximum angle of trajectory (for an alpha particle of energy E) that will results in the production of a latent track.

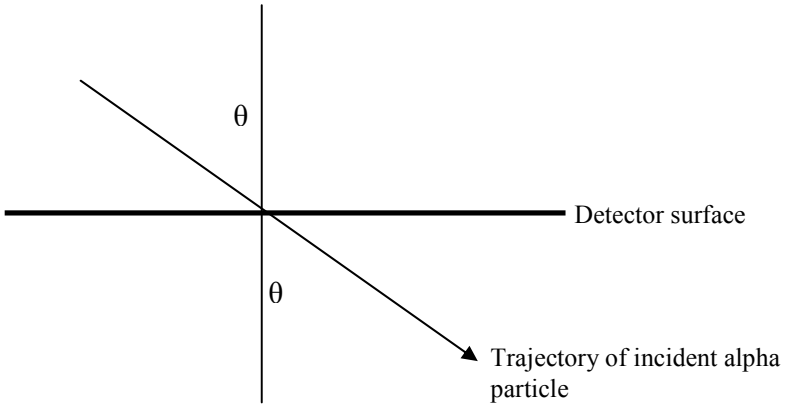

Figure 5.2 Angle of particle trajectory, θ

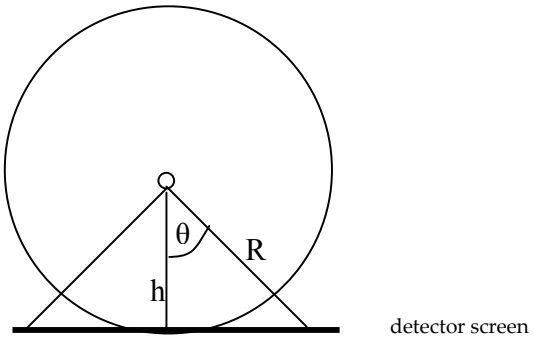

Fig 5.3 Cross-sectional representation of figure 5.1 in which the circle represents the number of directions in which the alpha particle may travel, and the cross-section of the solid cone (Cos θ =h/R) that represents the contribution of total alpha emissions that can reach the screen.

In cross section it can be seen that the angle (2 θ) must be equal to $360^o/4 = 80^o$ hence, angle θ must fall within the values of 0^o and 40^o between the values of h=0 and h<R

5.3 Development of tracks

Tracks can be developed in SSNTD materials because of the differential etch rates in radiation damaged and non-damaged areas of the material, where V_t and V_b refer to the track and bulk matrix etch rates respectively; V_t is proportional to the extent of localized radiation damage along the particle trajectory due to the energy transferred from incident particle.

If the energy of the particle is very low, the difference between V_t and V_b is likely to be insufficient to produce an identifiable track. The range of an incident alpha particle in the detector material is also proportional to the energy of the particle. Low energy alphas (<1 MeV) may not penetrate beyond the range of material that is etched away during track development; routinely this equates to approximately 20 μm for a standard etching protocol using 6N NaOH at 70^oC for 6 hours (Nikezic and Yu, 2003 ; Hermsdorf et al., 2007).

Thus, the development of latent tracks in SSNTD materials is a function of both the energy of the incident particle, and the critical angle of incidence and much research has been undertaken in this area (Barillon et al., 1995; El- Hawary et al., 1999; Nikezic and Yu, 2003).

The equation used in this work to calculate the theoretical number of alpha particles reaching the screen is based on the particles reaching the screen from within the confines of the solid cone (Cos θ =h/R), where it can be shown that θ falls within the values of 0^o and 40^o.

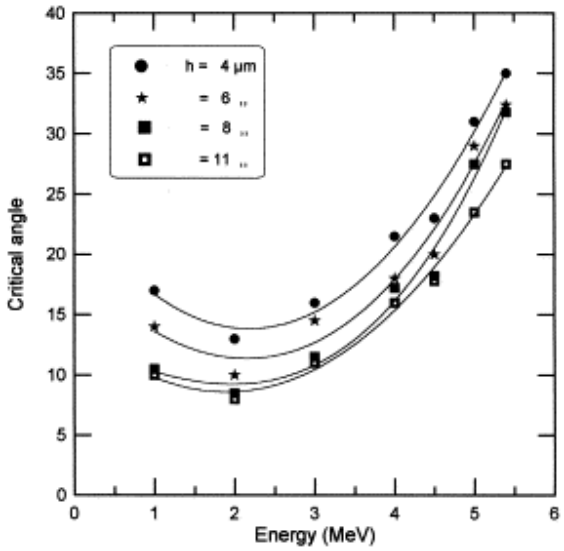

Figure 5.4 The variation of critical angle θ with alpha energy E, at different removal thickness layers (h) (from El-Hawary et al., 1999).

At critical angles falling between the values of 0^{o} and 40^{o}, alpha particles within the energy range 1 to 5.5 MeV (this range is potentially comparable to the likely energies of the alpha particles emitted by the U and Th decay series, having undergone varying degrees of energy loss due to matrix attenuation before reaching the detector) display the potential to produce latent tracks. Hence, when calculations are used to quantify detector efficiency later in this chapter, the efficiency factor is likely to be influenced predominantly by the energy of the incident particle.

The alpha particle energy values associated with the members of the U and Th decay series are well documented (see Tables 5.1, 5.2 and 5.3 below, values from Aitken, 1985) and it could be initially considered to be relatively straightforward, by using published values, to determine the critical angles of incidence

associated with each species. This is not the case however, as the energy values quoted do not include the energy loss caused by the attenuating properties of the matrix material from which the particle originates; alpha particles emitted from the surface of the material should have similar energy values to those quoted in the literature, however those originating from deeper in the material (up to a depth which is equal to the maximum alpha particle range within that material) would have substantially lower energy values, and have differing latent track development characteristics. Again, it is possible to calculate the loss of energy associated with energy deposition during the passage of an alpha particle of known initial energy, through the matrix material prior to detector contact if the depth of origin, material density and Z values are known.

In reality, the use of Monte Carlo based modeling techniques, or similar computational methods would be required to produce any quantitative probability data to effectively describe the complex situation associated with predicting track development in relation to even the most homogenous, well characterized distribution of alpha emitters within any type of material.

A suitable compromise for the prediction of the number of expected alpha tracks in CR-39, in relation to parent activity in a particular matrix type, may be achieved experimentally. A standard material of known U and Th activity, and in which there exists no apparent disruption to secular equilibrium (assessed by gamma spectrometry and discussed later), may be used to determine the typical detector response compared to the calculated expected number of tracks which would be produced if all alpha emissions resulted in the development of a countable track; the use of Eqn. 5.1 is appropriate in the determination of this value.

Gamma spectrometry is used routinely in the laboratory to determine standard material activity – existing laboratory data from these experiments may be used to produce a CR-39 detection coefficient that can also be used to quantify total activity, based on the number of countable alpha tracks produced. There is no assumption at this stage that it will be possible to produce a quantitative method for the determination of localized activity in the archaeological materials of interest as a number of assumptions, including equal thorium and uranium activities would need to be made. A second issue is the heterogeneity of the material in question; the activity estimates that could be provided by using a homogeneous standard of known activity would be applicable only to the determination of activity in homogeneous samples. There is currently no experimental procedure (using SSNTD materials) to differentiate between, for example, increased localized alpha activity that results from a 20 μm depth anomaly (a zircon grain for example) and a 2 μm depth area of slightly higher than average radionuclide concentration. The angle of incidence from which the alpha tracks originate may give information about the originating depth of the emission, but the exploration of this effect is not practical with CR-39 and the microscopy equipment available locally for use in this project.

A comparative, semi-quantitative assessment of surface derived alpha activity is feasible, and depending upon the sampling strategy used to generate test material, will provide very useful supplementary data to the general characterization of alpha emitter distributions.

TABLE 5.1 Thorium series alpha energies and range in pottery (Z=10.6, A=21.4)

Nuclide	Energy (MeV)	Intensity (% total emission)	Range (R_Q) ($\mu g/mm^2$)
^{232}Th	5.01	77	37.5
	3.95	23	
^{228}Th	5.42	72.7	58.5
	5.34	26.3	
^{224}Ra	5.69	95	62.5
	5.45	5	
^{220}Rn	6.29	100	72.5
^{216}Po	6.78	100	82.0
^{212}Bi	6.05	25.2	68.5
	6.09	9.8	
^{212}Po	8.78	64	124

		Average	69.5

TABLE 5.2 ^{238}Uranium series alpha energies and range in pottery (Z=10.6, A=21.4)

Nuclide	Energy (MeV)	Intensity (% total emission)	Range (R_Q) ($\mu g/mm^2$)
^{238}U	5.20	77	39.5
	5.15	23	
^{234}U	5.77	72	48.5
	5.72	28	
^{230}Th	5.69	76.3	48.0
	5.62	23.4	
^{226}Ra	5.78	95.5	48.5
	5.60	5.5	
^{222}Rn	5.49	100	59.5
^{218}Po	6.00	100	66.0
^{214}Po	7.69	100	100
^{210}Po	5.30	100	56.0

		Average	58.2

TABLE 5.3 ^{235}U series alpha energies and range in pottery (Z=10.6, A=21.4)

Nuclide	Energy (MeV)		Range (R_Q) ($\mu g/mm^2$)
^{235}U	5.40		42.5
^{231}Pa	5.01		51.1
^{227}Th	6.33		67.5
^{223}Ra	5.72		72.5
^{219}Ra	6.82		82.0
^{215}Po	7.39		95.0
^{211}Bi	6.62		80.0

		Average	68.6

5.4 Initial experimental considerations

5.4.1 Alpha activity

The initial stages of experimentation with CR-39 involved the exploration of the analytical parameters associated with the use of this detector to provide useful data for the materials in question; these parameters include sample contact time, etching efficiency for the development of tracks, the potential spatial resolution achievable and the level of magnification required to view and subsequently quantify the developed tracks.

The mean typical concentration values quoted by Aitken (1985) for thorium and uranium in archaeological ceramics are 10 ppm and 3 ppm respectively. A sample containing 1 ppm ^{232}Th in secular equilibrium displays a specific activity of 4.06 Bq kg^{-1}, whist 1 ppm of uranium (assuming natural abundance values of ^{235}Uand ^{238}U) has an activity of 12.9 Bq kg^{-1} (Adameic and Aitken, 1998).

In the case of secular equilibrium, where the activities of parent and decay chain daughter radionuclides display equal activity, the rate of radioactive decay of each member is defined by the value λN, where λ is the decay probability, related to the radioactive half life ($t^{1/2}$) of the radionuclide ($\lambda=0.693/t^{1/2}$). N refers to the number of atoms present that have not undergone decay.
In a state of secular equilibrium, the activity of each member of the decay series can be described by the following equation

$\lambda_1 N_1=\lambda_2 N_2= \lambda_3 N_3=\ldots\ldots \lambda_n N_n$

If the specific activity of ^{232}Th is 4.06 Bq kg^{-1} per 1 ppm content, the specific alpha activity, in a state of secular equilibrium must be equal to 6 x 4.06 = 24.36 Bq kg^{-1}

The multiplication factor is used to account for the total number of individual alpha emitting progeny in the decay series. A value of 6 is used for ^{232}Th instead of 7 as ^{212}Bi and ^{212} Po are regarded (in quantitative calculation) as a single emitter.

The parent activity of ^{238} U is 12.4 Bq kg^{-1} per 1 ppm and equates to -
(8x12.4) = 99.2 Bq kg^{-1} per 1ppm assuming secular equilibrium.
The parent activity of ^{235} U is 80.0 Bq kg^{-1} per 1 ppm and equates to –
(7x80) = 560 Bq kg^{-1} per 1ppm assuming secular equilibrium.
For naturally occurring uranium (99.29% ^{238}U and 0.71% ^{235}U, Adameic and Aitken, 1998) the specific alpha activity is ((560x0.0071)+(99.2x0.9929)) = 102.4 Bq kg^{-1} per 1 ppm

Using the quoted typical concentration values of Th (10 ppm) and U (3 ppm), it is possible to calculate a typical alpha activity value of $(10 \times 24.36)_{Th} + (3 \times 102.4)_{U}$ = 551 Bq kg^{-1} in archaeological ceramics.

Standard reference material (NBL107) contains 0.1% w/w Th, with members of the decay series in a state of secular equilibrium (verified by routine laboratory gamma spectrometry measurements).

The specific alpha activity can be calculated as follows

0.1 x 10000 x 24.36 = 24360 Bq kg^{-1} = 24.4 kBq kg^{-1}

Hence, the specific alpha activity of the NBL107 reference material can be assumed to be approximately 44 times greater than that seen typically (combined U and Th) in archaeological ceramics. The bulk standard composition (and hence Z value used in range calculations) is likely to vary from that of a typical archaeological ceramic, as it is primarily composed of silicon dioxide; the alpha particle ranges will vary slightly from those quoted for ceramics but not sufficiently to preclude the use of this material.

5.4.2 Detection parameters

It is reasonable to assume that short term initial tests using higher activity materials with similar compositions to the samples tested in this work will produce similar data to those derived from long term detector exposures using materials of typical natural activity.

The mean range of alpha particles from the U and Th decay series of 25 μm in typical archaeological ceramics mentioned earlier does not account for matrix heterogeneity, the presence of voids or other disruptions to matrix uniformity.

The range of higher energy alpha particles extends beyond this value and hence a proportion of particles reaching the detector will originate from beyond the average range; conversely, a proportion of lower energy alpha particles originating from within this range will not reach the detector; however, an average alpha range value is acceptable for the purpose of this investigation for a number of reasons. The techniques developed using autoradiography are semi-

quantitative with no initial requirement to distinguish between the alpha particles emitted from individual progeny of the U and Th decay series, as would be potentially possible using thin source alpha spectrometry. Additionally, it is not possible to calculate the exact alpha ranges associated with the heterogeneous materials studied here.

Deviation in Z values between naturally occurring component minerals is likely to be small except for those such as zircon which may be present as small localized inclusions (SiO_2, Z = 10: $SiAlO_4$, Z= 9.83: $ZrSiO_4$, Z =15.33)

Using typical values for alpha range (25 μm) and a detector area of 1 cm^2, the maximum volume of material from which alpha particles can reach the detector is approximately 0.0025 cm^3 which equates to a contributing material mass of 6.5 mg (derived using a value of 2.6 g cm^{-3} for the SiO_2 matrix, assuming maximal packing density and using the average alpha range value to estimate the contributing material thickness above the detector).

For the 0.1% Th standard material, with a calculated activity of 24.4 kBq kg^{-1} the number of alpha emissions resulting from 6.5 mg of material would be approximately 548 h^{-1} and the maximum number reaching the detector would be 137 h^{-1} (0.25 x 548)

For a 100% detector efficiency (i.e. every incident alpha particle will result in a countable track) the NBL107 – detector contact time required to produce a minimum of 10000 countable tracks on a 1 cm^2 area (or 100 tracks mm^{-2}, discussed later) would be ~70 hours.

For the uranium analogous standard material (0.1% U) NBL102 the theoretical maximum number of tracks that will reach the detector screen, per unit time, can be calculated by applying a simple alpha activity conversion factor to the previously calculated Th value.

The concentration specific U:Th activity ratio (102.4 / 24.36) = 4.20 (assuming secular equilibrium).

Hence, the calculated theoretical number of alpha particles reaching the detector (1cm2) per hour from a close packed 0.1 % Uranium (in SiO_2) standard would be (137 x 4.2) = 578 h^{-1} and required detector contact time for NBL102 to to produce a minimum of 10000 countable tracks on a 1cm^2 (or 100 tracks mm^{-2}, discussed later) would be ~17 hours.

5.5 Experimental procedures

CR-39 is supplied commercially by Tastrack Ltd. and as previously mentioned can be cut to the requirements of the end user. The detectors used in this series of experiments measure 1 cm x 1 cm x 1mm, and have been scribed on one side with a grid which separates the surface of the detector into 25 equal sections of approximately 0.4 cm^2 (not including scribing sections as the unscribed surface is placed in contact with the sample; the focal depth of the microscope is adjusted to view both the tracks on the unscribed surface, and the grid position on the underside).

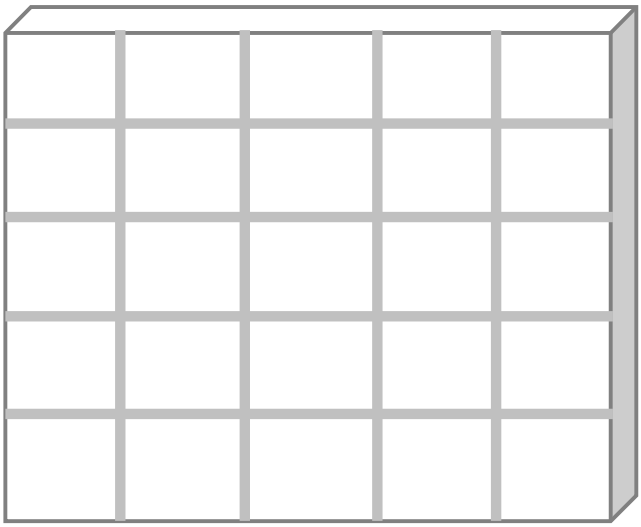

Fig 5.5 Representation of CR-39 SSNTD showing scribed surface.

5.5.1 Etching procedures

Numerous investigations of etching efficiency and track development have been made (for example, Nikezic and Yu, 2003 ; Hermsdorf et al., 2007). A routine etching procedure previously developed at Durham for work with ^{241}Am source calibrations using 6.25N NaOH solution at 70^{o}C, with varying etching times was adapted for use with archaeological materials. The development of partial tracks which can be counted effectively (for the determination of ^{241}Am alpha particles delivered to the detector from a plaque source, under vacuum), takes 2 hours using the aforementioned procedure; this is adequate for work of this type, where the alpha flux is high and the alpha particle energy range is very narrow (^{241}Am alpha energy with minimal attenuation). The optimum etching time needed to accommodate the wide range of alpha energies associated with the

different members of the U and Th decay series, and the variable rate (dependant on depth) of matrix associated energy loss, is expected to be significantly longer and to be close to 6 hours.

5.5.2 Chemistry of etching

Etching occurs primarily by the mechanism of alkaline hydrolysis and if the concentration of the etchant is sufficiently high to remain effectively constant, kinetics for bulk etching rate V_b are likely to be (pseudo) first order; this has been confirmed experimentally by the quantification of polymer material removed during etching as a function of etching time (Hermsdorf et al., 2007). Etching rate is highly temperature dependant and hence it is essential to maintain constant temperature during etching. The kinetics of the track etching rate V_t , are more complex due the extent and nature of radiation damage (energy deposition) along the trajectory of the incident alpha particle; the production of varyingly ionized species along this trajectory results in a potentially complex chemical environment.

5.5.3 Alpha autoradiography and digital photomicrography

5.5.3.1 Macro alpha autoradiography

During the initial developmental stages of using CR-39 to detect the presence of latent alpha particle tracks under ^{241}Am source irradiation, it was noted that localized regions where etched tracks are present have differing optical properties to the bulk material; the presence of etched tracks produces localized areas of semi-opacity which in extreme cases (high track density) can be seen by

the naked eye. If the detectors are placed on a flat non-reflective surface, with the track detection surface in direct contact with the substrate material, the application of light from a lateral direction results in the discrete illumination of the etched areas whilst areas of lower track density remain transparent. Using low power magnification (5X) coupled with post image-capture digital enhancement, a procedure has been subsequently developed to create macro-photomicrographs that represent the macroscopic (1 cm^2) distribution patterns of sample matrix constituent alpha emitters (Fig. 5.6).

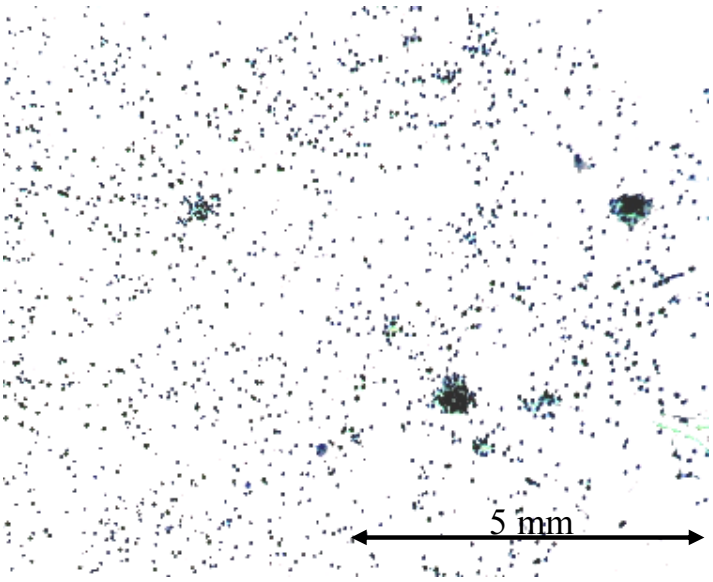

Fig 5.6 Digitally enhanced (image inverted) CR-39 alpha autoradiograph – dark areas indicate the presence of latent alpha tracks.

The use of this procedure is particularly effective in the investigation of any positive correlation between visual sample characteristics (mineral inclusions etc.) and the localized distribution of alpha emitters.

5.5.3.2 Digital photomicrography and track identification

The CR-39 detectors were placed contact side upwards on a standard microscope slide. Literature values for the typical etched track diameters (Nikezic and Yu, 2003) suggest that 100x magnification should be sufficient to view the developed tracks and this was confirmed experimentally using a standard laboratory microscope (Leitz – Leica) (Fig 5.7).

In order to calibrate the field of vision and subsequent image areas captured by coupling a digital camera (Nikon Coolpix) to the microscope eyepiece, a standard calibration slide (1mm scale with a resolution of 10 μm) was viewed and photographed at the same level of magnification used for track analysis.(Fig 5.8).

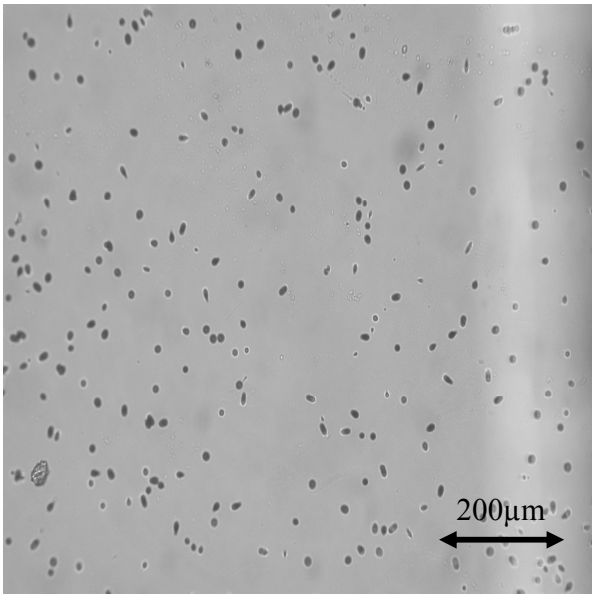

Fig 5.7 Photomicrograph of CR-39 detector (x100) exposed to reference sand NBL102 0.1 % U (5 days)

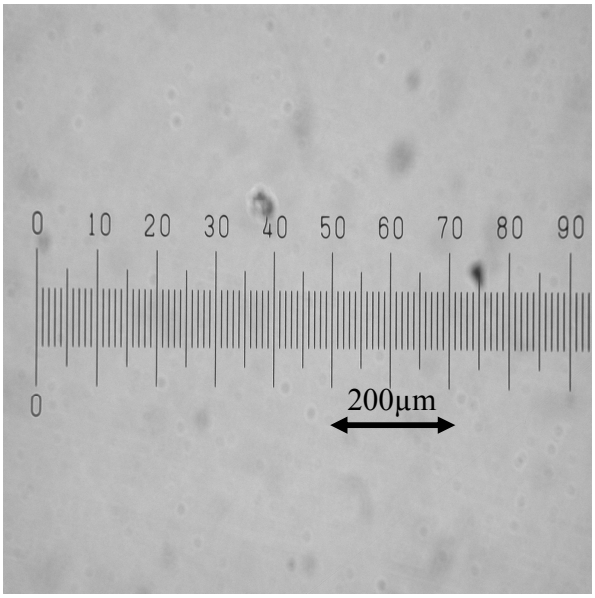

Fig 5.8 Photomicrograph of 1 mm calibration slide (x 100).

5.5.3.3 Track counting and standard error

Assuming accurate size reproducibility between subsequent photomicrographs, the countable area for the example shown can be calibrated effectively by measuring the ratio of the overall image dimensions to the known dimensions of the calibration slide. Using 100x magnification, the tracks produced by exposure to alpha particles from the members of the U an Th decay series are easily distinguished (from background) and for the exposure times estimated in Section 5.4.2, are present in suitable numbers to enable routine counting. Using this level of magnification, the countable area will be in the order of 0.8 – 1 mm^2 and must be calibrated for each series of determinations / photomicrographs taken to take into account slight changes in focal depth between individual determinations.

Using 400x magnification, 5-25 µm tracks can be resolved (Fig 5.9).

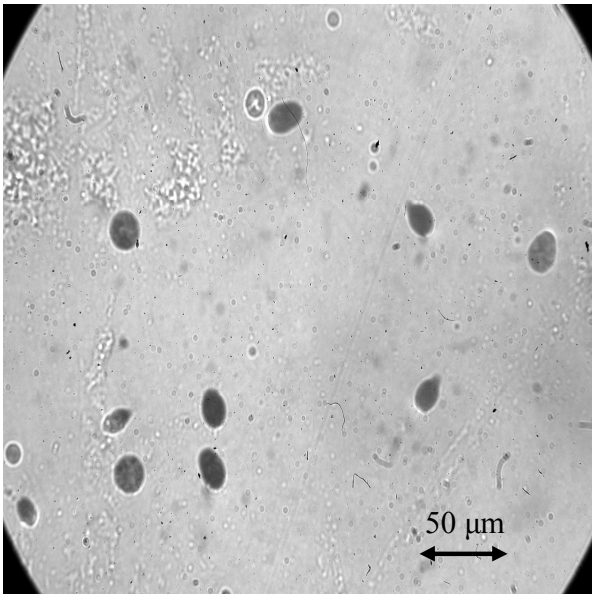

Fig 5.9 Photomicrograph of CR-39 detector (as in fig 5.6 viewed at (x400).

The estimation of the standard errors (s.e.) associated with counting techniques in general can be derived from the standard equation associated with Poisson distributions - s.e. = $N^{0.5}$, where N is the total number of counts. The following examples demonstrate the statistical advantage of counting the highest practicable number of tracks per unit area.

N= 10 s.e. = 31% (of total counts)

N= 100 s.e. = 10%

N= 1000 s.e. = 3%

N= 10000 s.e. = 1%

The CR39 detectors used in this project have a total area of 100 mm^2, with a scribed grid enabling simple visual resolution across the surface of the detector of 25 equal sections of ~4 mm^2.

To achieve a precision of +/- 3% (1000 counts) for a homogeneous track distribution, 10 sub-samples (discrete countable areas) is sufficient, providing the track density exceeds 100 tracks per mm^2.

5.6 Quantitative and semi-quantitative analysis

5.6.1 Initial Tests

Approximately 2 g of finely ground NBL107 (0.1%Th) reference material was placed in a circular, sealable Perspex container (used routinely for laboratory thick source alpha counting) and compacted manually to produce a dense layer (>5 mm thickness) . Four individual CR-39 detectors were placed (scribed side upwards) in contact with the compacted material and covered with a circular layer of neoprene foam. The Perspex cover was then placed above the neoprene and tightened to optimize the contact pressure between detector and sample, and simultaneously maximize the localized packing density of the standard material (Fig 5.10).

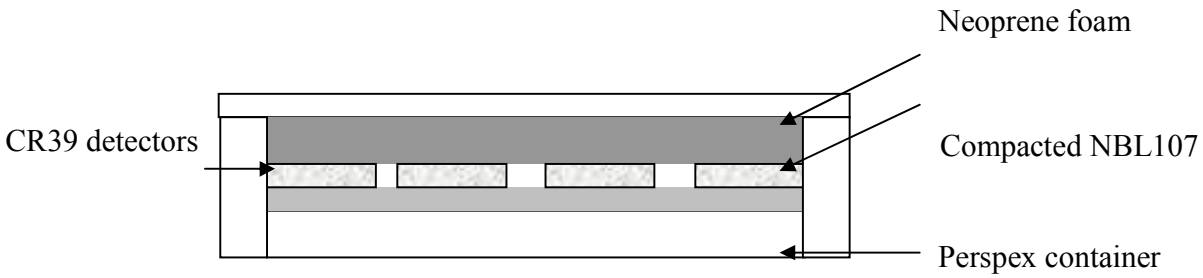

Figure 5.10 Cross sectional representation of apparatus used for CR-39 initial testing

After a measured exposure time, the detectors were removed from the Perspex container and rinsed thoroughly with de-ionized water to remove any traces of NBL107. The detectors were then etched at 70°C in a 6.25N solution of NaOH for 6 hours before being rinsed thoroughly with de-ionized water and allowed to dry at room temperature.

The procedures described above were performed with NBL107 and subsequently with NBL102 (0.1% U).

Photomicrographs (mag. x100) were taken from 10 different locations across the surface of the four CR-39 detectors exposed to the NBL107 and NBL102 as described above. The locations were chosen to represent central, peripheral and intermediate positions across the surface of each detector (see Fig 5.11); a total of 4 detectors were used initially to allow for subsequent adjustments to etching conditions and contact times if necessary.

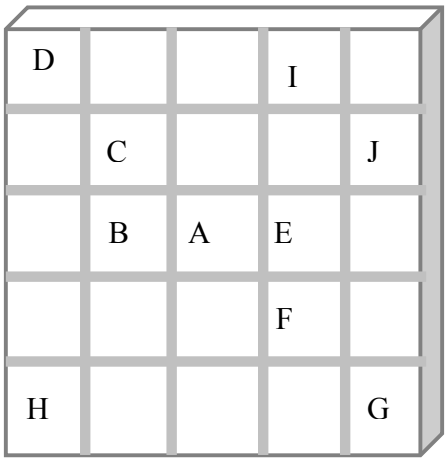

Fig 5.11 Diagram showing locations at which photomicrographs were obtained.

The total number of developed tracks was counted using a simple "marking off" technique with a printed copy of each photomicrograph. The area of each micrograph was calibrated, and a standardizing factor applied to produce values of track density (mm^{-2}).

Results

Detector number / position	NBL107 Tracks mm^{-2}	NBL102 Tracks mm^{-2}
D1-A	135	347
D2-B	133	315
D3-C	165	407
D4-D	121	351
D1-E	121	365
D2-F	148	323
D3-G	141	398
D4-H	137	374
D1-I	180	358
D2-J	139	322

Table 5.4 Measured track densities for standard 0.1% U and Th materials.

Calculations and discussion

NBL107

Sample-detector residence time	= 115 hours
Total counts	= 1299
Standard error	= 2.77%
Mean track density	= 129.9 tracks mm^{-2}
Adjusted track density	= 12990 (+/- 360) tracks cm^{-2}
Theoretical maximum track density*	= 15755 tracks cm^{-2}
Detector efficiency (Thorium)	= 82%

NBL102

Sample-detector residence time	= 116 hours
Total counts	= 3560
Standard error	= 1.68%
Mean track density	= 356 tracks mm^{-2}
Adjusted track density	= 35600 (+/- 597) tracks cm^{-2}
Theoretical maximum track density*	= 67048 tracks cm^{-2}
Detector efficiency (Uranium)	= 53%

*Theoretical maximum track density is calculated on the basis that all alpha particles reaching the detector will produce a developable track. In reality, a proportion of alpha particles will have insufficient residual energy (or strike the detector at an inappropriate angle) to result in the production of a developable track.

As track development is partially dependent upon incident alpha particle energy, it is unsurprising that the CR-39 detection efficiency for members of the Th decay series is higher than for the U series (members of the Th decay series have a higher mean energy and subsequent range value than members of the U decay series). In archaeological materials where secular equilibrium is assumed, and where the concentrations of uranium and thorium do not vary significantly from natural abundance values, it is reasonable to assume equal activity of U and Th; hence, a combined, initial detector efficiency factor may be suitable for routine determinations.

It should be noted at this point, that initial calculations based on the use of NBL107 reference material did not take into consideration the presence of uranium, which is naturally present in the NBL107 material and leads to a slight overestimation of the CR-39 detector efficiency with respect to alpha emission from the Th decay series. Assuming a contribution of ~5% (based on values derived from routine gamma spectrometry) the combined efficiency factor is 65%

This value indicates a mean underestimation of around 35% of the true alpha activity when using CR-39 detectors and is due primarily to alpha particle energy and detection geometry parameters; this factor is approximate and due to experimental time constraints, is based on a limited data set but is still valid in the determination of the sample-detector contact time needed to produce an appropriate track density.

The variable matrix compositions of typical archaeological samples preclude the production of a specific detector efficiency factor that would provide truly quantitative data such as those calculated by Azkour et al. (1998) that were

derived using homogeneous phosphate minerals. To test the experimentally derived detector efficiency values, the procedures described above will be repeated using standard clay sediment material (NCS DC 73373 Stream sediment, supplied by LGC Ltd.) which contains certified concentrations of uranium and thorium that are close to natural abundance values, within a silaceous / aluminosilaceous matrix, and where secular equilibrium exists between decay series progeny.

5.6.2 Further considerations

Reference has been made in this chapter to the use of alpha-autoradiography as a semi-quantitative technique and it is important to qualify further why this description has been used within the context of this work. Primarily, with regard to the detection of alpha particles in a homogeneous matrix, this technique is both quantitative and effectively matrix independent, and has been used to assess alpha activity in low radioactivity samples with around 5% uncertainty (Sanzelle et al., 1986). These determinations were performed using standard laboratory reference materials of known uranium and thorium content, but the potential of this technique for quantitative analysis is clearly demonstrated. In this respect, the initial determination of detector efficiencies for uranium and thorium species can be regarded as quantitative. The number of alpha particles striking the screen that will produce a detectable track α', can be further described by the modification of equation 5.1 –

$$\alpha' = ¼ \, AR \, \varrho \, n \, c \, f \qquad \text{Equation 5.3}$$

Here f is a variable factor (depending upon the radionuclide species present) that is a function of both alpha particle residual energy and the angle of incidence. This factor can be assumed to be made up of two components; a geometric component that is effectively independent of emitting species, and an energy component which is species dependent. The mean alpha particle energy of the alpha emitting members of the thorium decay series is higher than that of the uranium analogues. Higher detection "efficiency" is hence expected for the former species and this was confirmed experimentally (Th detection efficiency = 82%, U detection efficiency = 53%)

Effectively, for the levels of accuracy required for this project, the experimentally derived value of the detector efficiency factor can be used to replace the factor, f, which cannot be calculated without the use of complex computer-based modelling techniques. In heterogeneous matrices, the use of CR-39 is still quantitative with regard to alpha particle detection and the determination of alpha activity at specific locations across the sample surface. Within the scope of this study, and for the materials in question, the usefulness of this characteristic has been well established.

In this work, the alpha-autoradiographic determinations recorded only alpha particle events, without resolution of alpha particle energies and so cannot be used quantitatively to characterize uranium and thorium distributions i.e., it is not possible, in this context, to differentiate between alpha particles emitted from the different members of the associated decay series. Here, the term semi-quantitative has been used in the context of the alpha-autoradiographic determinations used throughout this work.

At this point it is also useful to mention that the work carried out during the production of this thesis does not involve any attempt to quantify the material matrix dose-rate, nor the dose-rate applicable to any single phosphor grain (quartz) of interest. The quantification of the former is possible for homogeneous matrices, in which secular equilibrium exists with respect to the radioactive decay series members for both thorium and uranium and in which overall activity of the two series is equal. If this were to be the case, it is possible to use quantitative alpha-autoradiography data to calculate the concentrations of each parent species. Once specific concentration values have been established, data are widely available to convert these to effective material matrix dose rate equivalents (Adamiec and Aitken, 1998). The dose rate attenuation factors appropriate to quartz grains of a particular size are also well known (Mejdahl, 1979; Brennan, 2003).

The determination of the dose rate applicable to a specific single phosphor grain situated within a heterogeneous matrix is theoretically possible, but in practice very difficult to achieve. An attempt to model this using could be made using experimental data derived from the analyses discussed in this work, but a number of assumptions would still need to be made. For example, that the distribution patterns and concentrations of the radionuclides present in the test sample were representative of those throughout the material surrounding an individual grain and from which the dose originates.

5.7 Differentiation between homogeneous and heterogeneous track distributions

5.7.1 Visual interpretation

As discussed in previous chapters, the main scope of this project is to investigate the mm and sub-mm distribution characteristics of U, Th and K in archaeological

materials. With regard to the use of CR-39 detectors, it is important to consider, initially, what the expected distribution patterns would be from a uniform distribution of alpha emitters. The emission rate of alpha particles can be described accurately by the radioactive decay constant for a particular series member, although essentially, radioactive decay is a random process. With respect to the use of CR-39, an additional random factor is introduced by the fact that for every alpha emission within the contributing mass volume, there is only a 25% chance that the alpha particle expelled from the parent will result in collision with the detector (described previously in the chapter with regard to the solid angle Ω) .

5.7.1.1 Simulations of homogeneous and heterogeneous alpha track distributions.

The typical distribution patterns in the CR-39 that could be expected to result from a homogenous distribution of alpha emitters, was simulated by the use of a relatively simple spreadsheet model (Microsoft Excel); using an XY scatter plot where the graph area is representative of the detector surface it is possible to generate points on the graph, the coordinates of which are determined by the use of a random number generation function. The number of points generated is representative of the number of emissions that have been detected which is likely to be around 25% of the hypothetical total number of alpha emissions for a given concentration of emitting species. This system is somewhat crude, and relies upon the assumption that the process by which random numbers are generated in Excel is appropriate to simulate the natural alpha emission patterns that will develop across the detector surface.

This technique has been proven to be quite effective in the demonstration of the potential for track clustering (Fig 5.12) and apparent visual heterogeneity (Fig

5.13) that may result from a (simulated) homogeneous distribution of tracks and using differing concentrations and sample-detector contact times. The use of these techniques is further validated by the similarity in distributions patterns between simulated and experimentally derived (Fig 5.7) distributions from homogeneous materials.

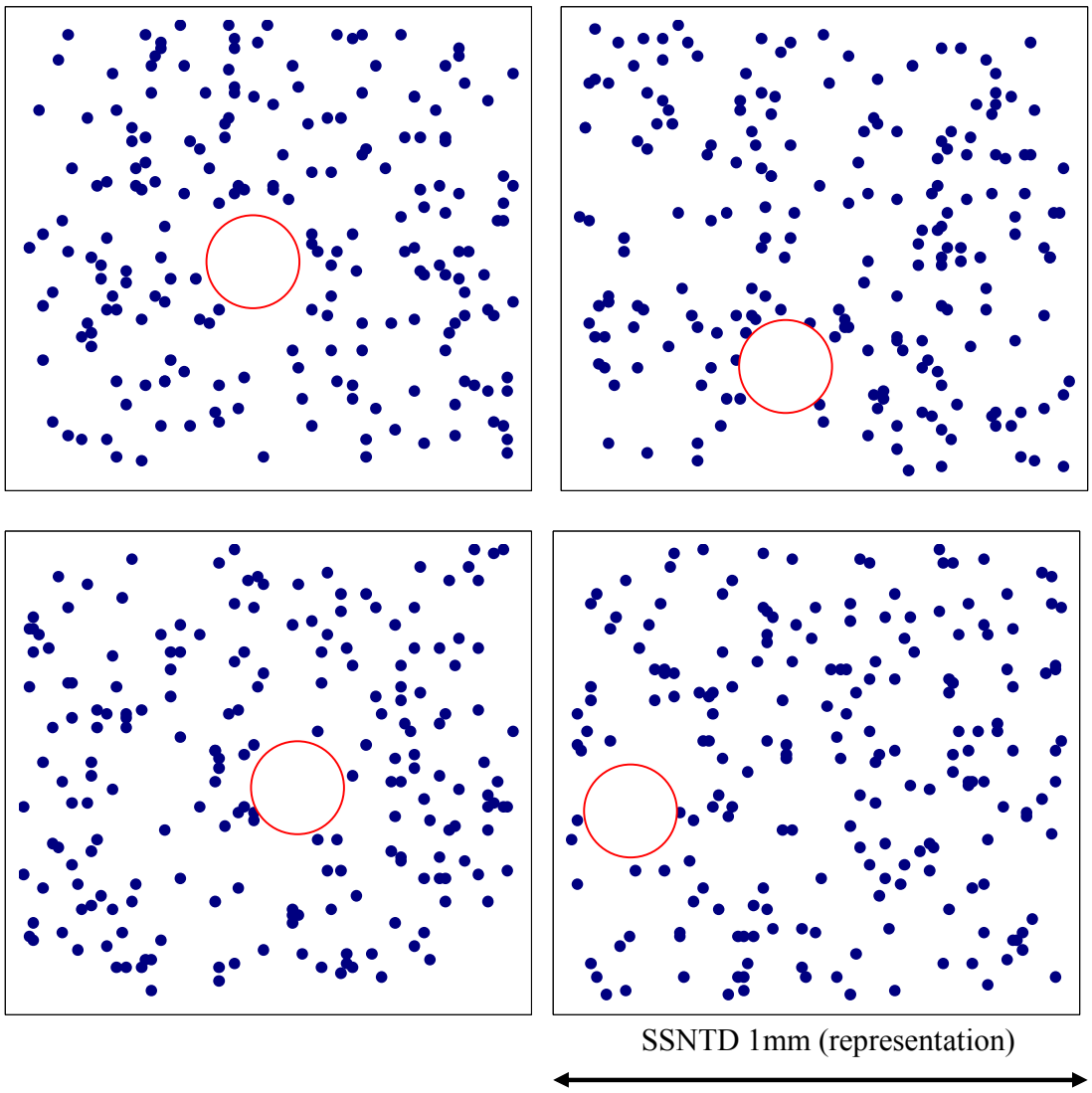

Fig 5.12 Simulated autoradiographs derived from a theoretically uniform distribution of alpha emitters. The total number of "tracks" = 200. Some clustering is apparent as is the appearance of areas of apparent lower activity (circled in red).

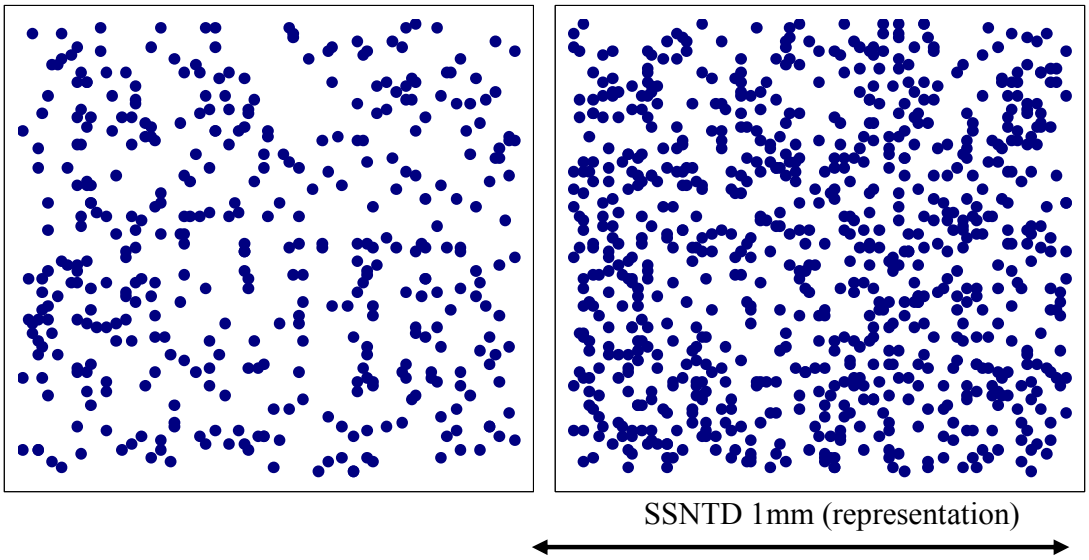

Fig 5.13 Simulated autoradiographs derived from a theoretically uniform distribution of alpha emitters. The total number of "tracks" are 400 (LHS) and 800 (RHS).

The visual interpretation of apparent areas of low / zero activity, particularly in the lower activity simulations is a characteristic that must be carefully assessed; the "patterns" `produced are interpreted subjectively by the onlooker and the assumption of heterogeneity (in such cases) must be made with caution. It must also be acknowledged that some clustering may occur in the events detected within the detector, as a natural consequence of the random process of decay.

The use of computer generated simulations is also useful in the determination of the appropriate limits of detection (visual) with regard to localized regions of genuinely higher activity, and the differentiation between these and the areas that result from the random clustering of tracks (Fig 5.14). By increasing the number of randomly generated data points (simulated tracks) within a defined area of the simulated autoradiographs shown above it is possible to determine

the extent to which a discrete area must differ in activity from the bulk value to become clearly visually apparent (Fig 5.15 and Fig 5.16).

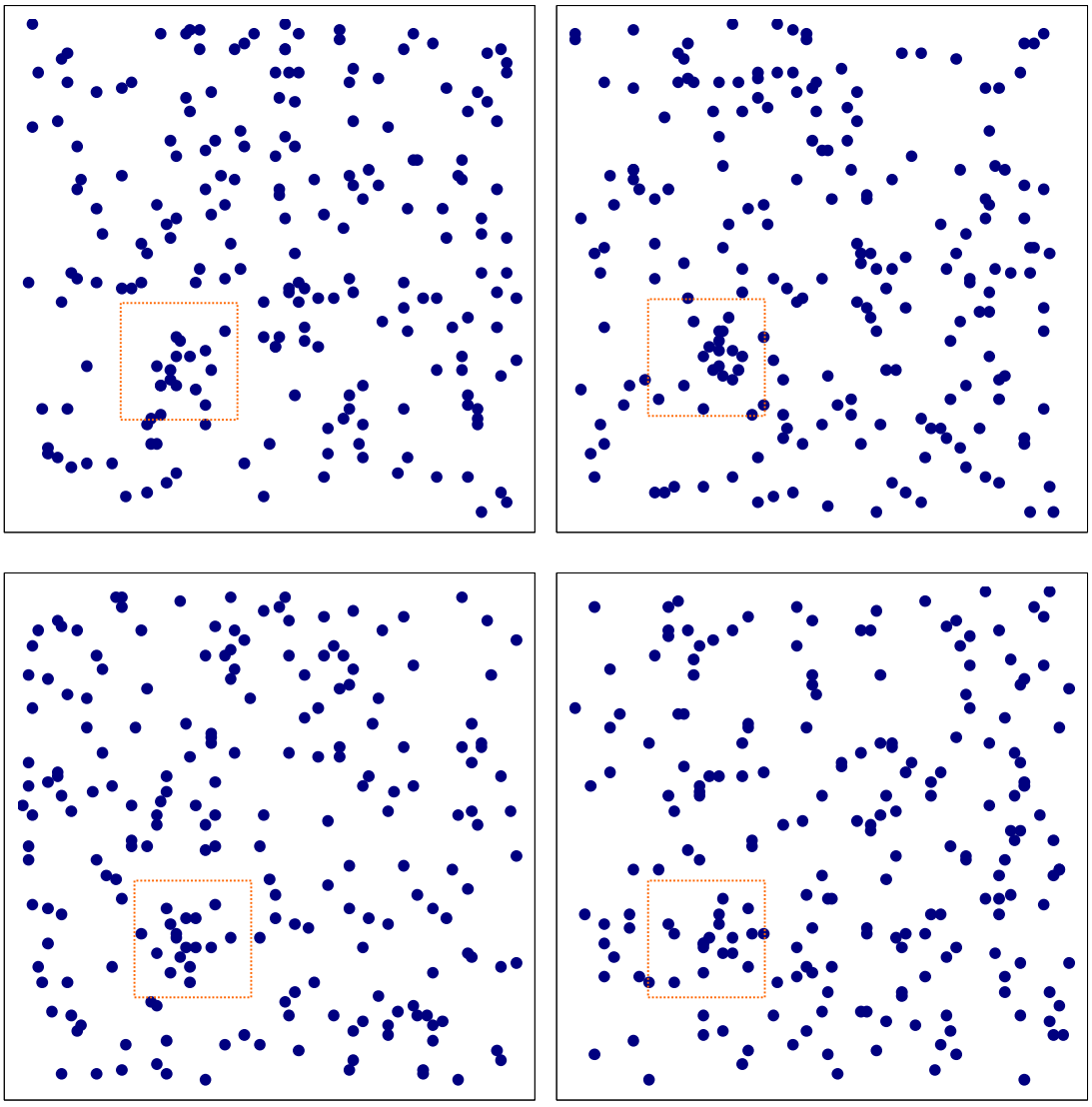

Fig 5.14 Simulated 1 mm^2 autoradiographs in which a localized area equivalent to 100 μm^2 has a simulated activity equivalent to 5x background activity. It can be seen here in the 4 randomly generated examples that the area of increased activity is not visually apparent.

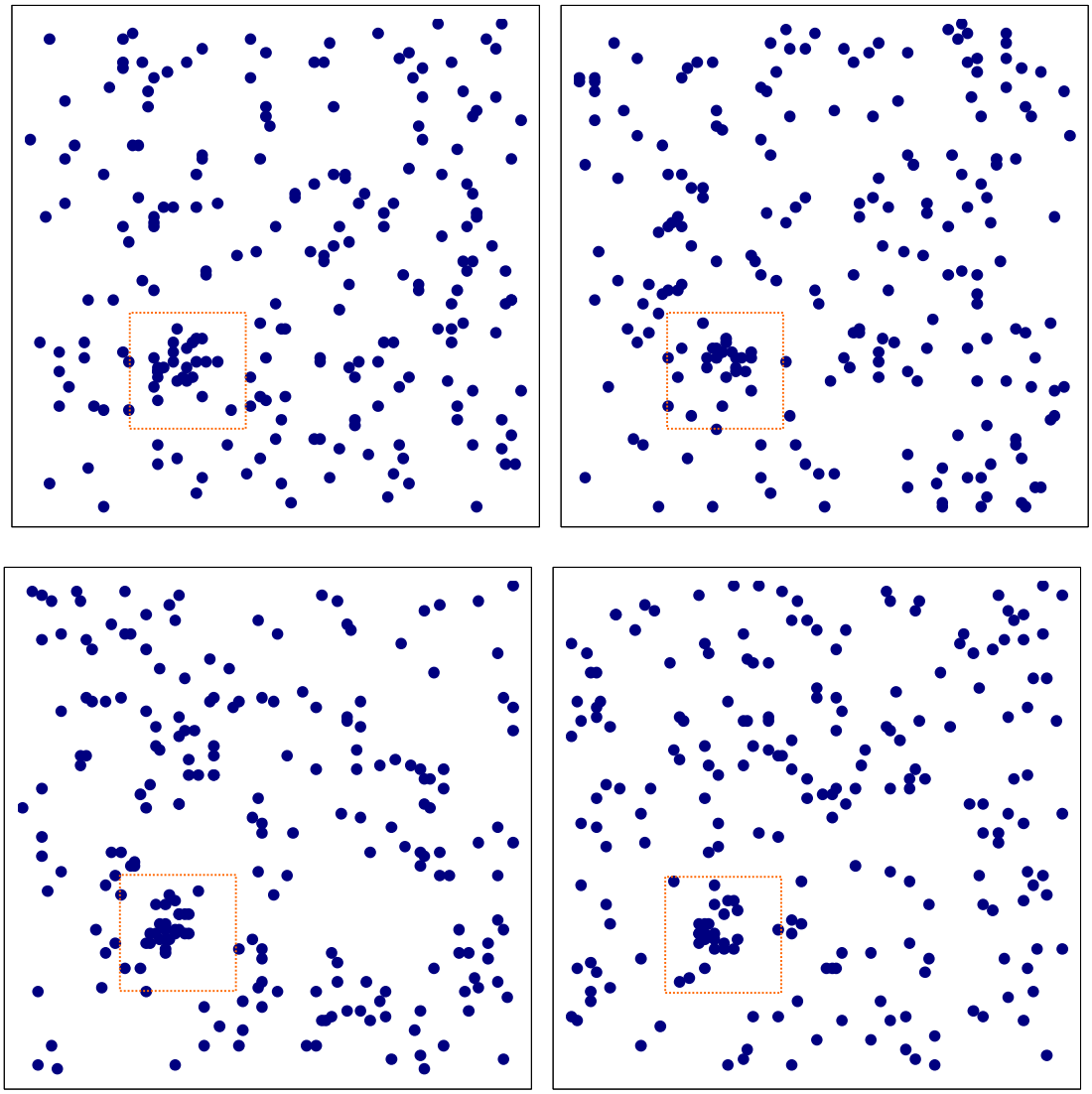

Fig 5.15 Simulated 1 mm^2 autoradiographs in which a localized area equivalent to 100 μm^2 has a simulated activity equivalent to 10x background activity. It can be seen here in the 4 randomly generated examples that the area of increased activity is starting to be more visually apparent, although in the first two examples these areas could be interpreted as random track clustering.

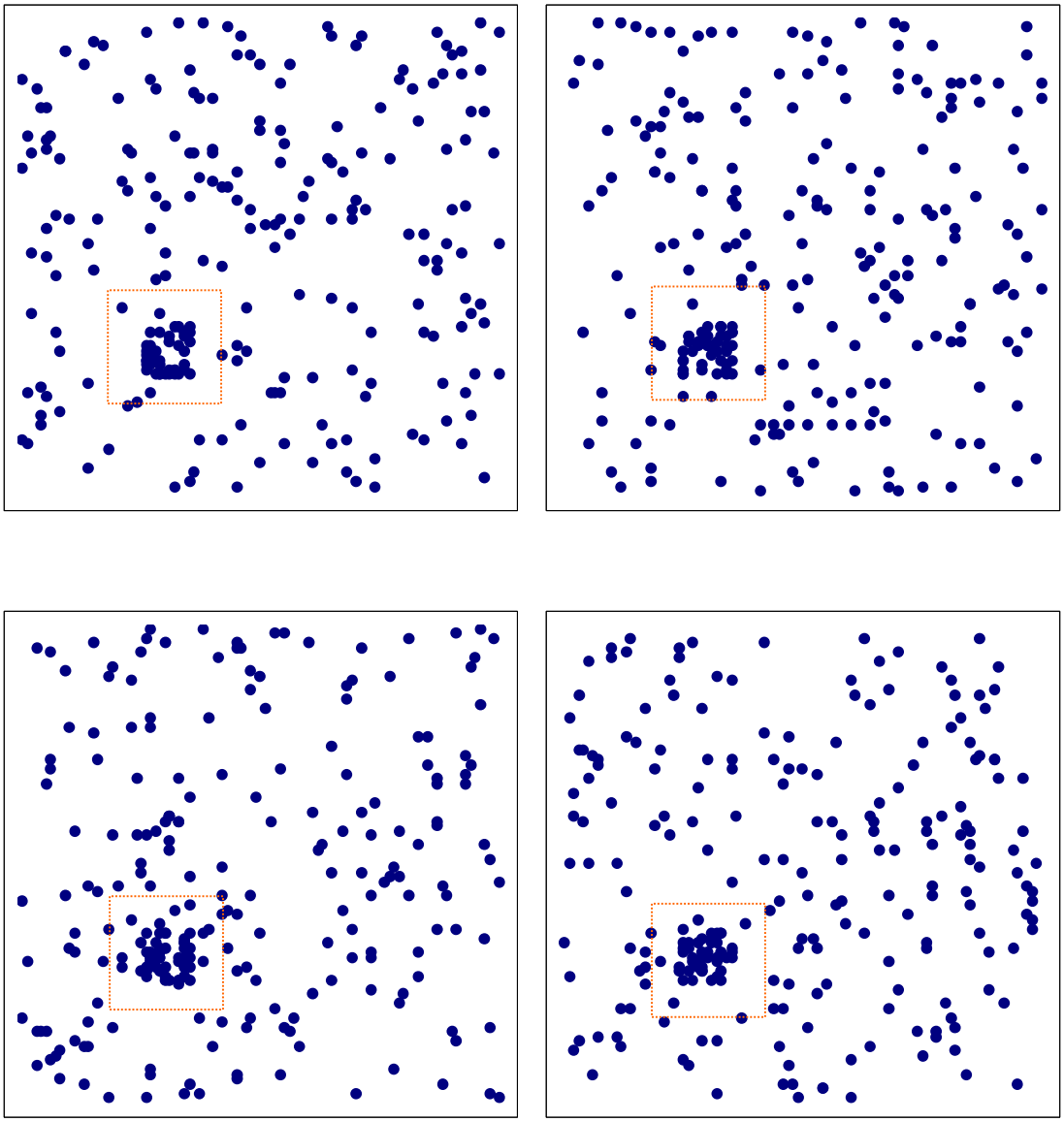

Fig 5.16 Simulated 1 mm^2 autoradiographs in which a localized area equivalent to 100 μm^2 has an activity equivalent to 20x background activity. It can be seen here in the 4 randomly generated examples that the area of increased activity has become clearly apparent and easily distinguished from random clustering and background track intensity.

The use of such simulations is extremely useful in the estimation of the applicable detection parameters for the use of SSNTD materials in the characterization of heterogeneity / homogeneity in distributions of this type. If a localized area of increased activity is only visually discernable at levels equating to 20 times that of the surrounding area, the assumption of uniformity due to a lack of such features must be made with caution as heterogeneity that results from smaller differences in concentration may be missed. Within the materials of interest to this project, areas of greatly increased activity (20x background) are likely to result from the inclusion of minerals such as zircon within the sample matrix rather than from other anomalous or random effects.

5.7.2 Track distribution heterogeneity – a statistical approach

Simple statistical procedures can be used to characterize the extent of spatial homogeneity or heterogeneity; the comparison of observed count rate between individual detector areas (sampled across the surface of a single detector) may be performed by the use of basic variance or standard deviation tests. Depending upon the level of spatial resolution chosen, the increase in determined variance or standard deviation (associated with the population of individual count areas) is expected to be proportional to the heterogeneity of the distribution of contributing alpha emitters. The likely values for variance and standard deviation for a uniform distribution of randomly emitting species for which only one emission in four results in detection can also be simulated by using a simple computer based simulation.

Using Excel, a hypothetical SSNTD count area was simulated in which a predefined number of cells produce a randomly generated number between 1

and 4. The application of a simple logic step enables the production of a positive outcome (i.e. a countable track) when a specified single number is generated; hence the number of cells in each grid can be used to simulate the total number of emissions, whilst the positive outcome produced when a specified number is generated (1 in 4 probability) represents an alpha emission that results in a detectable track.

By producing a grid that contains an appropriate number of cells, it is possible to simulate the production of tracks across the entire surface of the detector. If the cells are then sub-divided into a series of equivalent groups (to represent the degree of spatial resolution chosen for counting areas) the total number of counts for each group of cells can be quantified automatically. The resulting data can be used to represent the likely number of counts per unit area across the detector. If these series of values are subjected to statistical analysis, the typical ranges in values for variance or standard deviation can be produced for both homogeneous and controlled levels of heterogeneity.

The use of a numerical simulation provides the opportunity to rapidly generate simulations of theoretical counting outcomes that would take many months to derive experimentally.

5.7.2.1 Estimated relationship between variance and heterogeneity using Excel simulations

The Excel simulations described above have been used to provide introductory data regarding the relationship between track density spatial heterogeneity and expected changes in variance (σ^2, where σ is the standard deviation of a

particular normally distributed data series). It is likely that an increase in the degree of heterogeneity (depending upon resolution) is likely to result in an increase in variance but the levels of variance associated with the effectively random distribution of alpha tracks on the surface of an SSNTD detector is difficult to predict.

Simulations have been developed to correspond to a number of different distribution patterns and the associated variance value for each outcome has been calculated. A number of grids (400 in total) have been created, each containing 10 cells that generate a random digit between 1 and 5. A simple logic function returns a positive outcome (in this case a value of 1) if, arbitrarily, the number generated randomly was 4 (the number 4 allocated as a"hit"); i.e. approx 25% of the time, a value of 1 was generated to simulate the production of a detectable track. The grids were grouped into sets of 20 and the total number of positive outcomes recorded (out of a possible 200). The values were, as expected in the region of 50 counts, relating to the simulated 1 in 4 probability of a track reaching the detector. The total number "tracks" generated in each simulation is in the order of 1000.

Case 1 - Homogeneous distribution.

All cells within the simulation grid were assigned an equal probability of randomly producing a "track" to represent a hypothetical, completely uniform distribution. Variance in this situation can be regarded as a function of the random nature by which tracks are generated. The calculated variance will be compared to experimentally derived values to validate the use of this technique.

Results

Total number of simulations	100
Mean total count for each simulation (N)	1001.3
Mean variance (V)	37.39
Standardised mean variance % (V/N)	3.74
Standard error (68%)	1.27
Range of V/N (68% confidence)	2.47 – 5.01

Case 2 - introduction of 5% heterogeneity

The simulations were identical to those in case 1 but with a 100% increase in track probability in 5% of the composite grids. This simulation is used to represent a distribution that is effectively uniform but contains a small component (5%) of higher activity material.

Results

Total number of simulations	100
Mean total count for each simulation (N)	1051.5
Mean variance (V)	95.45
Standardised mean variance % (V/N)	9.08
Standard error (68%)	2.53
Range of V/N (68% confidence)	6.55 – 11.61

Case 3 – introduction of 10% heterogeneity

The simulations were identical to those in case 1 but with a 100% increase in track probability in 10% of the composite grids. This simulation is used to represent a distribution that is effectively uniform but contains a medium component (10%) of higher activity material.

Results

Total number of simulations	100
Mean total count for each simulation (N)	1107.1
Mean variance (V)	283.3
Standardised mean variance % (V/N)	25.59
Standard error (68%)	5.23
Range of V/N (68% confidence)	20.36 – 30.83

Case 4 – introduction of 20% heterogeneity

The simulations were identical to those in case 1 but with a 100% increase in track probability in 20% of the composite grids. This simulation is used to represent a distribution that is effectively uniform but contains a high component (20%) of higher activity material.

Results

Total number of simulations	100
Mean total count for each simulation (N)	1198.2
Mean variance (V)	457.2
Standardised mean variance % (V/N)	38.16
Standard error (68%)	5.78
Range of V/N (68% confidence)	32.37 - 43.95

Case 5 – Experimentally derived values.

The following values were calculated using data derived experimentally using CR39 alpha autoradiographs produced using standard glass (NIST 610, 500 mg/kg U) in which uranium and thorium (concentration – 500 mg/kg) species are distributed homogeneously. Photomicrographs were produced at 25 equivalent positions across the CR-39 detector and tracks counted using the standard technique.

Results

Total number of counts (N)	3198
Variance (V)	105.5
Standardised mean variance % (V/N)	3.27

Discussion

The calculation of variance appears to be a potentially useful technique in the determination of varying extents of deviation from uniformity. This has particular significance in the classification of track distributions in SSNTD materials that appear to be visually homogeneous. The results derived experimentally from Case 5 above, fall within the range of values for variance that were predicted using Excel simulations; these results are very encouraging and support the validity of this type of simulation.

5.8 Estimation of localized U and Th concentrations – further considerations.

The experimentally derived CR-39 detector response to known concentrations of U and Th can be used to estimate the minimum localized alpha activity derived from track density at a particular point on the CR-39 photomicrograph although CR39 cannot be used to distinguish between a detected area of increased alpha activity that results from, for example, a 2 mm^2 inclusion of 1 μm thickness (with activity equal to 100 x sample matrix activity) compared with a 2 mm^2 inclusion of 10 μm thickness (with activity equal to 10 x sample matrix activity). Within these limitations, and with respect to the production of semi-quantitative data, it is possible to calculate a *minimum* local activity value, based on the assumption that alpha particles detected emanate from within the full extent of the mean particle range.

This value is semi-quantitative but potentially useful in characterizing the minimum concentrations of U and/or Th within a (Th or U rich) inclusion.

A simple calibration of the CR-39 using experimentally derived track densities (tracks per unit area) for materials of known activity can be used to produce an initial factor which relates observed track density to unit activity and exposure time.

$$A_s = \frac{C_s \times D_{Std} \times T_{Std} \times A_{Std}}{C_{Std} \times D_s \times T_s}$$

Where

A_s = Calculated localized sample activity (Bq/kg)

A_{Std} = Activity of standard material (Bq/kg)

C_s = Tracks counted (sample)

C_{Std} = Tracks counted (standard)

D_s = Count area (sample) cm^2

D_{Std} = Count area (standard) cm^2

T_s = Sample – detector contact time (h)

T_{Std} = Standard – detector contact time (h)

This equation is only valid if the following conditions are met -

1. There is linearity of detector response between sample and standard activities
2. Equal activity of uranium and thorium
3. Comparable values of A,Z and density of sample and standard materials

5.9 Proposed methodology

For the production of alpha autoradiographs using samples appropriate to this work -

Ceramic materials

1. Production of thin slices (10 mm x 10 mm x 1 mm)
2. Detector - sample contact period of 12 months to reveal macro distribution patterns
3. Additional detector - sample contact period of 3 months (for step 5)
4. Photomicrography and calibration
5. Calculation of macro and local alpha activities and degree of variance

Sediments

1. Encapsulation using Epothin resin (Struers)
2. Production of thin slices (10 mm x 10 mm x 1mm)
3. Detector - sample contact period of 12 months to reveal macro distribution patterns
4. Additional detector - sample contact period of 3 months (for step 6)
5. Photomicrography and calibration
6. Calculation of macro and local alpha activities and degree of variance

Standard materials

1. Powder compression or pelletization using minimal binding agent
2. Detector contact time – as appropriate to known activity
3. Photomicrography to validate visual material homogeneity
4. Calculation of track density and calibration parameters

Chapter 6 Staining methods and digital analysis

6.1 Staining techniques - general

Unlike the microscopic methods used in many geological and ceramic petrology mineralogical determinations, the production of translucent thin slices of material is not necessary for the application of staining techniques. This is particularly useful as archaeological ceramic matrices may be friable in nature and would require encapsulation with an appropriate resin (low K content) to enable sectioning at this thickness (<100 μm); encapsulation will generally be required in determinations of mineral distributions in sediments, where maintenance of spatial integrity may be important , although staining techniques can also be used on disaggregated material, where for example, the bulk proportion of potassium bearing grains may be of interest.

Many staining techniques have been developed, the chemical nature of which depend upon the types of geological or ceramic materials in question, and the nature of the species which is to be determined.

6.1.1 Chemical aspects and staining mechanisms

Macromolecular structure, weathering, and the differing mechanisms by which potassium may be incorporated into naturally occurring minerals (see chapter 1), result in potential variation of the levels of concentration at which potassium may be present at the exposed areas of interest within a ceramic or geological matrix. Additionally, staining techniques rely upon the availability of an analyte to chemically react with the applied stain. For these reasons, the first stage of the staining techniques used within this project is the exposure of the sample surface to hydrofluoric acid vapour; the use of HF in the digestion of ceramic and geological

matrices is well established (Potts, 1987) and is based on the ability of HF to break the Si-O and Al-O bonds that form the molecular skeletons of these materials.

Typical empirical reactions are shown below -

$4HF + SiO_2 \rightarrow SiF_4 + 2H_2O$ or $6HF + SiO_2 \rightarrow H_2SiF_6 + 2H_20$

In the case of aluminosilicates, and importantly those in which potassium forms a structural or interstitial component, the reaction with HF serves two useful roles; firstly, the rate at which aluminosilicates are etched by HF is faster (cf. quartz) due to the greater susceptibility of the Al-O bond to attack. This results in the formation of a dullish, etched appearance on the surface of feldspathic minerals at a much faster rate than that associated with quartz and hence, enables basic differentiation between the two major species. The second useful process that occurs due to Al-O and Si-O bond cleavage in aluminosilicates is the "opening" of the tertiary molecular structure; this effect increases the surface availability of potassium when this species is present both structurally and interstitially, and hence enables surface reaction with the staining chemical. The non-stoichiometric reaction below between orthoclase feldspar and a dilute mineral acid (signified simply by H^+) demonstrates the potential to liberate potassium from this species, and indeed forms the basis for the leaching of potassium, and hence reducing surface availability, of this species generally in weathered feldspars.

$8KAlSi_3O_8 + H^+ + H_2O \rightarrow 8K^+ + 2Al_4Si_4O_{10}(OH) + 8\ SiO_2$

The sodium salt of the hexanitrocobaltate complex is very soluble in water and forms a deep red coloured aqueous solution. The solubility of the potassium analogue is greatly reduced and the addition of potassium salts to a solution of sodium hexanitrocobaltate, depending upon the concentration of the two species, results in the precipitation of the potassium complex as a vivid yellow solid. This reaction, which forms the basis of the staining technique, is well known and was exploited in classical analytical chemistry before the routine use of instrumental analysis (Schueler and Thomas, 1933).

6.1.2 Initial tests

In order to verify the effectiveness of the staining techniques described above for the types of material encountered routinely in luminescence dating procedures, two samples were chosen for initial testing that represented extreme cases in terms of visual heterogeneity.

Sample 321-1 (archaeological brick) was chosen to represent extreme visual heterogeneity with the presence of numerous crystalline inclusions of varying sizes and appearances, dispersed non-uniformly throughout a ceramic matrix that also displays visual heterogeneity with regard to colour and texture of the composite material.

Sample 2 329-1 (archaeological sediment) was chosen to represent visual uniformity with regard to the size and distribution of the composite materials. The sediment is composed of a very fine continuous matrix in which mineral grains (of a relatively narrow particle size range) are distributed uniformly.

6.1.3 Experimental procedures

Several 1 mm slices of these materials had already been prepared for single grain dating techniques (in situ) and surplus sections were used for the initial staining tests. The surface of each sample was initially exposed to hydrofluoric acid vapour by suspending the thin section from the lid of a sealed reservoir of acid (recycled photographic film canister (PE), 2 ml of VWR Analar HF 40%) for 30 minutes. The lid was carefully removed and without rinsing, 1 ml of staining solution (2.5 g sodium hexanitrocobaltate dissolved in 5 ml deionised water) was applied to the full surface area and left for 5 minutes to allow the stain to develop. After this time had elapsed, the sample was rinsed thoroughly with copious amounts of deionised water to remove traces of both hydrofluoric acid and staining reagent.

Hayes and Klugman (1959) also proposed the use of a general purpose stain to highlight the differences in etch rate observed between quartz and feldspathic minerals which are not stained in the initial stages described above. Eosin is a red/pink coloured stain used widely in microbiological analyses and initial tests indicated that this solution is absorbed preferentially by non-quartz matrix components, post HF vapour etching. Depending upon the characteristics of the individual samples in question (in cases where it may be difficult to differentiate between mineral species based on surface etching effects alone), the use of a final eosin stain (1% in ethanol) may be useful.

After the staining and rinsing stages, the samples were left to dry at ambient temperature before microscopic and digital analyses were performed.

The optimum vapour / sample residence and stain reaction times were determined experimentally, using the information supplied initially by Hayes and Klugman (1959) and a number of repeat experiments using archaeological ceramics. It was noted that over exposure to HF vapour caused subsequent material stability

problems – the underlying material beneath the surface stain became friable and was lost partially or completely during post stain washing. The use of a 5 minute staining reaction time is somewhat arbitrary as the surface reaction is almost instantaneous, however surface tension effects that may inhibit reagent – sample contact should be taken into account.

6.1.4 Results

Sample 321-1

On close visual examination (the use of digital enhancement will be discussed later in this chapter) the matrix material appears to be composed of two discrete phases (labelled A and B), with respect to colour and texture, that after staining with both sodium hexanitrocobaltate and eosin appear to be mineralogically different with respect to potassium content. The included species appear to be predominantly quartz like in nature (labelled D, translucent appearance is maintained and eosin is not absorbed onto the surface), however, several minor inclusions have increased opacity with some visual evidence of eosin absorption (labelled C). None of the large crystalline inclusions appear to have stained yellow to a substantial degree, which indicates that the non-quartz inclusions that are displaying increased opacity are likely to be plagioclase feldspars.

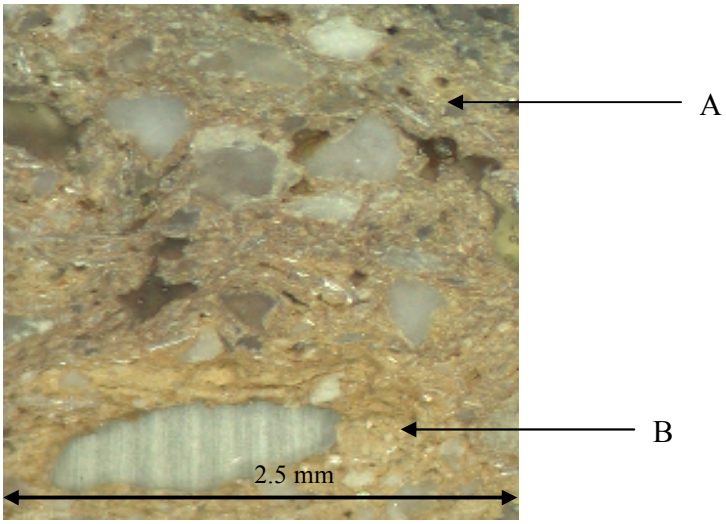

Fig. 6.1 Photomicrograph of sample 321-1 before treatment.

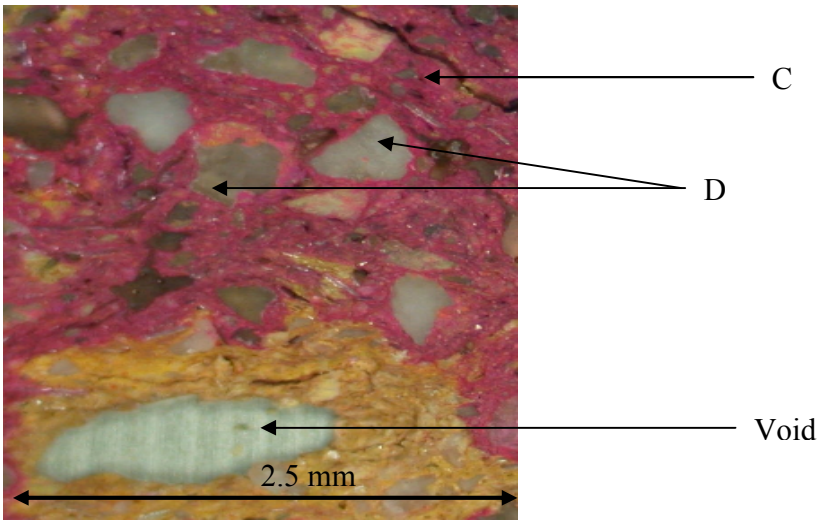

Fig. 6.2 Photomicrograph of sample 321-1 after staining treatments.

Sample 329-1

The material was examined after the initial HF etching, sodium hexanitrocobaltate and rinsing stages; the subsequent eosin stain was not employed as the variation in opacity and the fixing of the yellow stain in the included, non-quartz component minerals provided clear indication of the mineralogical species present.

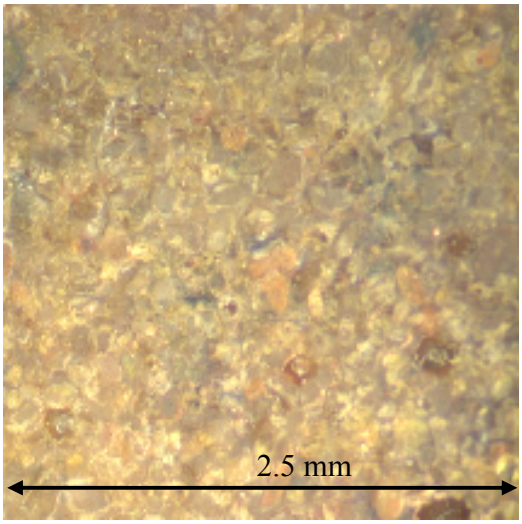

Fig. 6.3 Photomicrograph of sample 329-1 before treatment.

The included species appear to belong to three distinct mineralogical groups – quartz, K-feldspars (and potentially alkali feldspars) and plagioclase feldspars. After treatment, the translucency of the quartz inclusions appears to have remained generally unchanged in comparison to the pre-etch image (labelled E), where differentiation between these minerals and other translucent species was not possible by simple optical means. The opacity of a large proportion of the crystalline inclusions has changed substantially (labelled F) and indicates the presence of a

discrete plagioclase feldspar component. The third discrete mineral phase demonstrates a variable degree of yellow staining (G) which indicates the presence of potassium in varying concentrations; this phase may be regarded as a potential mixture of both K-rich and alkali feldspars (which are characterised by variable K and Na contents). The distribution patterns of the composite potassium bearing minerals are clearly visible but may be highlighted further by the use of digital enhancement.

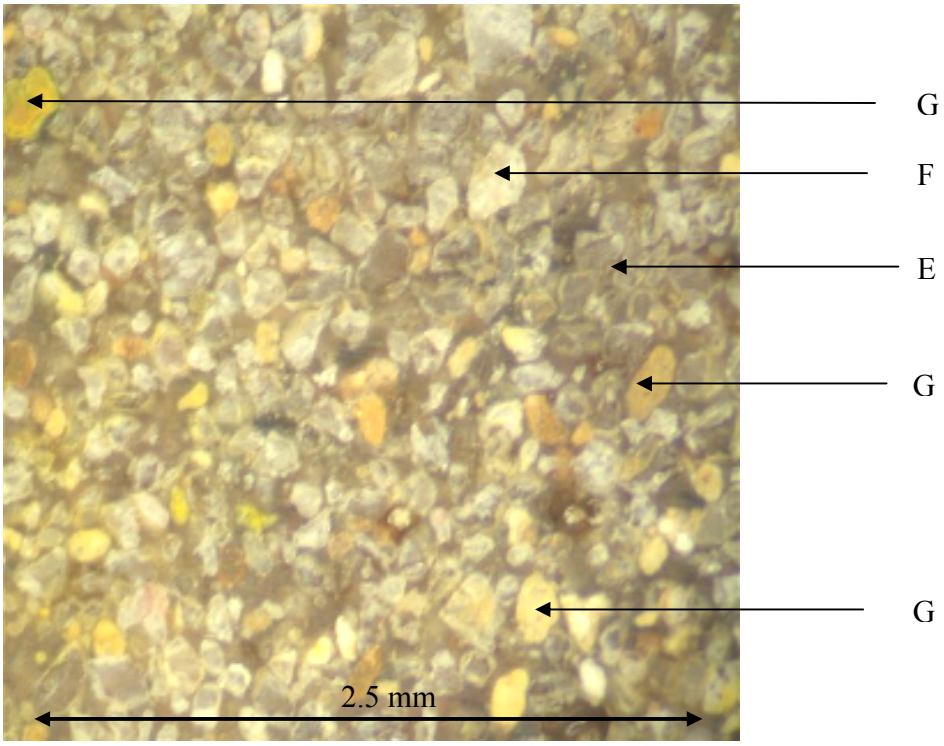

Fig. 6.4 Photomicrograph of sample 329-1 after staining treatment

The characterisation of the apparently random distribution of potassium bearing grains, made visible by the use of sodium hexanitrocobaltate staining offers potentially useful in formation in assessing the beta dose distribution characteristics of the sample as these grains represent localised areas of increased radioactivity

(beta) or "hotspots" (Mayya et al., 2006). In order to provide a clearer visual indication of these areas, an attempt has been made to digitally enhance the photomicrograph of the stained section.

Adobe Photoshop is a software package that has been used routinely for several years in the post production enhancement of digital images. One of the features of this software offers the ability to "sample" colour from a particular area of interest and to replace this colour (throughout the entire image) with a different colour of choice. By selecting the individual areas of the 329-1 digital photomicrograph that had developed a visible yellow stain, and replacing with a colour not present naturally in the image (in this case black), it is possible to increase the visibility of all such areas of the photomicrograph that displayed this feature, and potentially in small areas where this colouration was not immediately visible to the naked eye. By converting the enhanced image to grayscale, it is then possible to increase the levels of contrast and brightness so that the appearance of non-stained (now non-black) regions is highly, if not completely reduced, and subsequently producing an effective "map" of just the distribution of potassium bearing minerals as illustrated in Fig. 6.5

Fig. 6.5 Digitally enhanced view of stained regions (329-1)

The distribution of potassium bearing minerals is now much more clearly visible, and the presence of regions of increased potassium concentration that are not necessarily associated with larger single inclusions has been made apparent.

Image J is an image processing package (Author, Wayne Rasband, public domain) and was used to assess the use of automated techniques for track counting in SSNTD materials. The automatic quantification of the total number of discrete regions of increased localised potassium concentration is possible using this software. The results obtained are expressed in terms of the number of discrete regions falling within a specified pixel size range (pixel size in this instance can be regarded as a relative, arbitrary unit although future calibration is possible):-

Particle count: 923

Total Area: 148062.000 pixel^2

Average Size: 160.414 pixel^2

Area Fraction: 8.2%

(from Image J output text file)

The total image area is expressed in pixel^2, which can be converted to standard units if the image size is known. A semi-quantitative estimation of image size in this case is possible and equates to approximately 6.5 mm^2. The pixel^2 to mm^2 ratio can be approximated to 22800 which in turn enables the estimation of cross sectional area of the areas of interest to be expressed in standard units (~0.007 mm^2 in this case). If the assumption is made that grains are primarily spherical in nature, the average grain diameter can also be calculated ((0.007/3.142)^0.5 x2) which equates to approximately 100 microns and is typical for sedimentary material of this type. The cross sectional surface area taken up by potassium bearing grains is 8.2 %

These data may provide useful information for modelling-based dosimetric investigations but should be used with caution, as the identified grain sizes are a function of the cutting process and must be regarded as cross-sectional in nature, with no information about the grain depth at which cutting occurred (Bailiff, 2006).

If the grains are randomly distributed throughout the material it is, perhaps, appropriate to view the cross sectional grain diameters as representative of what is likely to be seen if a slice it taken randomly from any area within the material. In this case, ability to quantify the percentage of the total (cross sectional) surface area attributed to potassium bearing minerals may be useful. The Image J software offers the user the ability to perform this type of analysis and the results detailed below

relate to the image analysis of the enhanced photomicrograph of sample 329-1 seen above (Fig. 6.5).

6.1.5 Conclusions – staining techniques and subsequent analysis

The application of both staining techniques and subsequent digital analyses provided a useful tool in the visualisation and potentially the quantification of the distribution of potassium rich minerals in both ceramic and sediment matrices. The development of colour provides a qualitative indication of the presence of increased potassium concentration and identifies regions of interest for quantitative determination of K concentration by AAS in combination with micro-sampleing. The development of a surface coating of potassium hexanitrocobaltate will not compromise the quantitative determination of potassium as this element is effectively fixed, in situ, due to the solubility characteristics of the complex produced.

If the material in question is to be subjected to spatially resolved luminescence analysis (Bailiff and Mikhailik, 2003; Bailiff, 2006) the application of staining techniques should be done after all such analyses have been performed; if the quartz component of the matrix is the subject of such scanning techniques, it is possible that the regenerative luminescence characteristics may remain unchanged after staining; however, the use of HF vapour etching may produce subtle surface effects on the exposed quartz and so should be avoided.

6.2 Digital enhancement without staining - introduction

The application of digital techniques to enhance the appearance of image sections with differing colour characteristics may also offer the potential to highlight regions

that are composed of dissimilar matrix components, without the application of staining techniques, and particularly in ceramic matrices where inefficient mixing of more than one matrix component is apparent. Whilst the differentiation of matrix components by colour characteristics will not provide any compositional or mineralogical information, the ability to highlight such areas for subsequent sampling and quantitative analysis is useful; in the case of ceramic matrices, where quartz is present potentially as a tempering agent and as a natural constituent of the composite clay materials, the luminescence characteristics may vary, depending upon the source of the quartz. Spatially resolved techniques have shown that the luminescence signals recorded in procedures using disaggregated grains may be emitted primarily, from a very small percentage of the total number of grains present (McCoy et al., 2000). If these "bright" grains arise from a discrete component within the matrix (one of a number of different clay types for example) it will be useful to determine whether the radionuclide concentration of this phase differs from the matrix average.

6.2.1 Initial tests

Adobe Photoshop offers the user several functions to enhance digital images and in particular, the ability to alter brightness, contrast and colour saturation are useful in enhancing visual differentiation between different phases (Fig. 6.6 below). As described previously, the ability to sample subtle colour shades from discrete image locations and replace with intense or more noticeable colour is also useful in the identification of subtle variations in colour and texture.

6.2.2 Results and discussion

The image below is a digitally enhanced photomicrograph (see Fig. 6.1) taken of sample 321-1 before the application of staining techniques. It was previously noted that digital enhancement may offer a useful means of identifying differing composite phases without providing mineralogical or chemical information, it is possible in this instance to produce a direct visual correlation between the areas that have been highlighted digitally (labelled H) and those areas that developed a surface yellow stain due to increased mineral potassium concentration.

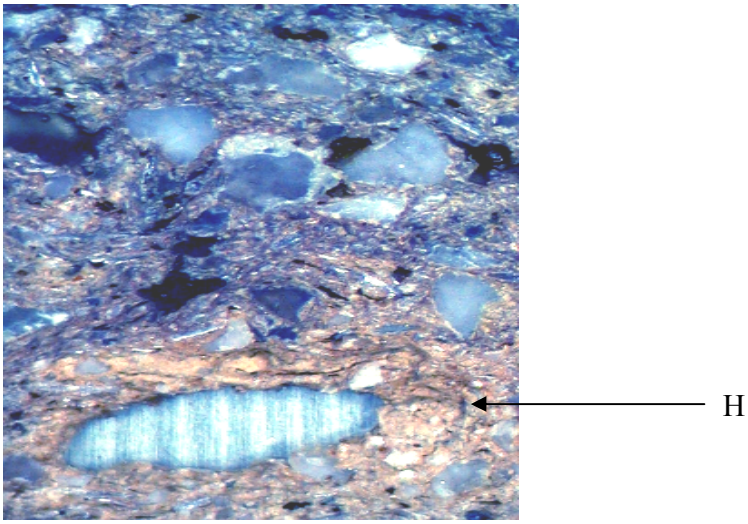

Fig. 6.6 Sample 321-1 digitally enhanced image (before staining)

The identification of a positive correlation between differing colour and texture and (effectively) radionuclide concentration in this example validates the use of photo micrographic and digital analysis techniques in the characterisation of archaeological materials encountered routinely in luminescence dating.

Chapter 7 Quantitative instrumental analysis

7.1 Inductively Coupled Plasma Mass Spectrometry

Inductively Coupled Plasma Mass Spectrometry (ICP-MS) was introduced briefly in Chapter 4 as a technique that can be used to determine the trace and ultra-trace concentrations of uranium, thorium and potassium associated with the materials and methods used in this project. The theoretical aspects of this section refer generally to the ICP-MS technique, whilst practical and experimental information refers specifically to the use of the ELAN6000 Inductively Coupled Plasma Mass Spectrometer (Perkin Elmer) which is currently housed within the class 10000 clean room analytical facility, based within the Department of Geography, Durham University.

Whilst some of the basic theoretical aspects of this technique were introduced in Chapter 4, this chapter focuses on the details associated specifically with the application of ICP-MS within the scope of this project.

7.1.1 Instrumental and analytical parameters.

The manufacturer's quoted values for the detection limits of uranium and thorium are <1 ng/L (less than 1 part per trillion) which enables the detection of these elements at the typical concentrations encountered within this research, even after dilutions of several orders of magnitude. The determination of potassium is less straightforward due to the presence of the interfering species ArH^+ (May and Wiedmeyer, 1998), an intrinsic constituent of the argon plasma used in the generation of ionic species and which forms the basis of the

technique. Methods of compensation for this problem will be discussed later, together with possible analytical alternatives.

Samples are introduced into the instrument via an auto-sampling system; liquid is drawn through an inert polymer tube by indirect peristaltic action and subsequently passed via a nebulizer to a spray chamber aspiration system where controlled flow argon carrier gas is used to introduce the solution in controlled aerosol form, and at a constant rate into the plasma torch. The rate at which sample is introduced into the plasma is critical as consistency is assumed between sample and calibration solutions.

The generation of plasma is achieved by passing the carrier gas through a conduction loop to which RF frequency current is applied where a primary spark provides sufficient energy to initiate plasma production; plasma generation is maintained by the continuous gas flow / application of current and provides conditions (including temperatures of around 6000K) that are conducive to both sample atomisation and ionisation. The chemistry of plasma / sample interaction is complex with a number of potentially competitive processes occurring simultaneously including atomisation, ionisation, recombination and oxidation.

The mass detection system requires that the analyte ions are differentially transferred from atmospheric pressure at a temperature of 6000K to a final pressure of 10^{-5} Torr. A series of sampler and skimmer cones are used to reduce the amount of material passing through the system; material from the central channel of the plasma is first passed through the 1.1 mm aperture of a sampler cone into a region of lower pressure (1-3 Torr) where most of the argon atoms are

removed by vacuum. The subsequent ion beam is refined further by the use of a skimmer cone which is used to introduce limited amounts of material into the low pressure environment (10^{-5} Torr) in which the ionic separation and mass detection systems are located. A solid disc known as a shadow stop is situated in the linear path of the ion beam to effectively block any photons that are present.

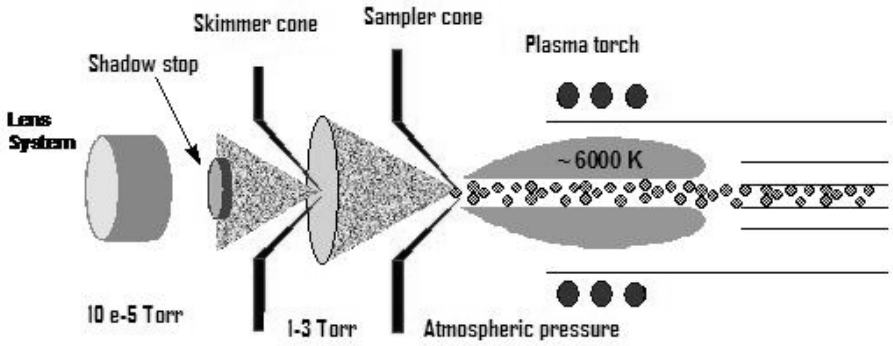

Fig 7.1 Schematic of the ion beam introduction system (adapted from Perkin Elmer training material)

The ion beam travels through a cylindrical ion lens which serves to focus the beam through a differential aperture into the quadrupole mass filter assembly whilst simultaneously excluding non-ionic species. The focussing and collimating functions of the ion lens system must be optimised to ensure that mass discrimination effects are minimal; in practice optimisation is routinely achieved by altering the voltage applied across the lens whilst monitoring system performance and this forms part of a series of procedures that are performed each time the ICP-MS is used.

The Elan 6000 ICP-MS falls into the category of instruments that are characterised by the use of a quadrupole mass discrimination system to selectively control the trajectory of the ionic species that pass through and ultimately reach the detectors. As previously described in Chapter 4, (section 4.2.2.1,), the quadropole consists of four rods, two positively charged and two negatively charged. Discrimination based on the ionic mass to charge ratio is achieved by the application of RF current across the system to which a constant base DC voltage is maintained; hence by altering the applied current it is possible to allow only species of a specific M/Z ratio to reach the detectors at any one time. The trajectories of ions with different M/Z ratios are unstable and result in the ions being lost into the vacuum.

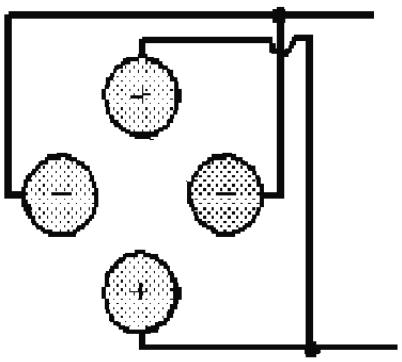

Figure 7.2 Cross section of quadrupole showing positively and negatively charged rods.

The typical mass resolution capability of a quadrupole system is in the region of 0.6-0.8 atomic mass units (amu) which provides sufficient selectivity to differentiate between species with a mass difference of >1 amu. Potential overlapping of species with a mass difference of <1 amu is problematic for the

determination of certain species, however in most cases it is possible to focus attention on a neighbouring isotope of the same element, or to use a mathematical formula based on typical abundance values to allow subtraction of the contribution to signal made by interfering species.

The detection system of the Elan 6000 is based on the use of an array of 21 discrete dynodes which provide a dual stage detection system. Signal is measured simultaneously by a pulse counting stage for relatively low count rate signals and an analogue counting stage (measured between dynodes 10 and 11) for higher signal intensity determinations.

Post detection data processing is achieved by the use of a Pentium grade computer and dedicated software. Data can be imported directly into Excel spreadsheets although the software package provides the facility to automatically present data in a custom report format.

The routine operation and monitoring of analytical parameters of the ICP-MS is also computer controlled; the dedicated software package is typical of the type associated with modern analytical instrumentation and allows the instrument to be monitored remotely from any PC linked to the same network as the primary control PC.

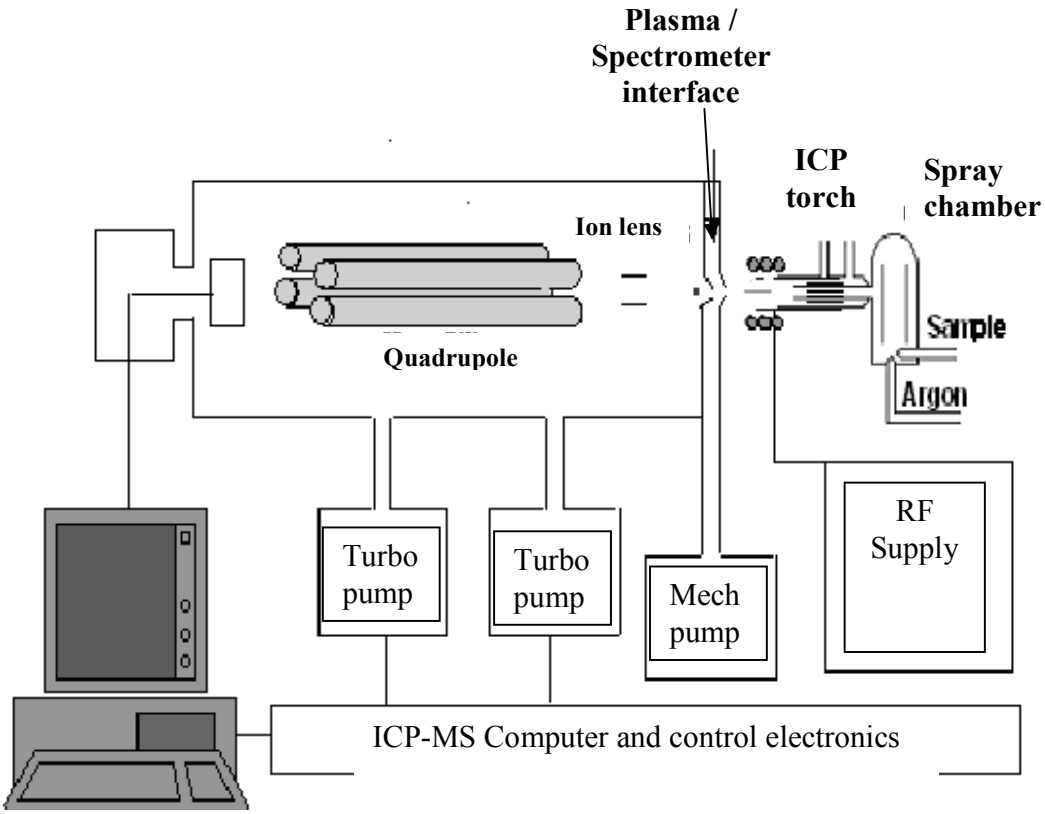

Figure 7.3 Overall Schematic of ICP-MS (adapted from Perkin Elmer training material)

7.1.2 Optimisation of operational parameters.

The detection and operating parameters of the ICP-MS must be checked each time the instrument is used to ensure optimal analytical conditions are maintained; routine checks include detection efficiency and precision across a range of masses, the sample introduction system and torch positioning and plasma optimisation including the monitoring of the production of oxides and doubly charged species within the plasma, both of which should be minimal.

The ICP-MS is turned on and the plasma torch allowed to stabilise for at least 15 minutes before any measurements are made. A standard solution is then aspirated to produce specific data that can be used to assess operating conditions.

Detector sensitivity

The sensitivity of the instrument (expressed in counts per second) is determined by recording the mean signal intensity of a series of masses (or more correctly mass to charge ratios) across the range of analyte masses to be determined. Magnesium, Indium and Uranium are used routinely and the manufacturer's guidelines for sensitivity (count rates) for a calibration solution containing a concentration of 10 μg/L of each of these elements are as follows –

Analyte	Measured mass	Optimal intensity
Magnesium	24.0	≥40000 counts/second
Indium	114.9	≥300000 counts/second
Uranium	238.1	≥300000 counts/second

Optimisation measurements are made with respect to standard operating conditions that control nebulizer gas flow, plasma gas flow, ion lens voltage, RF power and detection parameters.

If the desired sensitivities are achieved across the range of measured masses, the next stages of optimisation may be performed. If appropriate sensitivities are not achieved a number of manufacturer's prescribed operator checks and adjustments (not detailed here) must be performed to ensure that parameters fall within acceptable limits.

Plasma oxidation potential

A number of competitive reactions occur within the plasma phase of ICP-MS including the generation of oxidized species; the conditions of the plasma (gas flow rate, RF power and torch position) need to be tuned to reduce the presence of any species other than those detected in this technique i.e. singly charged ions. The oxidation potential of the plasma is assessed by the introduction of an easily oxidised analyte (routinely cerium), at known concentration. The ratio between oxidised and singly charged ionised species is monitored and must fall within prescribed limits to ensure optimal analytical conditions. Routinely, the ratio of CeO to Ce^+ should be less than 3%. Again, if these conditions are not fulfilled,

adjustments should be made including the reduction of nebuliser flow rate or the increase of RF power (which increase plasma temperature) or the reduction of sample aspiration rate which results in the reduction of the amount of water vapour present in the plasma.

Production of doubly charged species

As optimum analytical parameters are based on the detection of singly charged ionic species, the production of doubly charged ions (and hence a reduction in mass charge ratio by a factor of 2) is undesirable. In an analogous approach to that mentioned previously for the monitoring of plasma oxidation potential, the introduction of a known concentration of a species that is prone to further ionisation, routinely barium, is used to monitor this effect.

Optimally, the ratio of doubly charged to singly charges species (Ba^{++} to Ba^{+}) should routinely fall below 3%. Parameters which favour the production of doubly charged species are low nebuliser flow rate and low plasma temperatures. The adjustment of these parameters can successfully reduce the number of doubly charged species but care must be taken not to simultaneously increase the plasma oxidation potential whereby the concentration of oxidised species falls outside acceptable limits. A suitable compromise must be achieved whereby the concentrations of both species fall within desired limits.

Detection precision

The manufacturer's guideline value for acceptable detection precision is less than 2%. For example, the theoretical mass detection value for uranium should be

238.1, however a deviation of ± 2% (or ±.05 amu, whichever is lower) from this value is generally deemed to be acceptable. Precision is routinely measured (known as mass tuning) across a range of mass values provided again, by the introduction of standard species.

Measurement of background count rate

Count rate is measured at appropriate mass values (conventionally 220 and 8.5) and should routinely fall below the manufacturer's recommended threshold of 30 counts/second. Increased background signals can be reduced by following the manufacturer's guidelines for discriminator adjustment until an acceptable level is achieved.

Typical instrumental conditions from optimization file data (24/8/2008)

Nebuliser gas flow	0.91	L/min
Auxiliary gas flow	0.85	L/min
Plasma gas flow	15.00	L/min
Lens voltage	7.40	
ICP RF power	1100	
Analogue stage voltage	-2100	
Pulse stage voltage	1500	
Discriminator threshold	55.00	
Acquisition dead time	55 ns	
Current dead time	55 ns	

Daily instrumental performance checks (24/8/2008)

Table 7.1 Data from ICP-MS performance checks

Analyte	Mass (M/Z)	Mean Meas.intens. (counts per second)	RSD
Mg	24.0	78805.1	0.3
In	144.9	156442.0	0.5
U	238.1	160944.7	1.0
Ce	139.9	166722.9	0.5
CeO	155.9	3747.9	0.5
Ba	137.9	128101.9	1.1
Ba++	69.0	4098.2	1.2
220	220.0	0.6	34.3
8.5	8.5	3.73	27.0

It can be seen from the measurement data that all values fall within manufacturer's operational guidelines, except In and U, where the measured count rate is approximately half of the recommended minimum values. This situation is not ideal and further adjustment of the operational parameters should have been performed to optimise the count rates for these analytes. The ICP-MS operator, however, assessed the historic values of these parameters and found that they fall within experimentally derived acceptable limits for this particular instrument. Measured sensitivity for the uranium analyte (10 μg/L) would be acceptable for the concentration levels associated with the solutions produced during this work.

7.1.3 Calibration and internal standards

Instrument calibration is achieved by the aspiration of a number of standard solutions of the elements of interest, at a range of concentrations appropriate to the levels expected in sample solutions. The operating software includes a function to automatically produce a calibration curve from standard solutions of user specified elemental concentrations; in the range appropriate to this project (final solution concentrations of 0-50 μg/kg U and Th,) the calibration response is linear across the full concentration range. Also included in the calibration schedule is a blank solution which corresponds to zero analyte concentration but compensates for any ultra-trace levels of the analytes of interest which may be present in the reagents (2% nitric acid) used to stabilise the standard solutions.

The data recorded during ICP-MS determinations are derived from the measured count rate at a particular mass value, which, as mentioned previously, is a function of the voltage applied across the quadrupole. The count rate is dependant upon the number of ions reaching the detection system and this is primarily proportional to the concentration of the analyte in question in the solution being aspirated. It should also be noted at this point that the count rate is also dependant upon the stability of the plasma torch, the instrumental electronics and the rate of sample aspiration. It is possible that slight changes to the aforementioned systems may occur during the time taken to complete a series of determinations and as such the initial calibration may not be completely appropriate to samples that are aspirated at a later stage in the analytical routine. In order to compensate for this effect, and subsequently reduce the potential for

error, an internal standard is used. The internal standard takes the form of an additional analyte that is added at controlled concentrations to all test solutions including blanks, calibration standards and samples. The internal standard should behave similarly (chemically) to the analytes of interest and in the case of ICP-MS the element chosen should have a comparable first ionisation energy and a similar instrumental sensitivity. Ideally, the internal standard element should not occur naturally in any of the test materials although effects due to ultra-trace levels may be negated by increasing the concentration added to each test solution.

For the determination of uranium and thorium, terbium is routinely added as the internal standard; analytical data produced using these techniques are derived from the count rate ratios of the analytes and internal standard. The assumption is made that any system changes that occur throughout the analytical procedure would similarly affect the observed count rate for both the analyte in question and the internal standard; data reliability is maintained because the net count rate ratio is now independent of small system changes.

7.1.4 Potassium determination by ICP-MS

It should be mentioned at this stage that whilst potassium is likely to be found at higher concentrations than uranium and thorium in the materials associated with this project, the quantitative determination of this element by ICP-MS is not straightforward. The intrinsic compositional properties of the plasma torch result in the generation of the species Ar^+ and ArH^+ in relatively high concentrations and with mass values that are close to those of the isotopes of potassium.

The spectral overlap of these species results in the detected count rate from sub mg/kg levels of potassium being dwarfed by those associated with the interfering species. It is possible to use ICP-MS in the determination of potassium by switching to a different method of ion production, namely the use of a Dynamic Reaction Chamber, in which gaseous ammonia is used to replace the argon component and hence remove the interfering species mentioned above.

The DRC facility is not in routine use at Durham (Dept. of Geography) and the use of other quantitative methods may be more practical. Atomic absorption spectrometry is suitable for the determination of potassium at the levels associated with this project and suitable instrumentation is available locally.

7.1.5 Method development

To investigate the suitability of ICP-MS for the determination of uranium and thorium in the materials appropriate to this project, and at the levels of concentration associated with the use of micro sampling techniques discussed in earlier chapters, it was necessary to perform preliminary tests using standard materials of known analyte concentration. Commercially available standard material (NCS DC 73373 Stream sediment, supplied by LGC Ltd.) was chosen to provide a matrix that is mineralogically comparable to the materials of interest; this is particularly important with regard to the assessment of the efficiency and

stability of the preparation and dissolution stages associated with ICP-MS techniques.

The primary objective of the sample preparation stages is to separate the analytes of interest as efficiently as possible from the bulk material (and potentially problematic or interfering species) and to ultimately produce a sample medium that is suitable for introduction into the ICP-MS instrumentation (i.e., liquid) and in which the species of interest are chemically stable. Ottley et al. (2002) developed a method for the pre-ICP-MS dissolution of silicaceous minerals based upon experimental data accrued over several years; a scaled down version of this method has been developed for use with small aliquots of material (<10 mg versus 100 mg aliquots used routinely by Ottley et al.,2002).

Sample preparation – conventional and developed methods

The method developed by Ottley et al. (2002) involves the initial digestion of 100 mg of powdered sample material in a solution containing 4 ml HF (40% Romil SPA grade) and 1 ml HNO3 (69% Romil SPA grade); digestion is carried out in a pre-cleaned, 22 ml Savillex PFA vial at 150^{o}C for 48 hours followed by evaporation and the further addition of two separate 1 ml aliquots of HNO_3, which are each subsequently evaporated to near dryness at 150^{o}C. 12.5 ml of 20% HNO_3 are added before re-sealing the PFA vial and refluxing for 1 hour at 100^{o}C; the mixture is then allowed to cool and diluted to a volume of 50 ml with 18 MΩ grade water in a suitable container. The solution is then diluted (10x) in 3N HNO_3 before ICP-MS analysis.

In the version of this method, adapted for archaeological materials, up to 10 mg of sample were weighed accurately into 2ml Savillex PFA vials before the addition of 1 ml HF (40% Merck Suprapur grade) and 0.25 ml HNO_3 (69% Romil SPA grade). Reflux digestion was carried out as above (48 hr at 150°C) followed by the addition of two separate 1 ml aliquots of HNO_3, which are each subsequently evaporated to near dryness at 150°C. 1 ml 18MΩ grade water and 0.25 ml HNO_3 are added to the residue before re-sealing the vial and refluxing for 1 hour at 100°C. After cooling and agitation, a 1 ml aliquot is removed by an Eppendorf™ transfer pipette and transferred, quantitatively to a 15 ml clean PE sample vial together with 4 ml of 18 MΩ grade water. An appropriate volume of stabilised terbium internal standard solution is added at this stage before subsequent dilution with acid stabilised 18 MΩ grade water (2% HNO_3) to a final working volume of 10 ml. This solution is filtered before presentation for ICP-MS analysis to remove any particulate material that may interfere with the aspiration systems. It should also be noted that all laboratory equipment used in sample preparation is non-glass (pre-cleaned) to prevent analyte loss (and potential contamination) due to surface adsorption problems associated with the use of glassware. The working concentration of the internal standard must be consistent in blank, standard and sample solutions and in this case is maintained at a relatively high level (100 μg/kg) to negate the effects of any trace amounts of this element present in the sample.

Initial tests

Ten small aliquots of standard material were taken through the sample preparation procedures described above and presented for ICP-MS analysis. Calibration standards of 5, 10, 15 and 20 μg/L were made to accommodate the

typical values of uranium and thorium present in the standard material; The ICP-MS instrumentation is computer controlled, and an appropriate analytical procedure was written whereby the samples could be loaded into the associated auto-sampler and aspirated / analysed automatically. Standard instrumental optimisation procedures were performed and indicated that the ICP-MS instrumental parameters were in line with manufacturer's guidelines (detailed above). The calibration standards were aspirated first to generate appropriate calibration factors and again, later in the analytical schedule as an additional performance monitor.

Table 7.2 ICP-MS Results for initial tests using standard sediment.

Sample weight (mg)	[^{232}Th] µg/l in sol^{n}	[^{238}U] µg/l in sol^{n}	[^{232}Th] mg/kg in sample	[^{238}U] mg/kg in sample
10.31	5.059	1.307	12.27	3.17
8.88	4.427	1.195	12.46	3.37
12.38	7.232	1.650	12.58	3.33
11.31	5.788	1.627	12.79	3.60
10.41	4.841	1.374	11.63	3.30
11.37	5.503	1.497	12.10	3.29
18.20	8.028	2.122	11.03	2.91
14.17	7.360	1.652	11.22	2.91
13.87	5.991	1.724	10.80	3.11
12.97	7.712	1.864	12.94	3.59
Reagent blank	0.000	-0.004		

Chapter 8

Introduction to High Resolution Spatially Resolved Optically Stimulated Luminescence

Instrumentation has been developed over a series of years (Bailiff and Mikhailik, 2003) to enable the measurement of optically stimulated luminescence (OSL) across the surface of planar sections of material (ceramic and encapsulated sediments). Stimulation is achieved by the application of a focussed laser beam (Reliant 250D laser, principle wavelengths 488 nm and 514 nm i.e., blue/green stimulation). The position of the laser beam is effectively fixed, with spatial resolution being achieved by the employment of an X-Y motorised stage to effectively position the sample with sub-mm precision.

In common with other standard OSL measurement techniques, detection is achieved by the use of a sufficiently sensitive photomultiplier tube, positioned directly above the area of stimulation and incorporating an appropriate optical filtration system to prevent the detection of stimulating wavelengths.

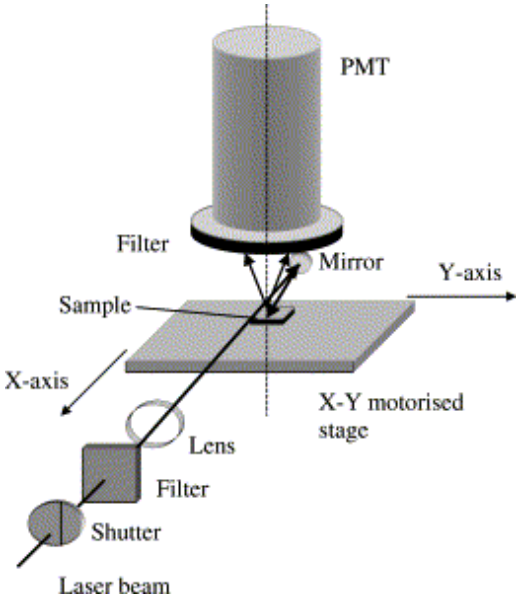

Figure X.X Schematic representation of spatially resolved OSL instrumnetation taken from Bailiff and Mikhailik, 2003.

The OSL signal can be measured at any pre-defined location on the sample surface (within the limits associated with the range and resolution of the motorised stage); the area to which stimulation is applied (and hence from which emission results) depends primarily upon the diameter of the laser beam and the optical properties of the chosen area (for example if stimulation is applied to a transparent crystal, the transmission / refraction of stimulating light may result in more diffuse emission).

Stimulation time is controlled by the use of a shutter mechanism (as used in photography) to interrupt the otherwise continuous laser beam. Beam intensity is controlled by the incident power applied to the laser and by use of a series of optical filters which may be removed or added depending upon the required intensity (e.g. neutral density filters). The beam diameter can be set to an appropriate value, routinely 250 μm.

The degree of spatial resolution is defined by the distance between each OSL measurement, and of course the beam size; by selecting a "step" size equivalent to the beam diameter (i.e. 250 μm) the entire surface of the sample can be scanned, although some areas may be missed due to geometric factors (i.e. a circular beam of area ~49000 μm^2 stimulating an effective sample area, (defined in this case by the "step" size of 250 μm) of ~ 62500 μm^2. In practice, the beam profile is likely to be such that stimulation will extend beyond the measured 250 μm diameter and effectively overlap slightly into neighbouring regions. For a typical sample (ceramic slice) the measurement area is 10 mm x 10 mm, which equates to a total of 1600 individual measurements when a step size of 250 μm is selected.

When the laser is used in "low-power" mode, and with the incorporation of neutral density filters to further reduce the beam energy, the system can be used to identify the presence of emitting species, without fully depleting the OSL

signal from emitting species. In this mode of operation, and by stimulating sequentially at pre-defined intervals, it is possible to "scan" across the entire surface of a sample, to detect localised areas of higher luminescence intensity that may subsequently be used individually in dose reconstruction procedures. Here, the beam position can be manually re-directed (by imputting experimentally determined X,Y co-ordinates) to highlighted areas of interest; The application of higher intensity stimulation, with data points recorded at pre-selected time intervals (typically 1 ms), enables the characterisation of the OSL decay curve as the signal is fully bleached (i.e. returns to background intensity).

Alternatively, scanning techniques may be employed initially at full laser power, and reduced beam attenuation, to attempt to fully deplete regions of OSL emission across the surface of the sample; The application of regenerative dose procedures, with subsequent repeat scanning enables dose-reconstruction to be performed simultaneously across the entire surface of the sample – areas of interest are highligted by the use of a simple Excel spreadsheet (see Fig 8.2, Fig 8.3, Fig 8.4). This procedure is useful for routine measurements where a number of individual luminescent regions may be present and negates the requirement for time consuming individual repeat determinations at numerous points across the sample surface. Decay curve characterisation, however, is not routienely possible with this "fast scanning" technique as accrued data are derived from the cumulative signal measured over a pre-defined time interval (typically 1 s). These techniques have been used in recent research which aims to date single grains in-situ (Bailiff, 2006)

The substitution of the blue/green stimulation source with an IR emitting diode enables the potential "mapping" of emitting feldspathic materials across the sample surface by measurement of the associated IRSL signal. Differentiation between quartz and feldspathic emissions may also be achieved by the use of

Time-Resolved Luminescence measurements, where the time difference between stimulation (excitation) and emission can be used to differentiate between the two mineral species (Clark and Bailiff, 1998; Bailiff, 2006).

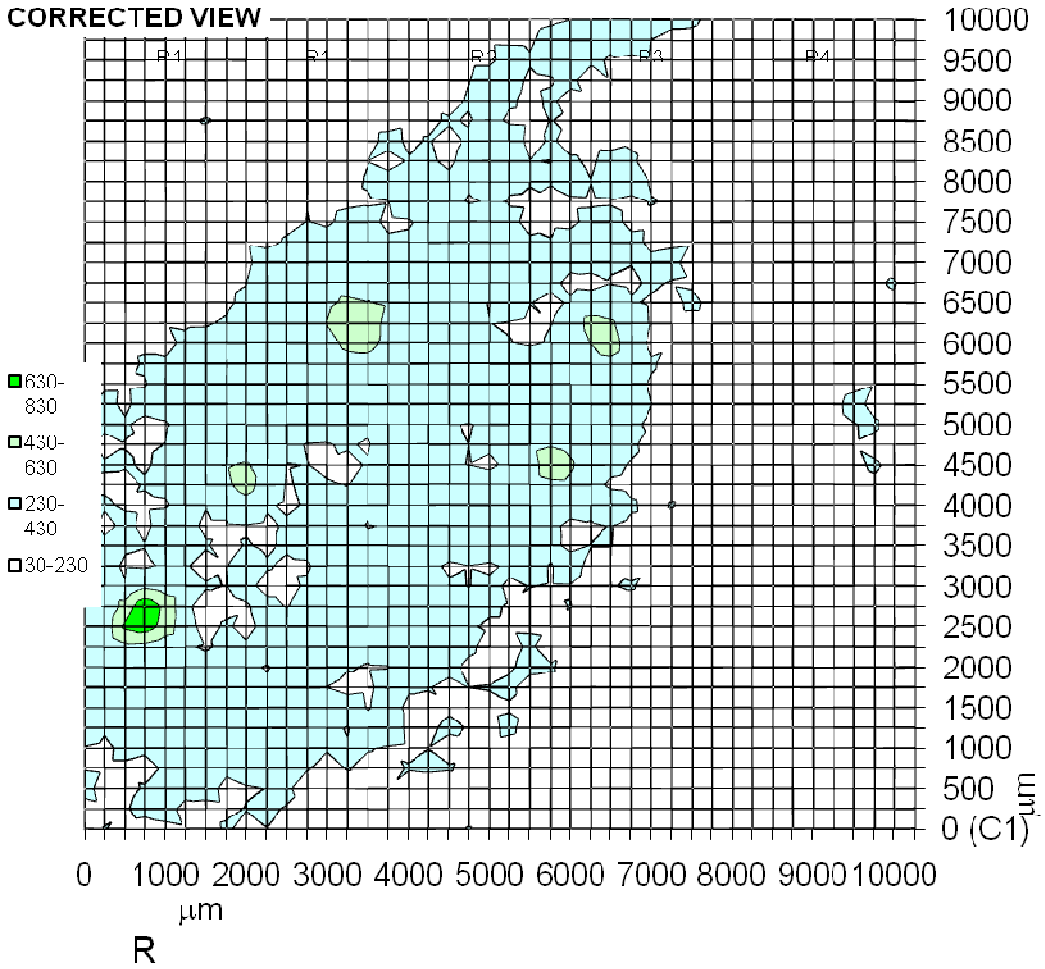

Figure 8.2 Graph showing measured OSL intensity across the planar surface of a sample of granite. In this example, areas of higher intensity are shaded blue/ green. This type of graph is produced by incoporating the numerical raw data (intensity) produced sequentially during scanning measurements into a standard grid format.

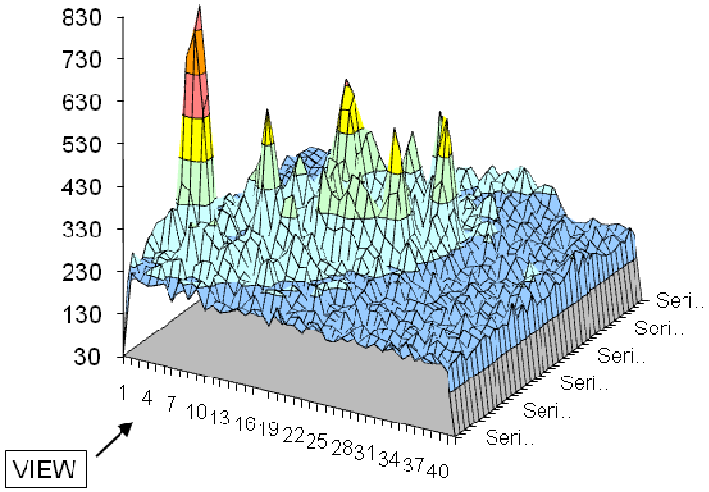

Figure 8.3 Graph shown in Fig 9.2 reproduced in a three-dimensional format whereby OSL intensity is expressed as "peak height" on the Z axis.

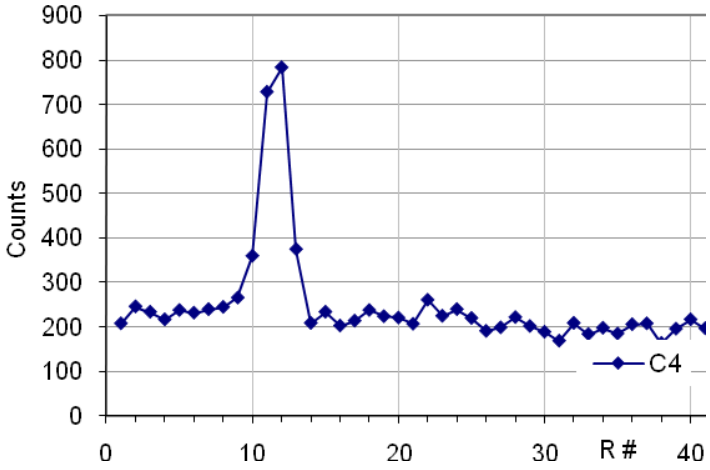

Figure 8.4 Line graph showing OSL intensity with relation to sample position across a single data row. This type of graphical representation can be useful in the recognition of areas of interest, when the photon count is only slightly higher than that associated with background / mean sample matrix rate.

A further routine application of high-resolution spatially resolved luminescence that has been developed in the laboratory is the determination of the frequency of occurrence of "bright" gains in the disaggregated material used in standard laboratory OSL measurements. This is particularly important in the dating of sediments, where individual grains may vary with respect to dose rate and bleaching history.

Pseudo-single grain OSL measurements are performed using very small aliquots of disaggregated material (typically 15-20 grains) on the assumption that OSL signal may be derived from a single bright grain (the validity of this assumption depends upon the ratio of bright grains to non-emitting or weakly emitting grains). After all OSL measurements have been made, the material is scanned in situ (i.e. still mounted on a stainless steel disc). The actual number of emitting species is often clearly apparent (Fig. 8.5 and Fig 8.6) and this value is used to provide important supplementary information to the paleodose determinations derived from each aliquot.

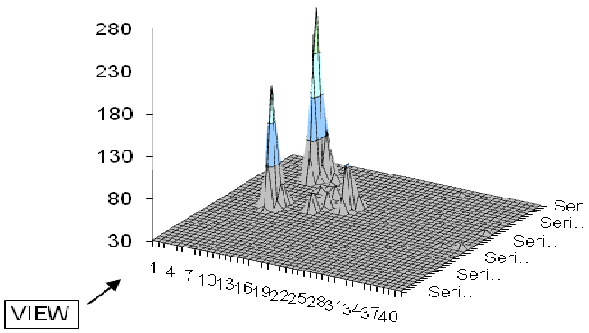

Figure 8.5 OSL scan of a very small aliquot of disaggregated material, in which it is apparent that emission is derived from at least two grains.

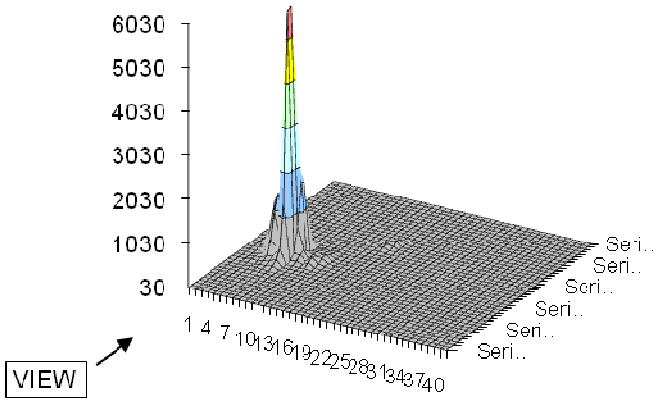

Figure 8.6 OSL scan of a very small aliquot of disaggregated material, in which it is apparent that emission is derived from one bright grain.

Chapter 9 - Case studies

Introduction

A number of samples were chosen for to represent the different archaeological materials encountered routinely. Numerous examples of archaeological brick were chosen to represent the variable nature of this material, whilst only one sediment was tested to represent a potentially complex example of this type of material.

A 321-1 (Brick)

B 316-2 (Sediment)

C 294-1 (Brick)

D 294-17 (Brick)

E 304 (Brick)

Case study A - Sample 321-1

Introduction

Sample 321-1 is one of a series of ceramic (brick) samples taken from the 9th century church of St. Philbert de Grand Lieu, located in north-west France. This site represents an important example of Carolingian architecture, and is the site from which samples were taken for a European collaborative research project involving the application of scientific dating methods to ceramic building materials.Work carried out by the participating laboratories of the "Groupe de Recherche Européen (GdRE) - Terres cuites architecturales et datation " involves the inter-laboratory comparison of a number of dating techniques applied to samples of building ceramic taken from identified sites of interest. This sample is also of particular relevance to the work carried out within the scope of this research topic as the sample matrix is particularly complex, with a number of variably sized crystalline inclusions dispersed throughout a continuous matrix that has non-uniform visual characteristics.

9.a.1 Digital analysis and photomicrography

1 mm x 1 cm x 1 cm slices were prepared from a small sub-sample of material for use in scanning experiments to measure the distribution of luminescent species across the surface of the sample. After all appropriate measurements were made, digital photographs of the slice were taken using a Nikon Coolpix digital camera, coupled to the eye piece of a binocular microscope using appropriate magnification (10x) to provide the best resolution across the surface area of the

sample (Fig. 9.a.1). Adobe Photoshop ™ was then used, as described in Chapter 6, (Section 6.2.1) to highlight subtle differences in matrix colour and texture in order to reveal the presence of multiple matrix component phases and / or effects caused by poor mixing during manufacture or heterogeneity of parent clay materials (Fig 9.a.2).

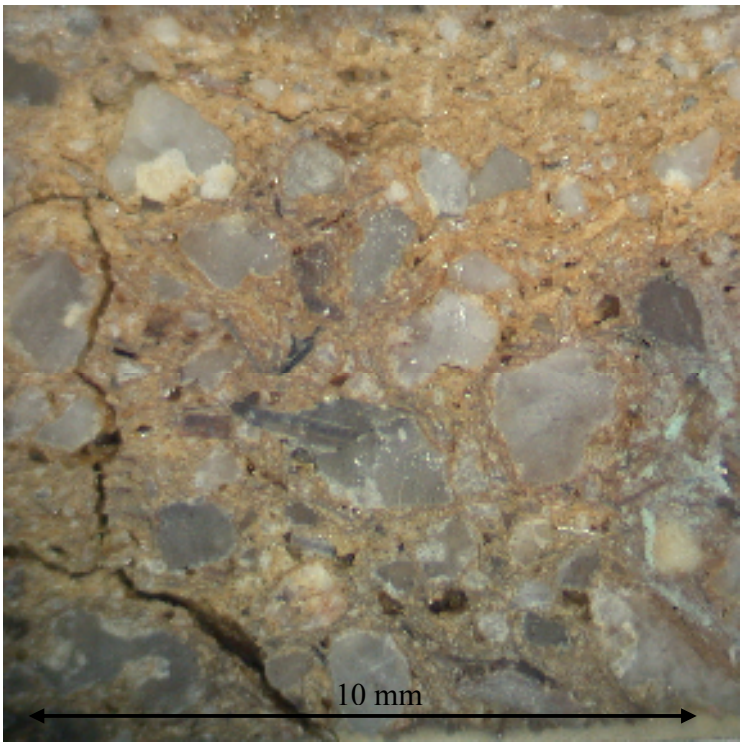

Fig.9.a.1 Digital photomicrograph of sample 321-1 (slice 7)

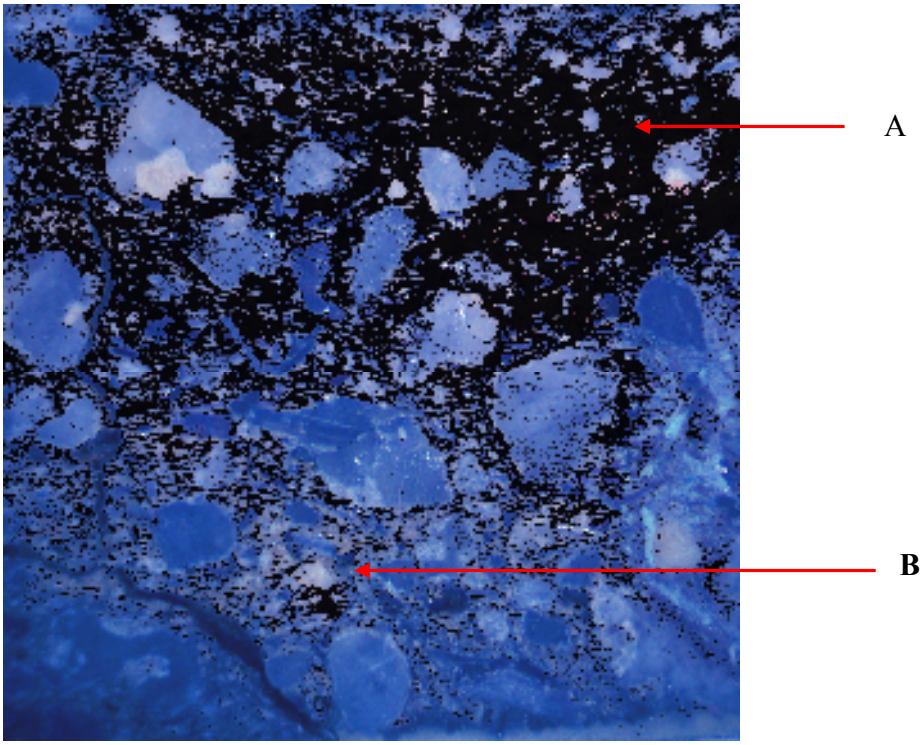

Fig 9.a.2 Digitally enhanced version of Fig.9.a.1

Sample 321-1 displays visual heterogeneity with respect to the size and distribution of the included crystalline materials and this sample appears to be composed of two different matrix components, where the term matrix refers generally to the fine grain phase in which crystalline and other mineralogical materials are embedded. The phase located towards the top of the image (A) that has been digitally altered to appear darker in colour forms the dominant material in this region, whereas the area towards the lower section of the image (labelled B) represents an interface between the two phases

.

Additionally, there appears to be a lower concentration of larger crystalline inclusions in phase A which may indicate a correlation between matrix component material and crystalline content.

It is feasible that in the manufacture of a structural ceramic, the addition of a second type of clay raw material, containing fewer included minerals could be used to enhance the physical and firing properties of an initial, inclusion rich clay type. The size of the included crystals implies that this material was present naturally (e.g., resulting from parent rock weathering) in the raw materials used, as the sourcing and use of quartz grains of this size for addition as a tempering agent would not be practical.

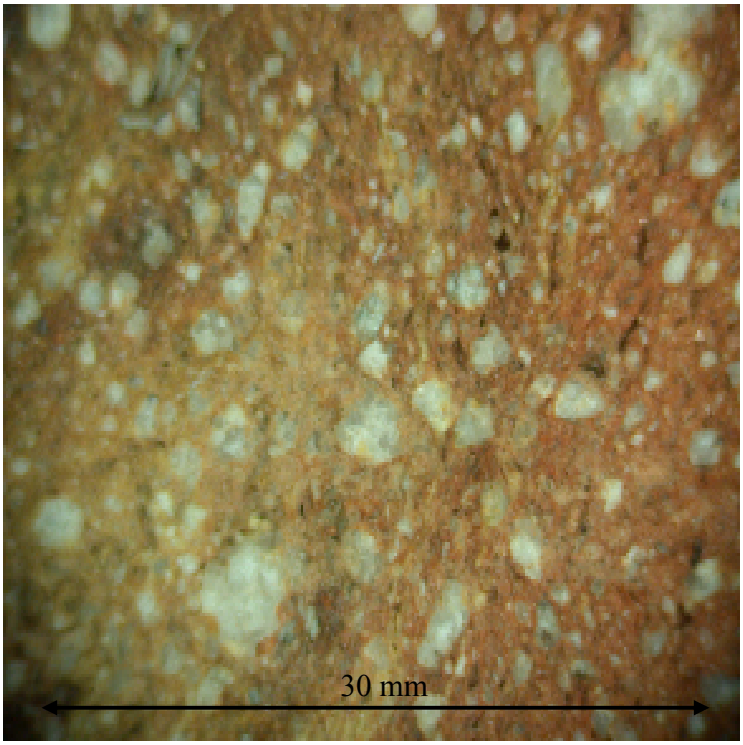

Fig 9.a.3 Digital image of sample 321-1 core cross section (30 mmx30 mm) which demonstrates material heterogeneity on a larger scale.

9.a.2 Staining techniques

The chemical staining techniques (Section 6.1.3) were applied to the sample after digital enhancement and SSNTD autoradiography techniques were performed. It was decided not to use an eosin stain, as the presence of potassium rich species was clearly evident.

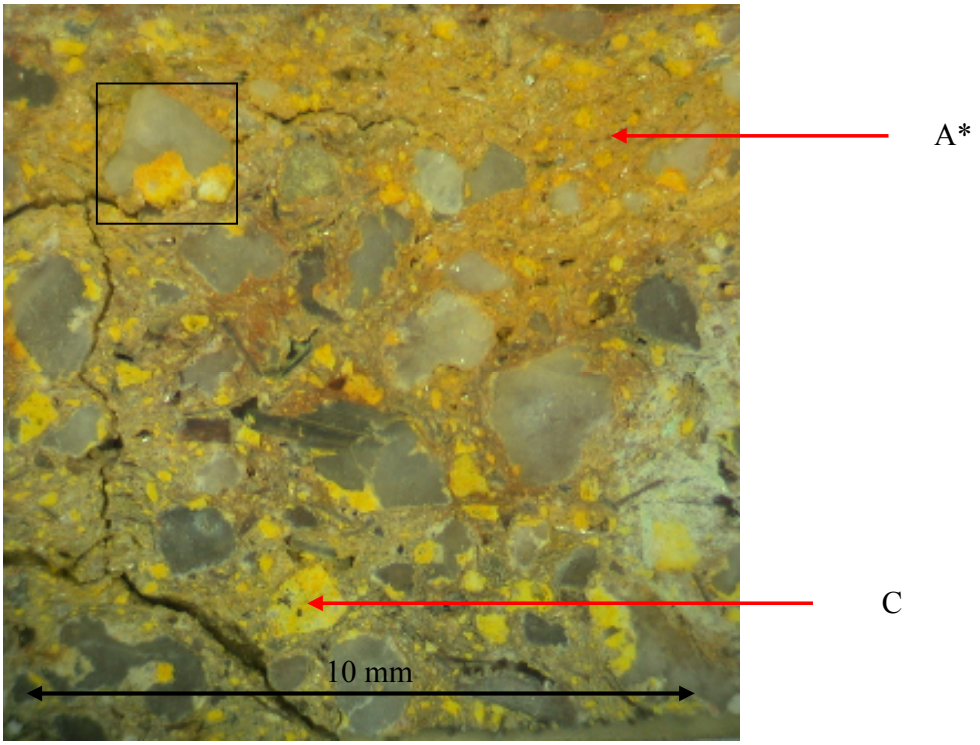

Fig 9.a.4 Digital photomicrograph of sample 321-1 (slice 7) after staining

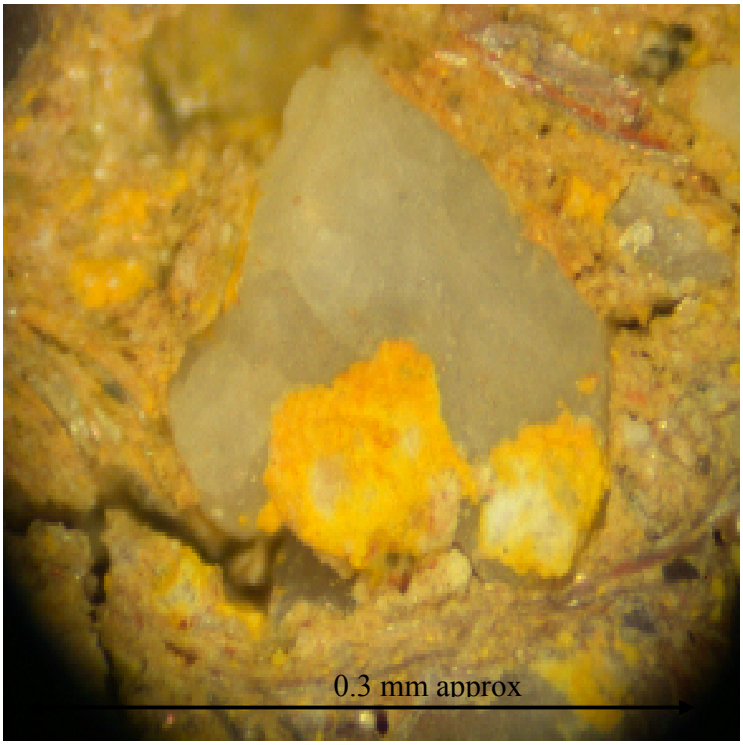

Fig 9.a.5. Digital photomicrograph of area of interest highlighted in Fig 9.a.4.

The staining techniques highlighted several interesting features with respect to the distribution of potassium - bearing minerals across the surface of sample 321-1 (slice 7 – Fig.9.a.4). Primarily, the mineral phase highlighted by digital enhancement (Fig 9.a.2 section A) demonstrated a positive reaction with the sodium hexanitrocobaltate (III) stain, (Fig 9.a.4 section A*) whereas the second phase (B) appeared to have remained unchanged. The observation that the two mineral phases have distinctly different potassium concentrations (with regard to staining potential) has important implications with respect to the assessment of localised heterogeneity of the ^{40}K beta derived matrix dose-rate.

The presence of a number of included potassium rich minerals was also revealed (Fig. 9.a.4 labelled C, for example).

A further interesting aspect highlighted by the use of staining techniques can be seen in Fig 9.a.5., where a photomicrograph has been produced at a higher level of magnification to reveal the presence of a potassium rich mineral which appears to be lying adjacent to a quartz grain and is dosimetrically important, being within the range of beta particles emitted by ^{40}K.

9.a.3 Alpha autoradiography

Following the experimental procedures described in Chapter 5, a 1 cm x 1 cm x 1 mm section of CR-39 SSNTD detector (non-scribed) was placed in direct contact with sample 321-1 (slice 7) and left, undisturbed, in a sealed container for 12 months (Fig 9.a.6). The experiment was then repeated with a sample-detector contact period of 3 months, using a CR-39 detector that had been scribed to produce a detector grid composed of 25 equivalent detection areas. In routine determinations for samples of typical activity (see Chapter 5) a contact period of 4 months should be sufficient to highlight any areas of increased local alpha activity. The initial extended contact period was chosen to enable the production of an alpha autoradiograph that could be used to qualitatively highlight the distribution patterns of alpha emitters across the full surface of the sample slice, without the requirement for the higher levels of magnification associated with shorter detection times.

The detectors were subsequently etched for 6 hours at 70^{o}C in a 6.25N solution of sodium hydroxide, before rinsing with deionised water and being allowed to dry at room temperature.

Individual tracks are clearly visible under 100 X magnification and this method is used (with the production of digital photomicrographs) to produce quantitative

counting data for track density for each of the 25 discrete grid sections across the surface of the detector.

When very large numbers of tracks are present, the optical characteristics of the CR-39 can be exploited to produce a macro autoradiograph in which the distribution patterns of alpha emitters across the entire surface of the detector can be seen. Using a binocular microscope and 10 X magnification, a "swan-neck" directional light source, was used to illuminate the sample transversely; light passes through the bulk detector material, but is absorbed / reflected by the areas of high track density; hence these areas become "visible" and enable the production of digital autoradiographs (Fig 9.a.7).

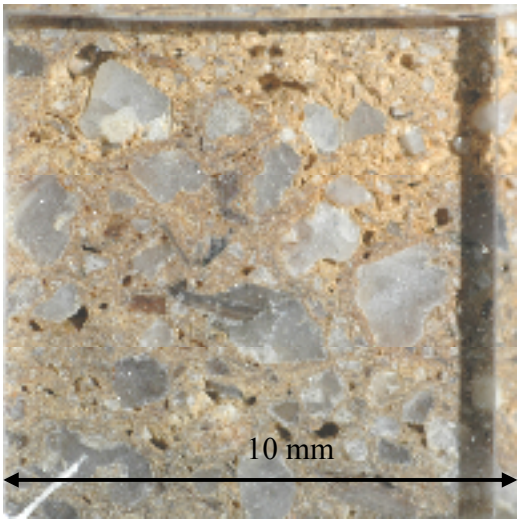

Fig 9.a.6 CR-39 detector in contact with sample 321-1 (slice 7)

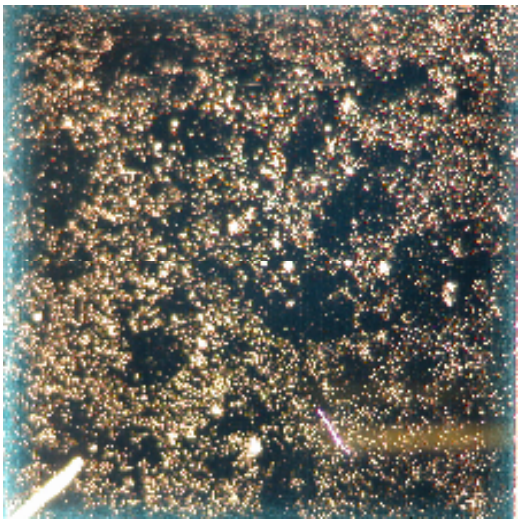

Fig. 9.a.7 Alpha autoradiograph of sample 321-1 (slice 7) 12 month contact time.

Discussion macro – alpha autoradiography

The distribution of alpha emitters across the surface of the sample is clearly heterogeneous; there is a positive visual correlation between larger crystalline inclusions and areas of reduced alpha activity (dark areas); the concentration of

uranium and thorium in quartz is expected to be lower than the clay rich matrix in which these crystals are included and this has been demonstrated in this example.

The discrete matrix phases that were seen to differ substantially in potassium concentrations do not appear to vary considerably with respect to the distribution of alpha emitters.

It is interesting to note that the presence of a number of small areas of increased alpha activity is evident throughout the material, appearing in the autoradiograph as small bright spots. The calculations below will be used to quantify the extent to which activity is increased in these, compared to "background" matrix activity, together with the use of additional analytical techniques to determine the chemical nature of these regions.

Initial Excel simulations using randomly generated points on a grid of arbitrary surface area (Chapter 5) indicated that an increased local activity equal to 10 – 20 times background matrix activity is required to "expose" such areas of higher activity; an attempt to quantify local activity in these areas will be performed later in this chapter, using high level magnification (400x) and the use of a microscope calibration slide to quantitatively determine counting area.

Detailed microscopic investigation revealed no apparent visual correlation between matrix composition and the presence of these localised areas of high activity; the occurrence of these areas, apparently located within the regions of low alpha activity that correlate visually with the cross section of several large crystalline inclusions is important to highlight with regard to dosimetric considerations.

As discussed previously, the presence of an internal alpha source has the potential to significantly increase the localised levels of radiation dose absorbed

by a phosphor grain and this may increase the levels of uncertainty associated with the luminescence dating technique if undetected, particularly if the grain displays high luminescence sensitivity. The routine use of ICP-MS to determine the concentration of uranium and thorium in the quartz grains used for luminescence dating may potentially highlight this effect; current techniques are based on the analysis of bulk quartz samples (recycled grains from several aliquots) rather than individual grains and as such determinations provide an average concentration value without offering the capability to identify the existence of high alpha activity inclusions that originate from within individual quartz grains.

The 90-150 μm grain size fraction was used in OSL dating techniques (disaggregated grains) for this sample; because the extracted purified quartz was somewhat friable in nature, it was not possible to attempt single grain determinations of U and Th concentration. As ICP-MS is a destructive technique it must only be used during the final stages of the experimentation to provide quantitative data about the chemical composition of single grains extracted directly from the sample matrix.

Semi-quantitative autoradiography

Photomicrographs of individual grid sections were taken at 40x magnification which was sufficient to allow alpha track recognition and to enable counting across each full grid section (1.6 mm x 1.6 mm). Two areas of increased alpha activity were examined at higher magnification (100x) and subsequent photomicrographs were calibrated using a 1 mm calibration slide, with 10 μm resolution to enable calculation of localised activity per unit area.

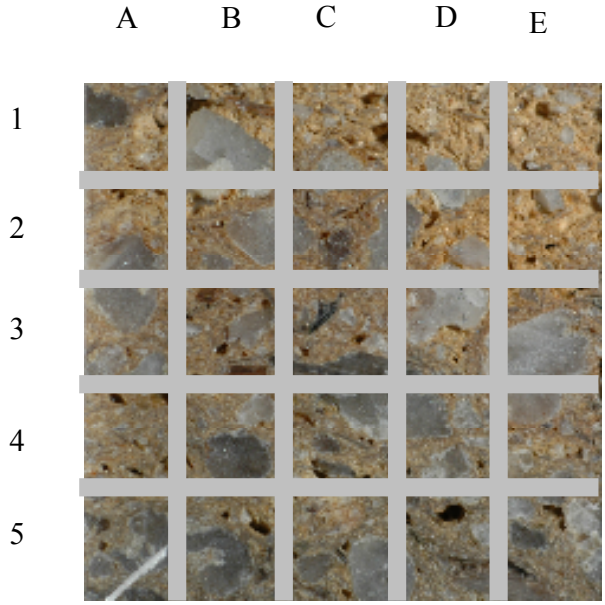

Fig 9.a.8 Representation of scribed CR39 detector/ 321-1 (S7)

81	106	83	61	53
160	127	88	166	63
100	157	169	138	265
128	122	117	224	125
85	128	139	114	144

Fig 9.a.9 Grid showing tracks per counting area with higher track densities shown in red

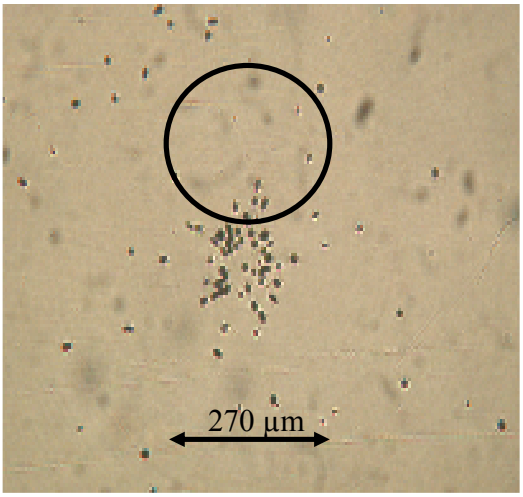

Fig 9.a.10 Photomicrograph (100x) showing an area of high activity (CR-39 grid section E-3)

Calculations

The sample – CR-39 detector contact time was 90 days. The counting area per individual grid section is effectively reduced by the grid scribing process in which a surface channel of 0.5 mm thickness is removed per scribed gridline. Each effective countable area measures 1.6 mm x 1.6 mm (2.56 mm^2).

Results based upon 25 equivalent measurements made across the detector surface -

Mean track density	= 125.7 tracks / 2.56 mm^2.
Total number of tracks counted	= 3143
Variance (of calculated mean)	= 75.5 %
Adjusted track density	= 4910 tracks cm^{-2}

Using a mean alpha range of 25 μm, a CR39 detector area of 1 cm^2, and an arbitrary material density of 2.6 g cm^{-3}, the volume of matrix material from which alpha particles can reach the detector is 0.0025 cm^3 which results in a contributing material mass of 6.5 mg (derivation given in Chapter 5, and further validation given in Appendix A).

In reality, the density of archaeological bricks is likely to vary considerably due to porosity and inherent material heterogeneity. The true alpha range value is also likely to vary substantially due to density and compositional effects; the density and range values used below are applicable to typical archaeological ceramics (Aitken ,1985) and as mentioned earlier in Chapter 5, calculated values for activity should be regarded as semi-quantitative.

The number of alpha particles that reach the detector with sufficient energy, and at an appropriate angle, to result in the production of a developable track is significantly lower than the total number of alpha emissions occurring within the material; The application of a geometry factor (1/4) and an efficiency factor (an initial value was derived experimentally in Chapter 5, with an approximate value of 65% for U and Th assuming equal activity levels) must be applied.

The calculated total number of alpha emissions (per 6.5mg of sample) in 90 days is now ((4910 x 4) / 0.65) = 30215

Rate of emission = (30215 / (90*86400) = 3.89 $x10^{-3}$ emissions per second.
Converting to standard units, (and still assuming a contributing mass of 6.5mg) the mean sample activity is 598 Bq kg^{-1}

Assuming equal activity for thorium and uranium, with no disruption to secular equilibrium it is possible to calculate the concentrations of both species.

Uranium concentration
299/ 102.4 = 2.9 ppm uranium (where 102.4 refers to complete decay series alpha activity of ^{238} U and ^{235} U at typical levels of abundance).

Thorium concentration
299/ 24.36 = 12.3 ppm thorium (where 24.36 refers to complete decay series alpha activity).

The mean surface activity of sample 321-1 agrees well with the previously calculated typical value of 558 Bq kg^{-1} (Chapter 5) and the verification of the calculated concentrations of uranium and thorium by the use of quantitative methods will be discussed later. The high standard deviation value (variance = 75.5% of mean count value) is unsurprising given the heterogeneous nature of the distribution of alpha emitters highlighted previously by macro – alpha autoradiography.

Calculation of localised high activity levels.

By comparing the observed track density in the two areas of localised high activity (Fig 9.a.9 sections E-5 and E-3) to the mean surface track density it is possible to estimate the extent to which activity is increased in this area. The calculations below assume that alpha contributing material thicknesses for the two areas of high activity is equivalent to the calculated value used previously. In reality, the contributing thickness may be considerably less (described in chapter 4) in which case the calculated localised activity values must be regarded as minimum values only.

Grid section E-5

Localised area = approximated circle of radius 170 μm = 0.0908 mm^2

No of tracks	= 135
Track density (135/0.0908)	= 1487 tracks mm^{-2}
Adjusted track density	= 148700 tracks cm^{-2}
Mean matrix track density	= 4910 tracks cm^{-2}
Localised activity / mean activity	= 30.3
Estimated minimum thorium concentration	= 370 ppm
Estimated minimum uranium concentration	= 86 ppm

Grid section E-3

Localised area = approximated circle of radius 135 μm = 0.0573 mm^2

No of tracks	= 47
Track density (47/0.0573)	= 820 tracks mm^{-2}
Adjusted track density	= 82024 tracks cm^{-2}
Mean matrix track density	= 4910 tracks cm^{-2}
Localised activity/ mean activity	= 16.70
Estimated minimum thorium concentration	= 204 ppm
Estimated minimum uranium concentration	= 48 ppm

The calculated values for minimum thorium and uranium concentrations in the selected regions of high alpha activity are based on the assumption of equal U and Th activity, in accordance with natural abundance values.

9.a.4 Scanning Electron Microscopy

The use of SEM facilities located at one of the GdRE partner laboratory (Bordeaux) were kindly made available for the examination of this sample. Current facilities did not include scanning multi-elemental SEM determination and hence a number of key sample areas were highlighted for examination, based on the results from macro autoradiography. Sample 321-1 (slice 7) was kindly taken to the University of Bordeaux by Sophie Blain, who has involvement at the luminescence laboratories in both Durham and Bordeaux. SEM analyses were performed at the highlighted areas (Fig 9.a.11) and an interpretation was provided by specialist SEM staff. The SEM model used was the JEOL-6460LV (low vacuum) with a 20 k eV electron beam.

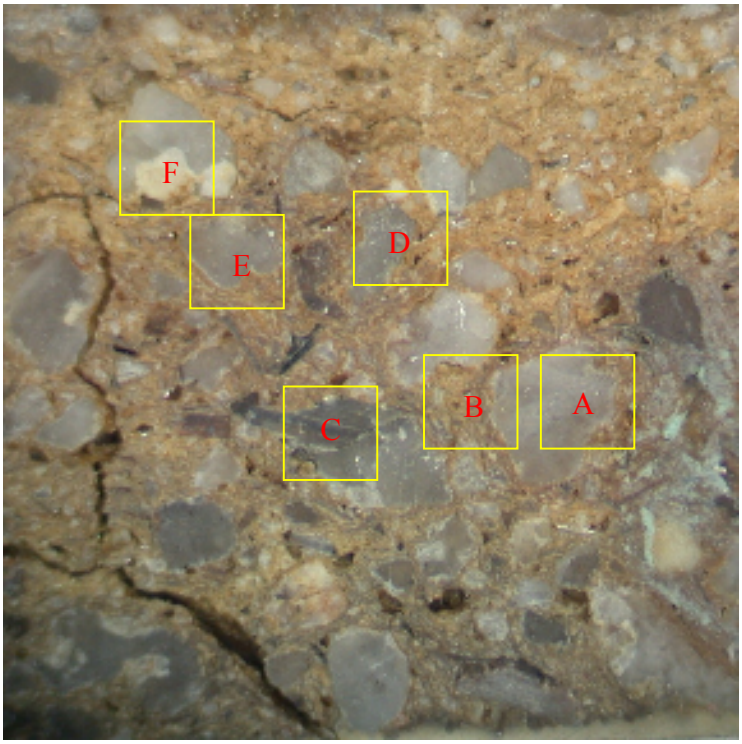

Fig 9.a.11 321-1 (S7) Highlighted SEM locations

9.a.1.4.1 SEM results Section A

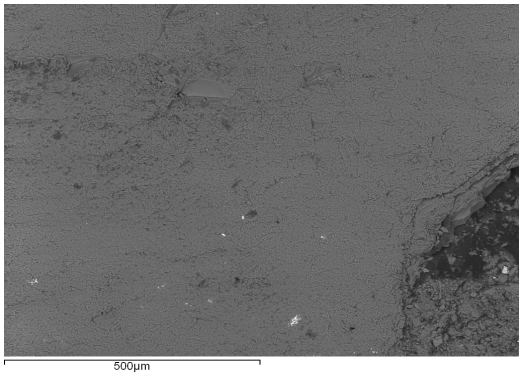

Area A: Electronic picture

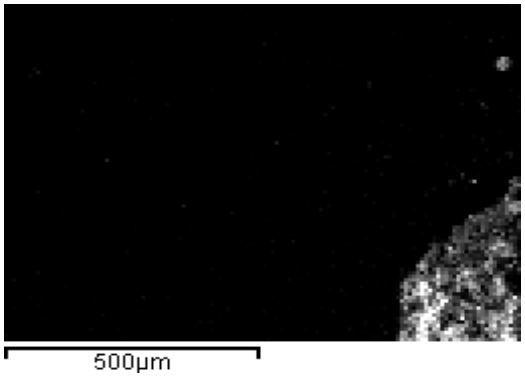

Al-map

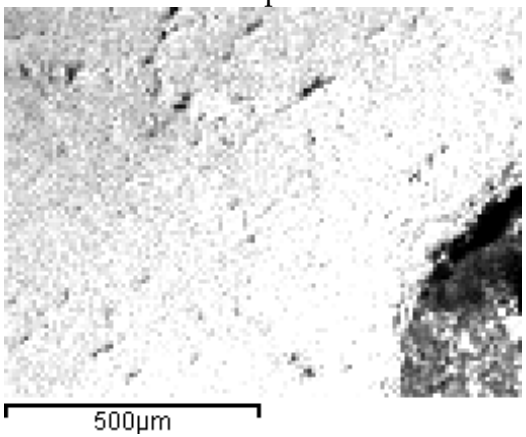

Area A: Si Map

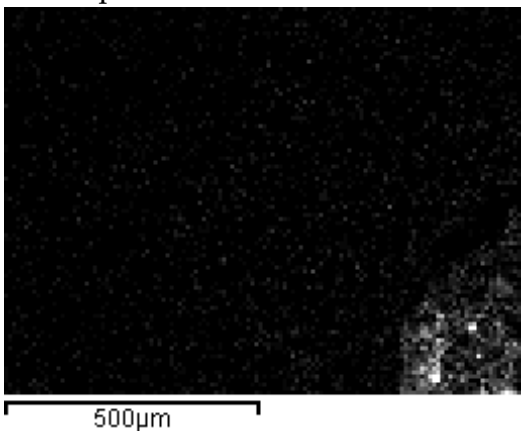

K Map

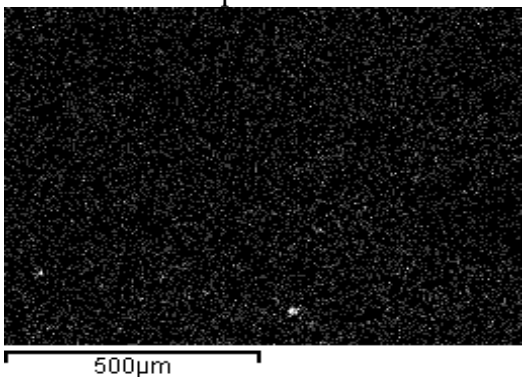

Area A: Ce map

9.a.1.4.2 SEM results Section B

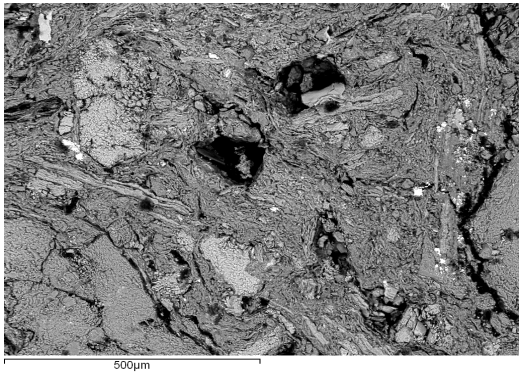

Area B: Electronic picture

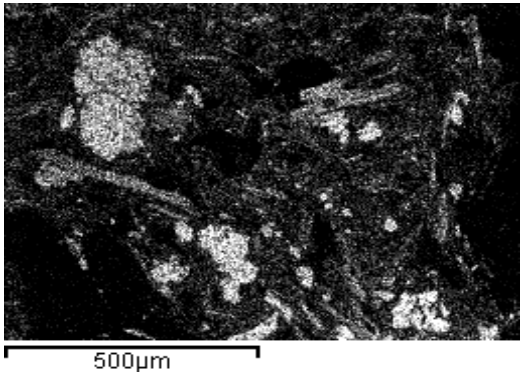

K map

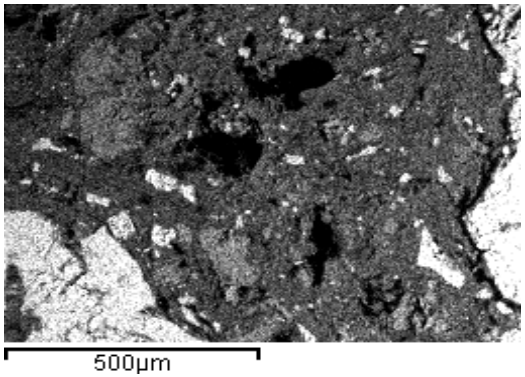

Area B Si Map

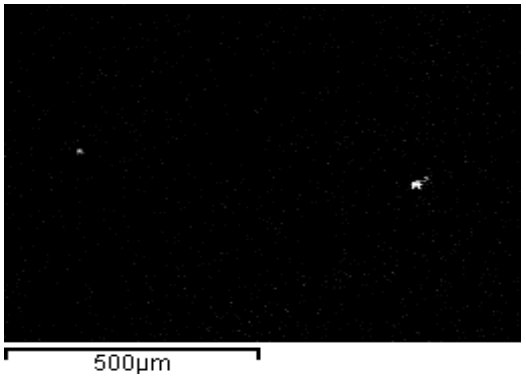

Zr Map

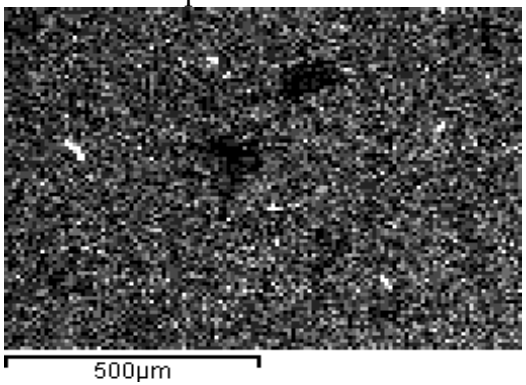

Area B: Ce map

9.a.1.4.3 SEM results Section C

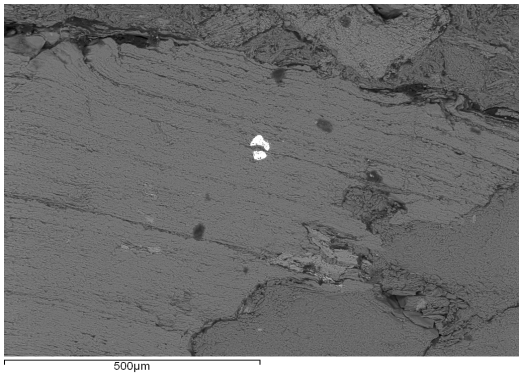

Area C: electronic picture

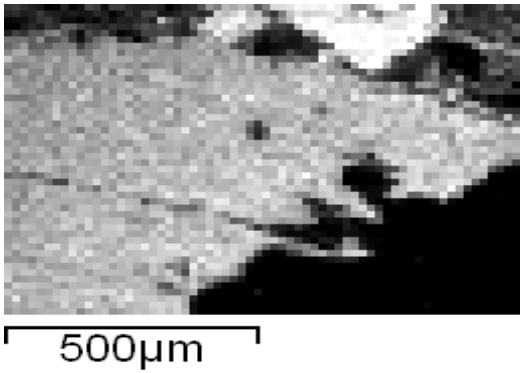

K map

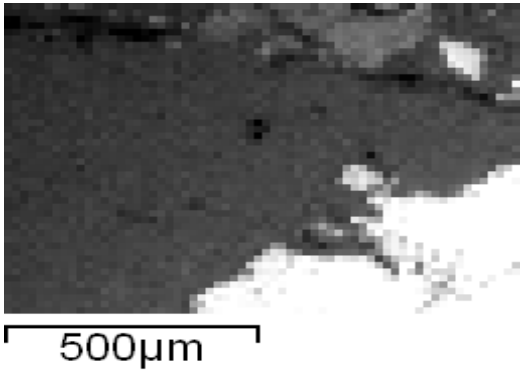

Area C: Si Map

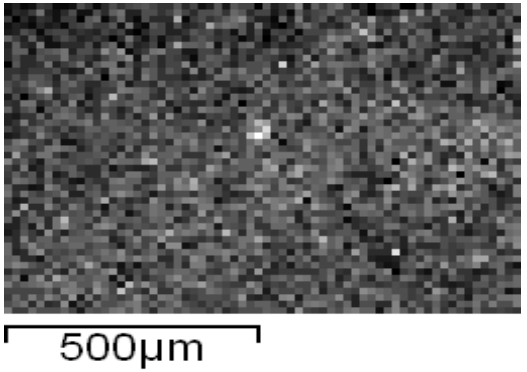

Th Map

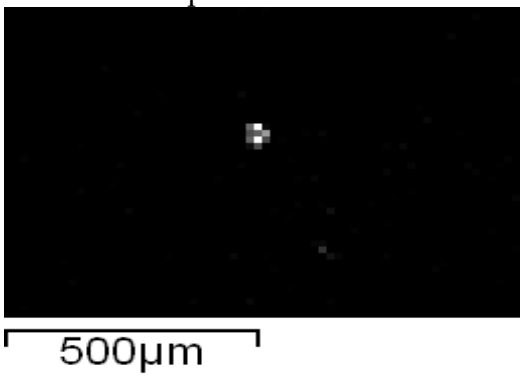

Area C: Ce map

9.a.1.4.4 SEM results Section D

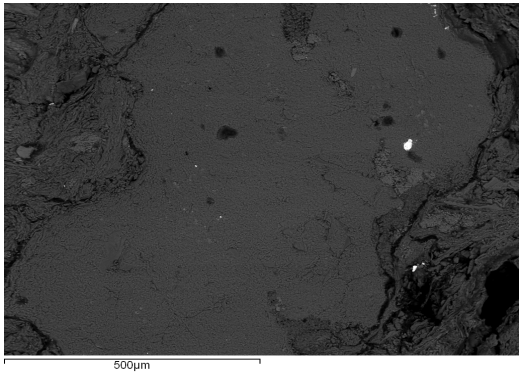

Area D: Electronic picture

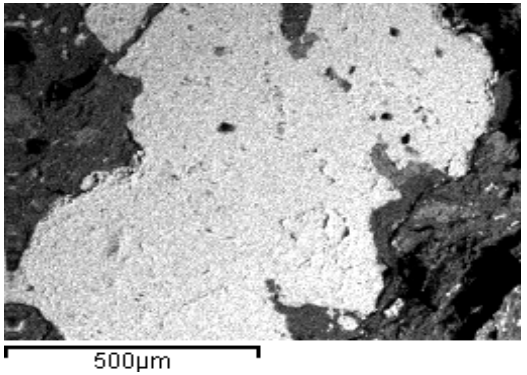

Si Map

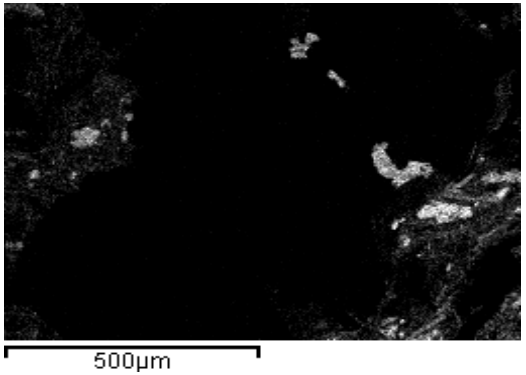

Area D: K Map

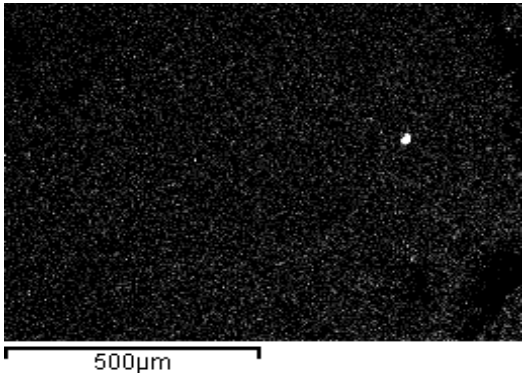

Ce map

9.a.1.4.5 SEM results Section E

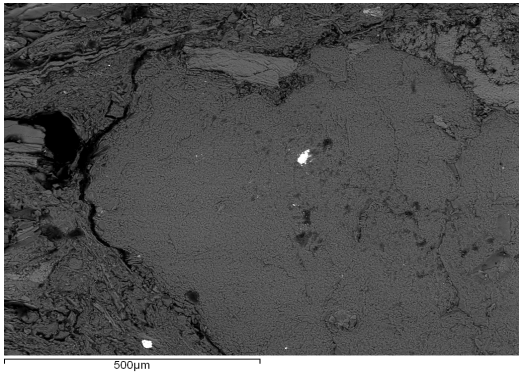

Area E: electronic picture;

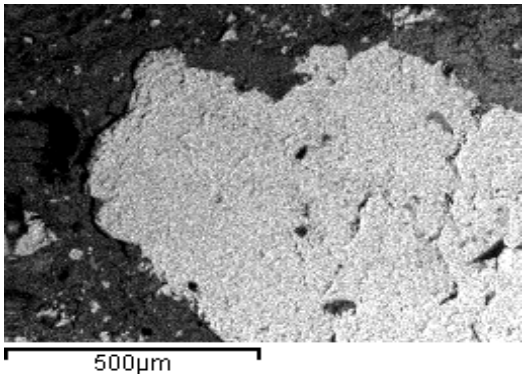

Si map

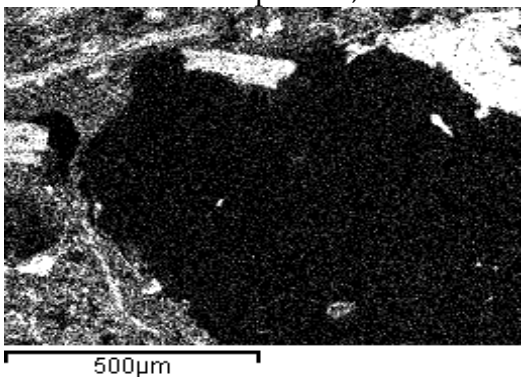

Area E: K map

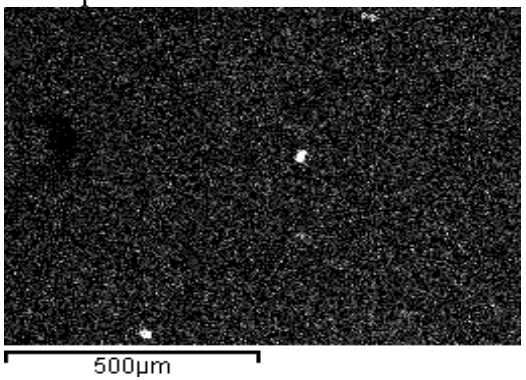

Ce map

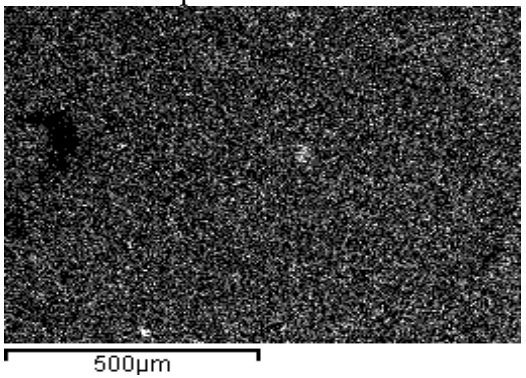

Area E: Th map

9.a.1.4.6 SEM results Section F

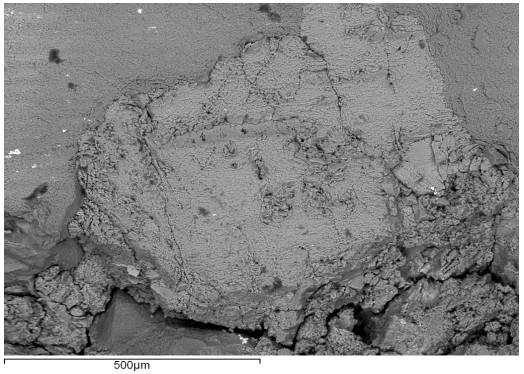

Area F: Electronic picture;

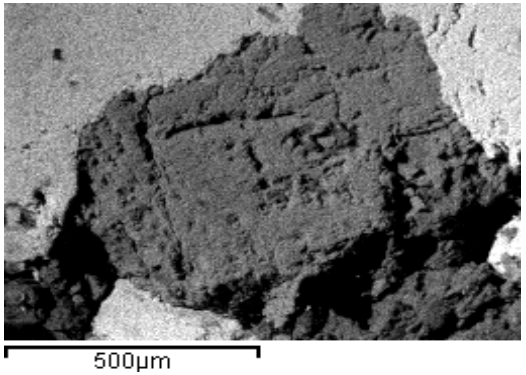

Si Map

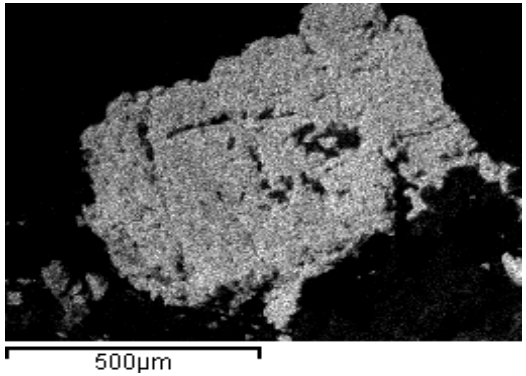

Area F: K map

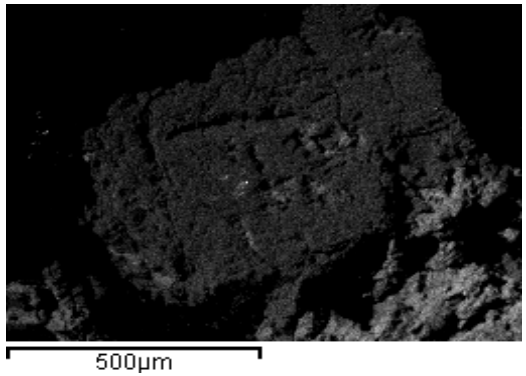

Al Map

SEM – Interpretation of results

Section A

This section was chosen as the macro alpha autoradiograph highlighted (Fig. 8.7) what appeared to be a region of high activity situated within an area of reduced activity, assumed to be quartz. SEM analyses confirmed the absence of any major elemental components other than silicon, however the presence of thorium, zirconium or cerium (an indicator for the presence of Monazite) was also undetected. Whilst this method is not sensitive to the presence of uranium, it is unlikely that this element would be present without zirconium or other associated elements. In this case it is possible that the area of high activity highlighted by alpha autoradiography was particulate in nature and was displaced during transportation of the sample or was not included in the relatively small area on which SEM analysis was performed. See Fig. 9.a.1.4.1 for electronic picture and elemental maps (Al,Si,K,Ce).

Section B

This section was chosen due to the presence of regions high alpha activity at what appeared to be the quartz inclusion – matrix interface. SEM analysis revealed the presence of both zircon and Monazite grains embedded within the clay matrix. The sub-mm asymmetry in the distribution of potassium bearing minerals was also highlighted. See Fig. 9.a.1.4.2 for electronic picture and elemental maps (K,Si,Zr,Ce).

Section C

This section was chosen because of the presence of localised high alpha activity and the appearance of a mineral inclusion which displayed

different visual characteristics to the other large inclusions. SEM analysis revealed the presence of an interface within the inclusion between two differing minerals (quartz and feldspar). The presence of a fractured monazite grain within the feldspathic component was also detected. See Fig. 9.a.1.4.3 for electronic picture and elemental maps (K,Si,Th,Ce).

Section D

This section was chosen because of the presence (from alpha autoradiography) of a localised area of high alpha activity, apparently located within an area of low activity (assumed to be quartz). SEM analysis revealed the presence of both feldspathic and monazite inclusions within the quartz inclusion. See Fig. 9.a.1.4.4 for electronic picture and elemental maps (Si,K,Ce).

Section E

Again, this section was chosen because of the apparent presence of a region of high alpha activity located within an assumed quartz inclusion. As with section D, the presence of both feldspathic and monazite inclusions within the quartz grain was confirmed. See Fig. 9.a.1.4.5 for electronic picture and elemental maps (Si,K,Ce,Th).

Section F

This section was chosen because of the apparent visually differing phases within a single mineral inclusion. The presence of potassium rich feldspar was subsequently highlighted by the application of staining techniques and this result was confirmed by SEM analyses which indicated the presence of a feldspathic inclusion within, and peripheral

to, the quartz grain. Thorium, zircon and monazite were not detected (hence absence of elemental maps) which corresponds to the region of low alpha activity seen in Fig. 8.7. See Fig. 9.a.1.4.6 for electronic picture and elemental maps (Si,K,Al).

9.a.5 ICP-MS and AAS.

Micro sampling procedures (described in Chapter7, section 7.1.5) were performed at several regions of interest across the surface of sample 321-1 to provide quantitative data for the concentrations of potassium, uranium and thorium (fig 9.a.) associated with the discrete phase components highlighted by the use of the auto radiographic and staining procedures.

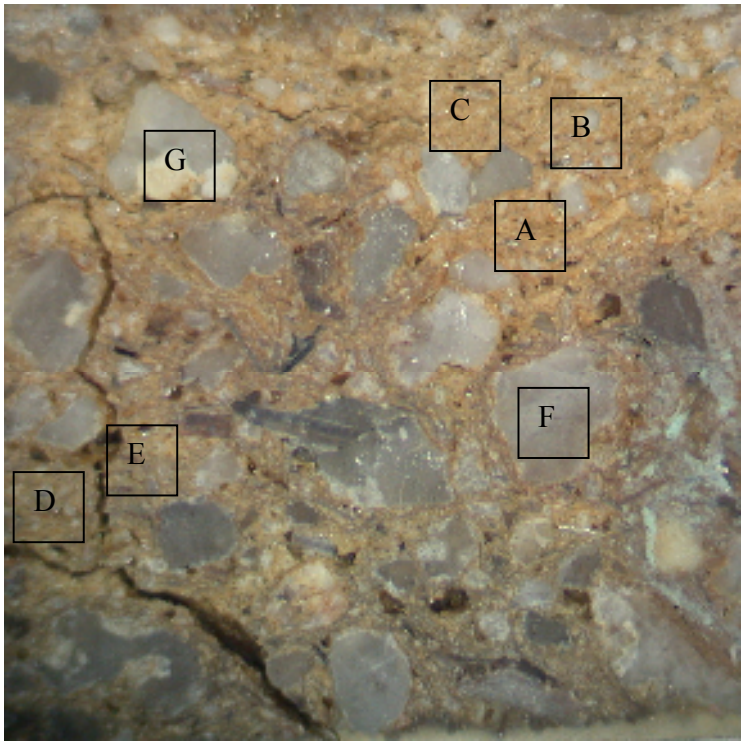

Fig. 9.a.12 Representation of phase components chosen for ICP-MS and AAS analysis. Samples A,B,C,D and E were chosen to represent the

continuous phase in which the large mineral inclusions are dispersed, and which appear to contain variable numbers of areas of localised high alpha activity (macro-alpha autoradiography). Sub-samples A, B and C were taken from the phase identified by staining techniques that appeared to contain a higher concentration of potassium bearing minerals than the other major phase (represented by sub-samples D and E). Sample F is representative of a large quartz inclusion whilst sample G was chosen to represent an area of high potassium content.

The sample material produced by micro-drilling was transferred quantitatively to individual Savillex™ digestion vessels; the digestion and dilution procedures described in Chapter 7 (section 7.5.1) were used to produce solutions that were subsequently presented for ICP-MS and AAS analyses.

Results ICP-MS and AAS

Sample Ref.	[Th] mg/kg (ICP-MS)	[U] mg/kg (ICP-MS)	[K] % (AAS)
A	6.93	4.32	3.83
B	11.2	7.11	5.30
C	13.04	5.40	3.38
D	8.04	6.12	3.76
E	8.01	5.72	3.33
F	2.05	0.65	1.08
G	2.69	0.79	6.08

Control Blank	<0.1	<0.1	<0.0001

Table 9.a.1 Concentrations of U, Th and K determined by ICP-MS and AAS

Discussion ICP-MS and AAS

Although based on a very limited number of determinations, the results from sub-samples A,B, and C indicate variability in the concentrations of both uranium and thorium throughout the potassium rich continuous phase of the sample matrix. In this phase, the concentration of potassium is also variable, with a maximum value of 5.30%, probably due to the presence of included K-rich minerals in the drilled material. The mean Th content is 10.39 mg/kg and the mean U content is 5.61 mg/kg.

The results from sub-samples D and E demonstrate good inter-aliquot comparability for all elements of interest, but with a lower mean thorium concentration (8.03 mg/kg vs 10.39 mg/kg) compared to the K-rich phase.

Interestingly, the thorium concentration values agree quite well with previously quoted values of typical natural abundance (from Aitken

1985 – 10 mg/kg Th, 3 mg/kg U), whilst the mean concentration of uranium (5.61 mg/kg) is almost double the expected typical value.

The quantitative results from sample F (large quartz inclusion) are perhaps slightly higher than expected, but not entirely atypical, with respect to potassium concentration; this element may be present as an intrinsic impurity as a charge compensator for aluminium which is, as discussed previously, a common impurity in natural quartz and as such, the extent to which both elements are present is a function of the intrinsic purity of the parent crystal (quartz).

The presence of uranium within the crystal at a level of concentration that is equivalent to approximately one tenth that of the surrounding matrix is not atypical, however the concentration of thorium (2.05 mg/kg) is perhaps higher than anticipated.

The concentration of potassium in sub-sample G, as expected, was substantially higher than the mean matrix value (6.08% versus 3.92%), and falls within the typical concentration values associated with the elemental composition of K-rich feldspars. Uranium and thorium were present at concentrations similar to those found in the quartz inclusion.

9.a.6 Discussion of analytical results and summary of material characteristics

Sample 321-1 is clearly a very complex material, consisting of a number of distinct composite phases. The use of digital enhancement and

staining techniques indicated the presence of two fine grain phases that form the continuous phase in which a number of mineral inclusions are present. These two phases differ both visually and in staining characteristics, highlighting a difference in basic mineralogical composition and variation in the associated concentrations of potassium between the two phases. The presence of two distinct phases is indicative of either poor mixing of differently sourced raw materials, and / or intrinsic material heterogeneity.

Alpha autoradiography revealed the presence of numerous localised areas of high alpha activity distributed evenly (but not exclusively) throughout the two continuous phases which were subsequently found to display minimum alpha activities of up to 30 times those associated with "background" matrix values. The size and activity of these areas may be indicative of the presence of heavier, resistant mineral species such as zircons or monazites, where the concentrations of uranium and thorium are likely to by significantly greater than natural abundance values. Subsequent SEM determinations confirmed the presence of both zircon and monazite grains.

The use of micro-sampling and ICP-MS analysis confirmed the presence of uranium at higher than expected values compared with typical natural abundance (~6 mg/kg vs. 3 mg/kg), together with apparently uniform distribution characteristics, suggesting an even dispersion of zircon (or other U rich minerals) inclusions throughout both continuous phases. The mean thorium concentration for both phases fall within expected typical values at 10 mg/kg for the K-rich phase and 8 mg/kg for the second phase. The inter-aliquot variability in determined thorium

concentrations throughout the K-rich phase, however, suggests that the distribution of this element is less uniform than in the second phase, where inter-aliquot variability was lower. This behaviour could be accounted for by the presence of an additional, inhomogenous distribution of thorium rich inclusions in the K-rich phase only.

The estimated mean values of uranium and thorium derived by semi-quantitative alpha-autoradiography (~3 mg/kg and 12 mg/kg respectively) were calculated on the assumption of equal activity between the uranium and thorium decay series (which is clearly not the case in the continuous phases); these values however, were derived from the cut, cross sectional surface of the sample, including the areas of low activity attributed to the presence low activity inclusions and whilst the estimated concentrations of uranium and thorium differ from those derived by quantitative means, the calculated mean sample activity should be reasonably accurate.

Alpha-autoradiography also revealed the presence of high activity micro-inclusions within some of the larger quartz crystals, which were later confirmed as either monazite or zircon by SEM analysis.

The distribution of potassium rich inclusions (and hence ^{40}K) throughout the material appears to be complex and includes the presence of feldspathic inclusions in close proximity to, and in some cases actually within quartz inclusions. The localised concentrations of potassium vary considerably between 1% and 6% across the surface of the sample, with an apparent mean value of around 3% in the fine grain continuous component.

With respect to the use of this material for luminescence dating, and indeed for inter-laboratory comparisons, it is difficult to indicate which of the phase components, if any (inclusions or fine grain) could provide reliable results. Spatially resolved measurements (Fig.9.a.13) indicate high variability in luminescence intensity (associated with larger inclusions) across the surface of the sample, that, in combination with a clearly complex dose–rate environment, on both the mm and sub-mm scale is likely to severely affect the integrity of any subsequent results.

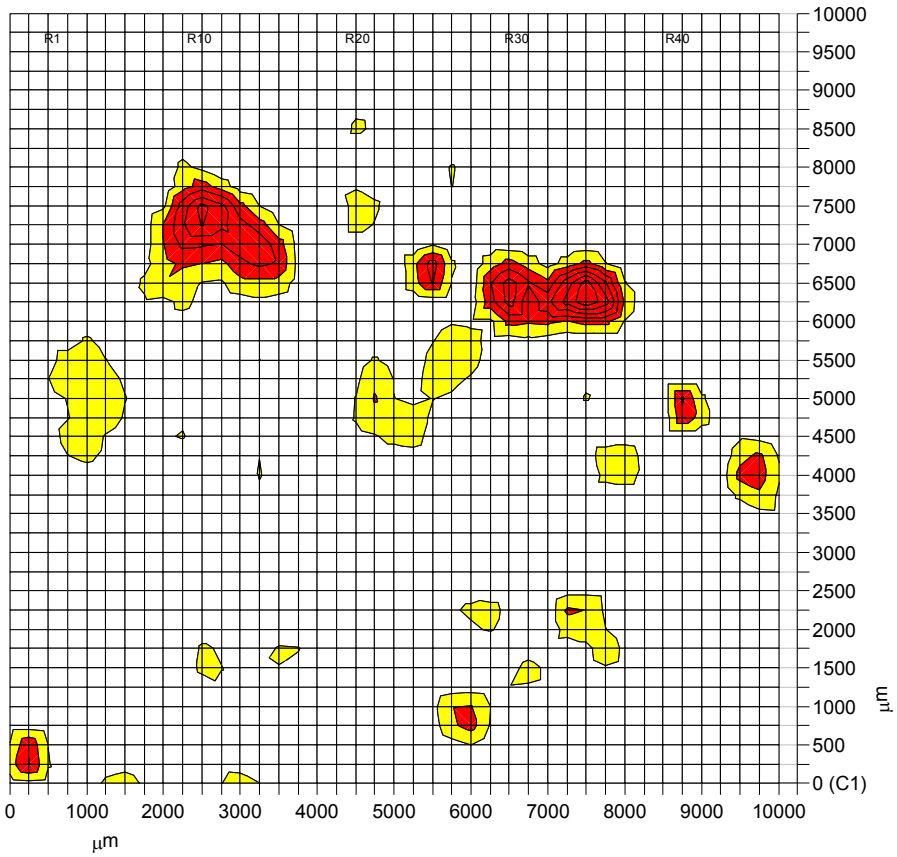

Figure 9.a.13 Map of natural luminescence intensity (OSL – 457-514 nm stimulation wavelength)across the surface of sample 321-1 (S7). Areas shaded red represent the highest levels of luminescence emission, whilst areas shaded yellow represent luminescence emission at levels that are substantially (X2 or more) above sample background levels.

Case study B - Sample 316-2 (Sediment)

Introduction

Laboratory reference 316-2 is one of a series of sediment samples taken from the open-air paleolithic site of West Cliffe St Margaret, Dover, and has been the subject of a number of continuing investigations into the feasibility of the luminescence dating of material of this age, where the paleodose can exceed 200 Gy and associated issues of luminescence signal saturation can be problematic. 316-2 was included in this project for several reasons; primarily, the sample is a sediment and was included to represent this category of archaeological material in addition to the presence of a very fine textured, apparently homogeneous matrix.

9.b.1 Digital analysis and photomicrography

Photomicrography and digital enhancement techniques (as described in chapter 8) were applied to the 1 mm x 1 cm x 1 cm slice of sample 316-2 which had been previously encapsulated using Epothin™ resin. The chosen material had previously been used for both spatially resolved luminescence measurements and a series of preliminary, investigative procedures using the commercial SEM services at the University of Newcastle.

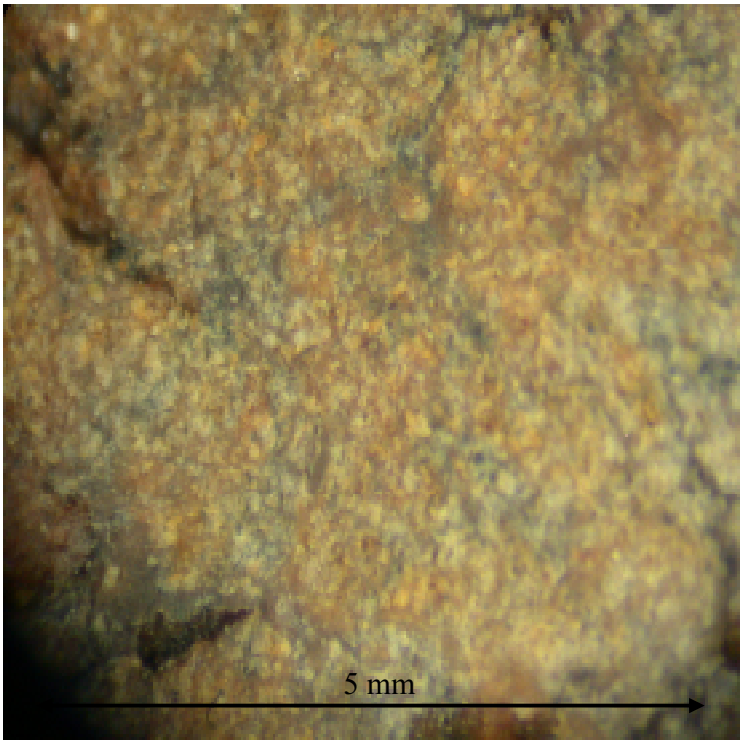

Fig 9.b.1 Photomicrograph of sample 316-2 (slice2) showing slight variation in colour across the sample and several "veins" of encapsulating resin.

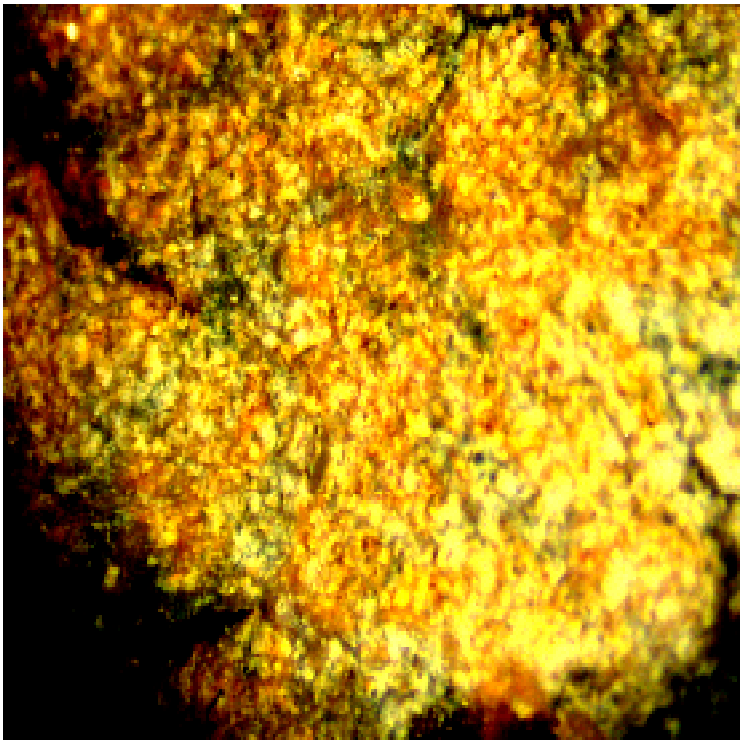

Fig 9.b.2 Digitally enhanced photomicrograph of sample 316-2 (slice 2)

Sample 316-2 consists of a very fine, apparently uniform matrix in which there is a noticeable absence of larger (>100 μm) mineral inclusions. In Fig 9.b.1, it is possible to observe numerous "veins" of encapsulating resin which have formed during the encapsulation process as a possible result of cracking (due to dehydration) during the initial stages of preparation where moisture is removed from the sample by the addition of acetone. There is some evidence of the presence of areas which differ slightly in colour; however, the texture remains consistent across the surface of the sample. The variation in colour may be an artefact of the encapsulation and cutting process and does not necessarily indicate the presence of a second matrix phase in this instance. The digitally enhanced image (Fig.9.b.2) highlights the effects described above.

9.b.2 **Staining techniques**

The chemical staining techniques described previously (section 6.1.3) were applied to the sample surface. After initial inspection, it was decided that the use of subsequent eosin staining would be useful to increase the colour contrast between stained areas and the background matrix. See Fig.9.b.3, Fig.9.b.4, and Fig.9.b.5.

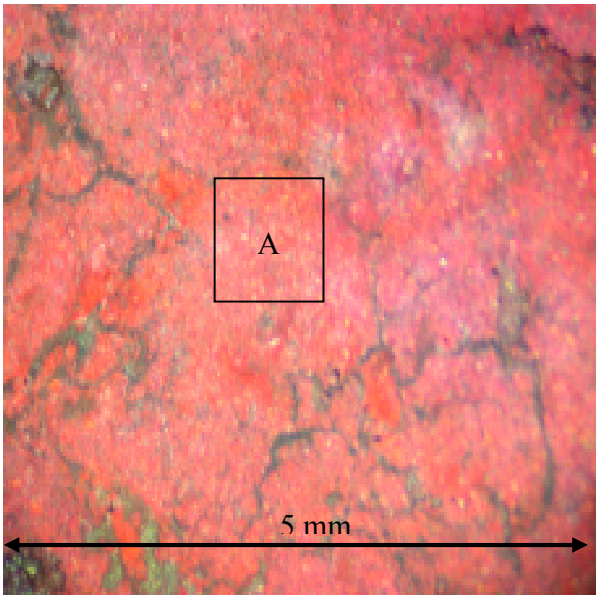

Fig 9.b.3 Photomicrograph of sample 316-2 after staining with sodium hexanitrocobaltate (III) and eosin. The veins of encapsulating material have become more evident due the HF vapour etching process, and addition of the eosin stain. At this level of magnification it is difficult to identify the presence of areas that have developed a positive stain.

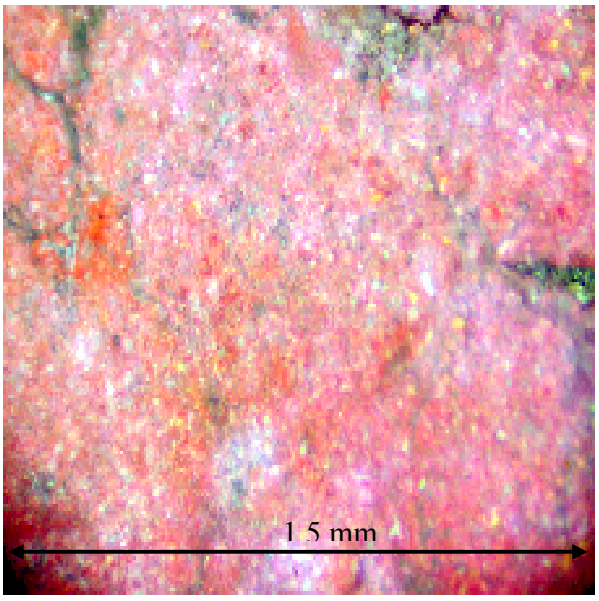

Fig 9.b.4 Digital photomicrograph of sample 316-2 (post stain) using 40x magnification (section A). It is now possible to differentiate small, well distributed areas that have stained yellow due to the presence of potassium.

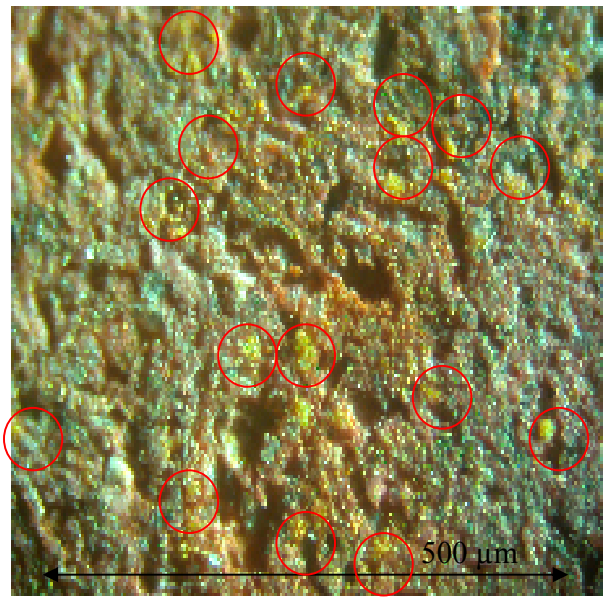

Fig 9.b.5 Photomicrograph of sample 316-1 (S7) after staining. 100X magnification and a green optical filter were used. Areas of localized high potassium concentration are circled (100µm diameter) in red and fall typically within the approximate size range of 30-75µm.

The application of staining techniques has revealed the presence of a uniform distribution of small (30-75 µm approx.) potassium rich grains that appear to be distributed evenly throughout the sample matrix. There is no apparent visual correlation between colour or textural characteristics and potassium content, although this would be potentially difficult to identify due to the size and distribution characteristics of these grains. The elemental map produced by the commercial SEM services at the University of Newcastle (Fig 9.b.6) highlights the presence of a number of larger potassium rich grains that are distributed throughout the material together with the "background" potassium present within the continuous phase of the matrix. It is interesting to note here that the application of staining techniques has proved useful in the differentiation between potassium rich mineral inclusions and the continuous matrix phase,

even when the latter clearly contains a potassium bearing component that is detectable by SEM. The potential to differentiate between such features by staining is of course dependant upon the actual variation in potassium concentration between the two components; the ability to differentiate between two species of alkali feldspar, for example, based on differences in potassium concentration may prove very difficult using surface staining techniques.

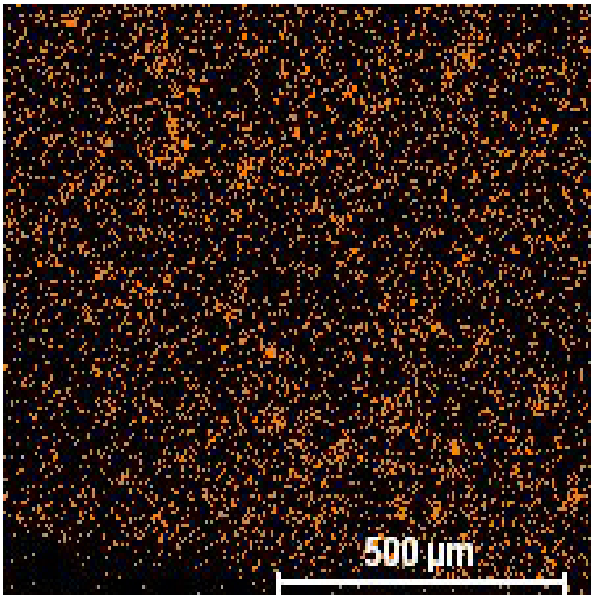

Fig 9.b.6 Elemental map (K) of sample 316-2. The lighter areas correspond to the presence of potassium.

9.b.3 Alpha autoradiography

Autoradiographs were produced using the procedures described earlier (section 8.a.3).

Results - macro alpha autoradiography

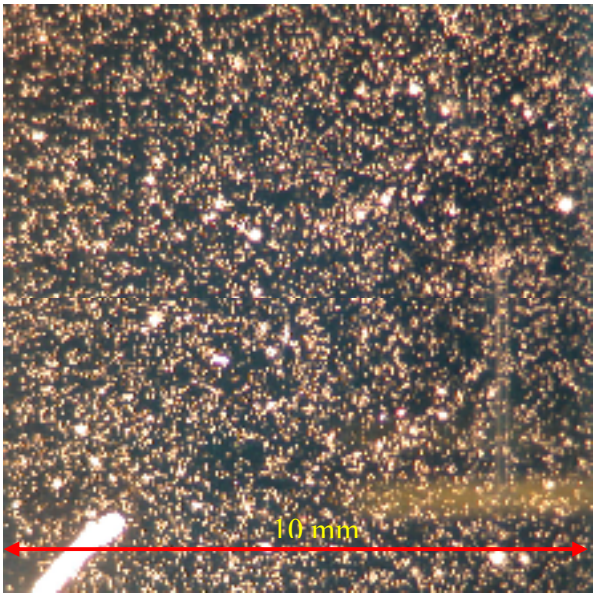

Fig 9.b.7 Macro alpha autoradiograph produced following a sample-detector contact period of 12 months. The distribution of alpha emitters appears to be generally uniform in nature, with the presence of a number of evenly distributed areas of increased localised alpha activity (seen as “bright” spots on the image).

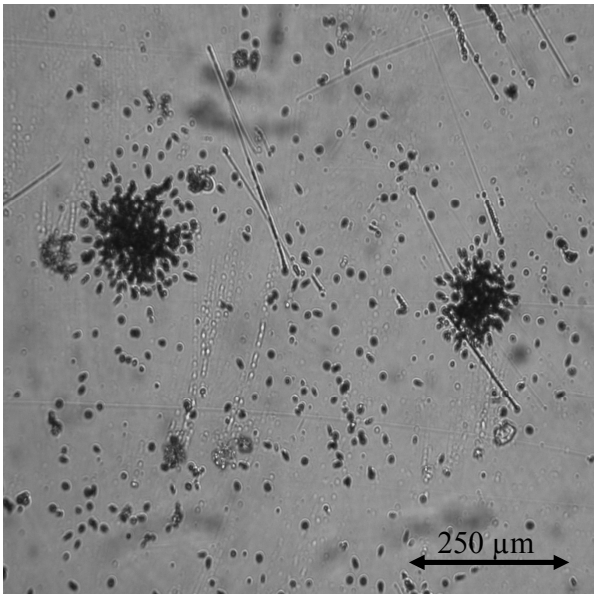

Fig 9.b.7 Photomicrograph of 316-2 (100x) showing areas of increased localised alpha activity.

Discussion

It is not possible to identify any visual correlation between the areas of increased potassium concentration identified by staining methods, and the localised areas of increased alpha activity seen in Fig. 9.b.7. Additionally, there is no apparent difference in the distribution patterns of alpha emitters between the areas that demonstrate slight variations in colour across the surface of the sample.

The presence of several areas of localised increased alpha activity indicates heterogeneity in the distribution of uranium and thorium (and associated daughter species) on the sub mm scale. The distribution of these areas across the sample surface however, can probably be regarded as uniform on the scale associated with the homogeneity of the beta radiation derived dose rate (associated with the luminescence dating techniques based on the use of etched grains).

Close examination of the autoradiograph (made after the appraisal of quantitative data regarding the localised concentrations of U, Th and K) has highlighted a potential correlation between seemingly randomly distributed areas of lower activity (characterised by a lack of developed tracks) and the veins of encapsulating resin that are made more apparent by the application of eosin staining solution.

Semi-quantitative alpha autoradiography

147	136	142	153	140
148	149	158	140	141
139	143	141	121	173
171	152	151	151	150
143	167	163	145	151

Fig 9.b.8 Grid showing tracks per counting area

Calculations

Mean track density = 148.6 tracks / 2.56 mm^2.

Total number of tracks counted = 3715

Variance (of mean) = 3.57 %

Adjusted track density = 5804 tracks cm^{-2}

Mean sample activity = 707 Bq kg^{-1}

Uranium concentration = 3.4 ppm

Thorium concentration = 14.4 ppm

9.b.4 Quantitative analyses

As the distribution patterns of uranium and thorium appear to be generally uniform (on the 1 mm scale associated with micro-sampling resolution) sampling locations for subsequent ICPMS and AAS analyses were selected to provide quantitative information regarding the concentrations of potassium, uranium and thorium across the surface of the sample, with the expectation that the uniformity characterised using other techniques will be verified quantitatively. The availability of resources (financial, ICP-MS time and laboratory equipment) limited the potential number of individual quantitative analyses performed.

Micro-sampling was performed at the areas highlighted below.

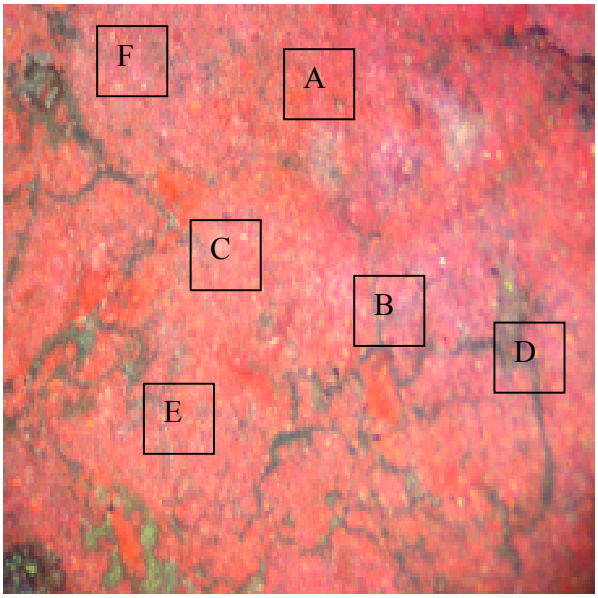

Fig 9.b.9 Digital photomicrograph of sample 316-2 (post stain) showing IC-PMS / AAS sampling locations.

Results ICP-MS and AAS

Sample Ref.	[Th] mg/kg (ICP-MS)	[U] mg/kg (ICP-MS)	[Zr] mg/kg (ICP-MS)	[K] % (AAS)
A	20.89	5.67	469.7	1.33
B	11.75	3.43	467.1	1.85
C	12.90	2.98	361.1	1.82
D	12.24	2.91	405.2	2.19
E	6.38	1.91	240.2	2.63
F	10.24	3.22	518.5	2.08

Table 9.b.1 Concentrations of U, Th, Zr and K determined by ICP-MS and AAS

Discussion

The quantitative results for these elements of interest indicated a somewhat unexpected degree of variability across the sampling locations chosen (Table 9.b.1). Sample location A displays a particularly elevated concentration of both thorium and uranium, whilst the concentration of potassium is lower than seen in other areas.

Material aliquots sampled from areas B,C, D and F contain comparable concentrations of U, Th and K between aliquots, with the degree of variability associated with a quasi-uniform distribution of the elements of interest.

Sample location E displays lower than expected concentrations of both uranium and thorium, whilst the determined concentration of potassium is slightly elevated compared to other aliquots. Interestingly, the concentration of zirconium in this aliquot is approximately half that seen in other samples, which may indicate the presence of a significant amount of encapsulation resin present in this sample.

9.b.5 Discussion of analytical results and summary of material characteristics

The results from the quantitative analyses are interesting and rather complex, but may be explained by the use of encapsulating resin to maintain the structural integrity of this sample during other phases of analysis, particularly in the production of thin sections for spatially resolved luminescence measurements.

The assumption was made during the encapsulation process that the specialist resin would penetrate evenly through the apparently uniform fine grain/clay matrix associated with this sediment. The appearance of veins of resin, (highlighted particularly after the application of eosin staining solution) indicated that this may not be the case, and closer inspection of the macro-alpha autoradiograph does seemn to indicate a number of regions where encapsulating resin may have reduced the local alpha activity.

If this is the case, the presence of resin, in varying concentrations, within the aliquots of sampled material could be responsible for the unexpected variability in the concentrations of the elements of interest.

In future quantitative determinations, it would be advisable to simultaneously quantify other compositional elements, and to compare elemental ratios to determine the presence of encapsulating resin.
The higher concentration of thorium seen in one of the aliquots may result from the sampling of an apparently random distribution of high alpha activity regions associated with the presence of U/Th included minerals, and where natural clustering of minerals at the point of sampling would result in the concentrations seen.

Regardless of the problems associated with the use of encapsulating resin, it is still reasonable to assume dose-rate heterogeneity across the sample, on the scale associated with the beta radiation derived dose component, appropriate to the use of disaggregated grain techniques.

Spatially resolved luminescence measurements made across the surface of this sample (Fig 9.b.10) indicate a reasonably uniform distribution of brightly emitting species. The combination of a uniform dispersion of emitting species of comparable luminescence sensitivity throughout a generally uniform matrix represents an optimal situation with respect to phosphor characteristics and dose rate environment for luminescence dating.

Work is still ongoing with this sample due to the complexities associated with material of this age.

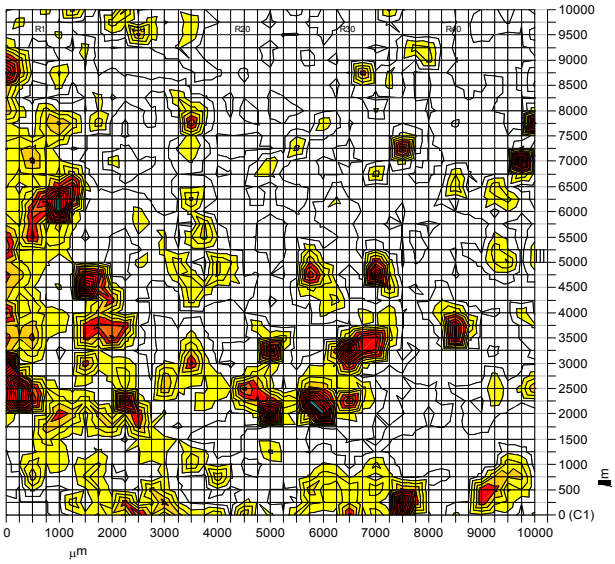

Fig 9.b.10 Map of natural luminescence intensity, measured across the surface of sample 316-2. Areas shaded red represent the highest levels of luminescence emission, whilst areas shaded yellow represent luminescence emission at levels that are substantially (2X or more) above sample background levels.

Case study C - Sample 294-1

Introduction

Sample 294-1 represents one of two examples of late medieval brick taken from the Sandhill area of Newcastle upon Tyne. This sample was taken from the same building as sample 294-17 (discussed as case study D), and as part of the same dating project, but from a different context with regard to the assumed phasing of the building. Sample 294-1 was included in this project because of the visually heterogeneous nature of the matrix material, with respect to the colour and textural properties of what appear to be two distinct phases which may result from poor mixing of the raw materials, or inherent heterogeneity within the composite clay.

9.c.1 Digital analysis and photomicrography

Photomicrography and digital enhancement techniques (as described in Chapter 6) were applied to the 1 mm x 1 cm x 1 cm slice of sample 294-1. Slice 1 was chosen as this sub-sample had previously been used to perform a number of spatially-resolved OSL experiments and provides a visually representative section of the material.

Due to the variation of colour and texture seen in archaeological materials, the exact nature of the digital enhancement techniques is optimised for each sample, based upon both colours and textures present. Hence, the digitally enhanced photomicrograph (Fig.9.c.1) represents the best compromise with respect to the identification and highlighting of visual heterogeneity for each specific sample.

Adobe Photoshop ™ was then used, as described in Chapter to produce a digitally enhanced version of Fig 9.c.1

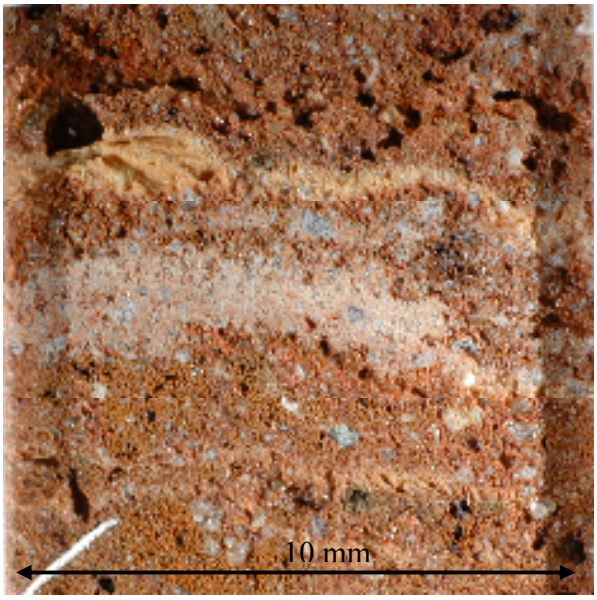

Fig 9.c.1 Digital photomicrograph of sample 294-1 (slice 1)

Visual heterogeneity is clearly apparent, with striations of lighter coloured material across the surface.

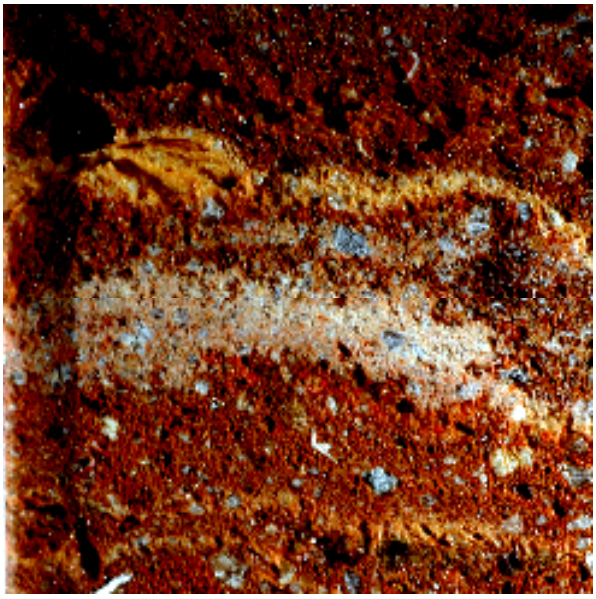

Fig 9.c.2 Digitally enhanced version of Fig 9.c.1

This sample was included in this project because visual heterogeneity is clearly apparent; digital enhancement was used here to increase the visual contrast between different phases, but did not reveal the presence of any features that were not previously identifiable without enhancement. The distribution of mineral inclusions appears to be slightly more well-defined

9.c..2 Staining techniques

The chemical staining techniques described previously (Section 6.1.3) were applied to the sample after digital enhancement and SSNTD autoradiography techniques were performed.

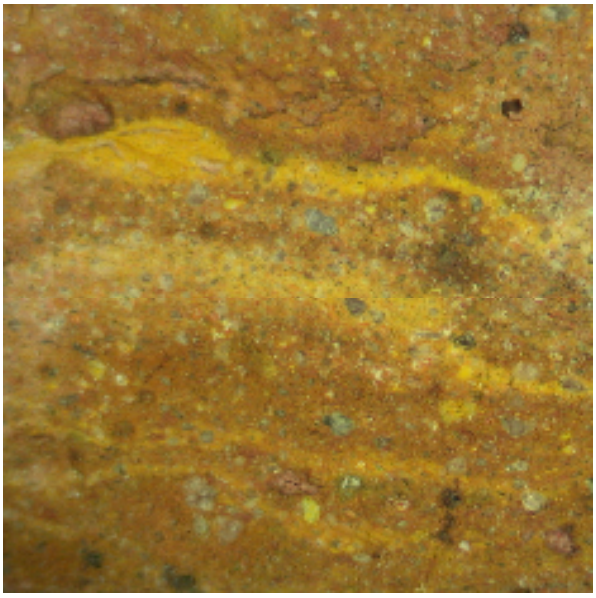

Fig 9.c.3 Digital photomicrograph of sample 294-1(slice 1) after staining.

The striations of material that display differing textural and colour characteristics to the major, continuous matrix phase have clearly displayed a positive reaction with the sodium hexanitrocobaltate (III) stain.

The minor phase components identified visually, and highlighted further by the application of digital enhancement techniques, appear to contain a higher concentration of potassium in comparison to the major, continuous phase component. The identification of a positive correlation between visual and elemental heterogeneity (with respect to K) is important;, however, in this case, the staining results must be interpreted with caution because consideration must be given to the base colour of the material phases before the application of staining reagents. The development of the yellow stain in the minor phase is a clear indication of the presence of potassium, but it is conceivable that the lighter coloured phase component could demonstrate an apparently increased reaction to the staining reagents (in contrast to the major phase) because of the differences in initial colour and texture in addition to potassium concentration alone.

In this case, the subsequent application of quantitative techniques (AAS) should be used to confirm the results produced by staining.

As discussed in earlier chapters, the disruption of the homogeneity of the local beta radiation derived dose rate due to heterogeneity in the distribution of potassium bearing minerals has important dosimetric consequences, and particularly with respect to luminescence dating techniques, if the sensitivity of the component phosphor grains is variable.

9.c.3 Alpha autoradiography

Autoradiographs were produced using the procedures described earlier (section 8.a.3).

Macro alpha autoradiography

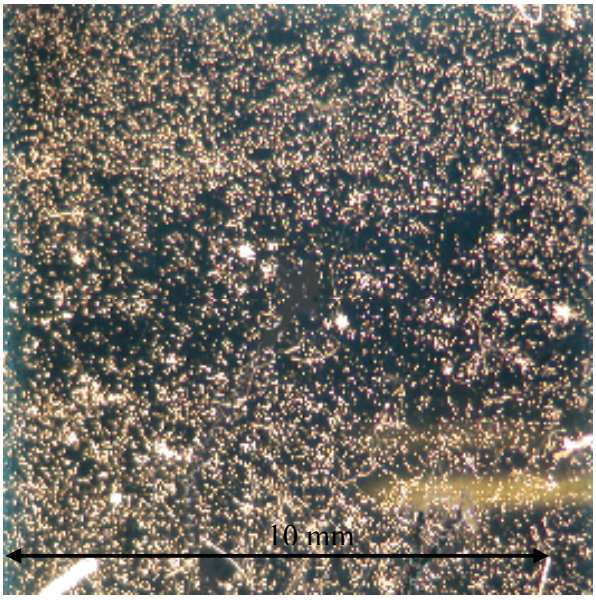

Fig 9.c.4 Macro Alpha autoradiograph of sample 294-1(s1) - 12 months

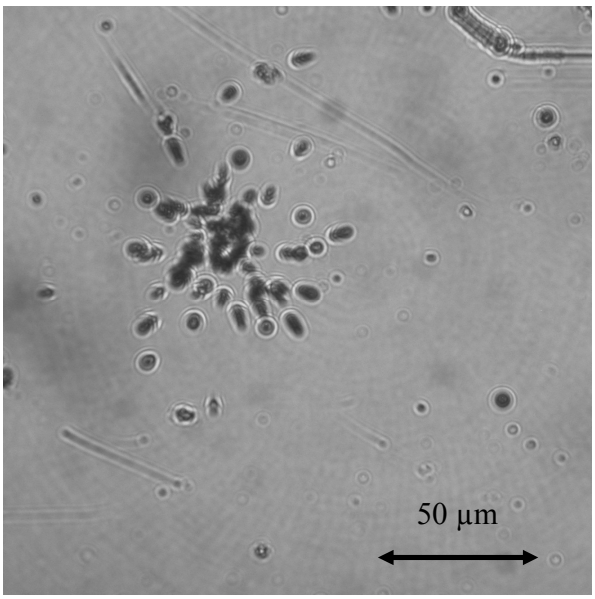

Fig 9.c.5 Typical area of increased localised alpha activity (200x magnification)

The macro autoradiograph shows a distinct central region of differing alpha activity, highlighted by the presence of a number of areas of high local alpha activity (seen as bright spots, Fig 9.c.4) situated within a band of lower surface alpha activity (compared to "background" activity).

The sample areas that displayed both visual and textural differences, together with a positive staining reaction for increased local potassium concentration, appear to demonstrate different characteristics with regard to the concentration and distribution of alpha emitters, compared to the continuous material phase. The alpha emitters in the minor phases (seen centrally on the autoradiograph) appear to be concentrated within small, uniformly distributed areas of high localised activity that can be associated with the presence of heavy mineral inclusions; the material in which these points of higher alpha activity are dispersed appears generally, to contain a lower concentration of alpha emitters than the major phase component.

Semi-quantitative alpha autoradiography

110	135	112	124	103
115	115	77	123	110
131	88	111	96	114
117	109	132	107	121
128	108	115	119	109

Fig 9.c.6 Grid showing tracks per counting area

Calculations

Total tracks counted	= 2829
Mean track density	= 113.2 tracks / 2.56 mm^2.
Variance (of mean)	= 6.4 %
Adjusted track density	= 4420 tracks cm^{-2}
Mean sample activity	= 538 $Bqkg^{-1}$
Uranium concentration	= 2.5 ppm
Thorium concentration	= 11 ppm

Although there is a clear difference in the distribution characteristics of alpha emitters across the surface of this sample (identified by macro-alpha autoradiography) the estimated concentrations of these species, at the resolution used for semi-quantitative autoradiography, is consistent with a generally uniform distribution. Subsequently, the associated beta radiation derived dose rate (from U and Th decay series) is also likely to be uniform at this level of resolution and hence, heterogeneity in this context is likely to result from the potassium derived contribution to dose-rate.

9.c..4 Quantitative analyses

Micro-sampling was performed at the areas highlighted in Fig 9.c.8.

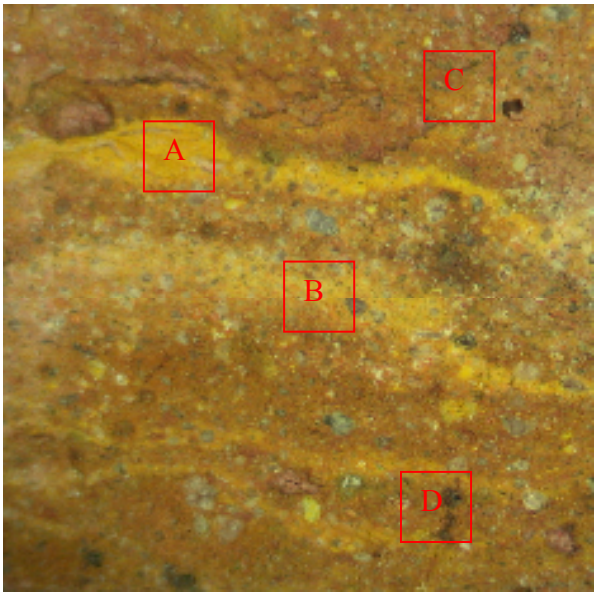

Fig 9.c.8 Digital photomicrograph of sample 294-1 (S1), post staining, showing ICP-MS and AAS sampling locations. Sample A and B were taken to investigate the potassium concentration in the areas of apparently higher concentration , whilst material from samples C and D was combined to provide a mean matrix concentration value.

Results ICP-MS and AAS

Sample Ref.	[Th] mg/kg (ICP-MS)	[U] mg/kg (ICP-MS)	[Zr] mg/kg (ICP-MS)	[K] % (AAS)
A	14.37	3.29	519.4	1.97
B	15.85	4.71	714.2	1.56
C,D	11.77	3.12	508.8	0.67

Table 9.c.1 Concentrations of U, Th, Zr and K determined by ICP-MS and AAS

As expected, material sub-samples taken from areas A and B contain significantly higher concentrations of potassium than the surrounding matrix. The mean matrix concentration is actually substantially lower than seen in other samples tested during this work and in particular sample 294-17 (1.79%K), which was taken from the same building.

The concentration of thorium is elevated in areas A and B, whilst uranium is present at higher levels in sample B only. The analysis of zirconium concentration was included to provide additional information for this sample and is present at seemingly higher levels in sample B.

9.c.5 Discussion of analytical results and summary of material characteristics

This sample was included in this work because of the presence of visual heterogeneity, in the form of numerous striations across the surface of the sample that had different colour and textural properties. Staining techniques confirmed an elevated concentration of potassium in these areas, and this was subsequently quantified by the use of AAS, indicating the presence of potassium at around 3 times that found in the major matrix phase.

Alpha autoradiography revealed a difference in the distribution characteristics of alpha emitters in the K-rich phases, with a high number of "bright spots" indicating the presence of Th or U rich included species.

Whilst results from semi-quantitative alpha autoradiography indicated a generally uniform concentration (but not dispersion) of alpha emitters across the surface of this sample, ICP-MS analyses performed using sub-samples taken

at strategic locations revealed an increase in thorium and (in one case) uranium concentrations in comparison to expected typical abundance values.
On assessment of the data relating to zirconium concentration it is reasonable to propose that Th-rich mineral inclusions are present in both of the discrete K-rich phases sampled, whilst in sample B, the presence of additional U-rich material (probably zircon due to elevated Zr concentration) is indicated.

The provision of comments relating to the suitability of this sample for luminescence dating is difficult without further investigation. Spatially resolved measurements of the natural luminescence signal measured across the surface of the sample (Fig 9.c.9) appear to indicate an increased number of "brighter" grains in the regions associated with increased concentrations of K, U and Th. As the material characteristics of this sample are complex and indicate the presence of at least two distinct mineralogical phases, it is possible that the quartz inclusions associated with these individual phases display differing degrees of luminescence sensitivity.
When using disaggregated grain techniques, the presence of quartz inclusions that display variable degrees of sensitivity (within a uniform matrix) is not necessarily problematic, providing the occurrence of "brighter" grains is sufficient to result in an even inter-aliquot distribution of these species when measurements are performed.

If "bright" grains are associated with a particular matrix phase, in which the dose rate is elevated (in comparison to the bulk sample value) the validity of the luminescence age calculation is compromised as the calculated annual dose component may not be applicable to the phosphor grains from which luminescence signal may be largely derived.

It is also feasible that the "bright" grains are demonstrating increased levels of luminescence due to higher local dose rate and do not actually vary considerably in luminescence sensitivity.

The application of further spatially resolved measurements to characterise the regenerative dose characteristics of the minerals associated with this sample are needed to provide more information about the suitability of this sample for luminescence dating. Alternatively, the extraction of quartz grains from single phase components, together with specific dose-rate measurements may improve the accuracy associated with dating this material.

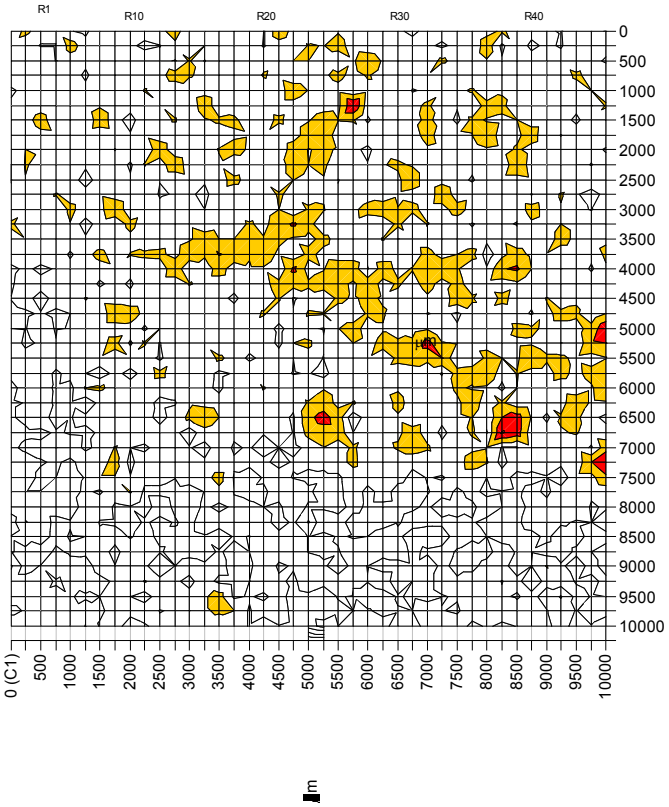

Fig 9.c.9 Map of natural luminescence intensity, measured across the surface of sample 297-1 (S4) Areas shaded red represent the highest levels of luminescence emission, whilst areas shaded yellow represent luminescence emission at levels that are substantially (2X or more) above sample background levels.

Case study D - Sample 294-17

Introduction

Sample 294-17 is an example of late medieval brick taken from the Sandhill area of Newcastle upon Tyne. This area of Newcastle upon Tyne has formed the basis of previous studies (Bailiff and Holland, 2000) and this sample was taken in the course of a subsequent project that aims to apply luminescence dating techniques to provide information about the dates of different construction phases in a late medieval building. Data from this project will form part of a future publication when additional dating evidence (e.g., dendrochronology) has been considered. With respect to the aims of the current project, this sample was also chosen because of the matrix properties, where a number of crystalline inclusions are distributed uniformly throughout a fine, apparently uniform matrix. This sample was taken from the same building as sample 294-1 (discussed as case study C).

9.d.1 Digital analysis and photomicrography

Photomicrography and digital enhancement techniques (as described in Chapter 6, section 6.2) were applied to the 1 mm x 1 cm x 1 cm slice of sample 294-17. Slice 4 was chosen as this sub-sample had been used to perform a number of OSL scanning experiments and provides a visually representative section of the material.

Due to the variation of colour and texture seen in archaeological materials, the exact nature of the digital enhancement techniques is optimised for each sample, based upon both colours and textures present. Hence, the digitally enhanced

photomicrographs represent the best compromise with respect to the identification and highlighting of visual heterogeneity for each specific sample.

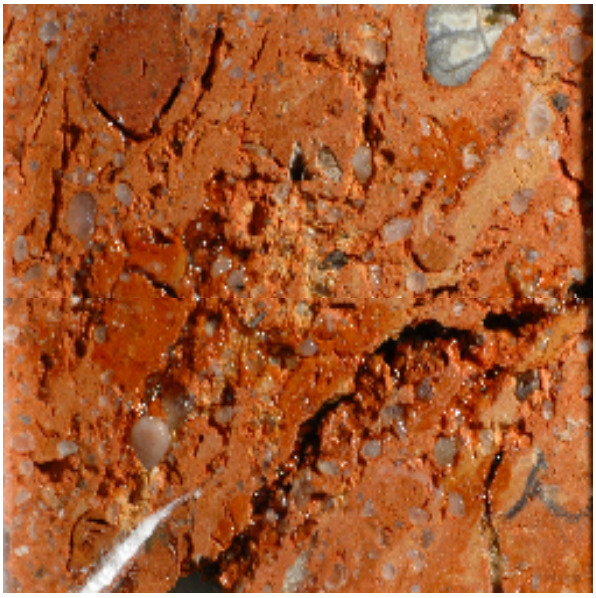

Fig 9.d.1 Photomicrograph of sample 294-17 (slice 4).

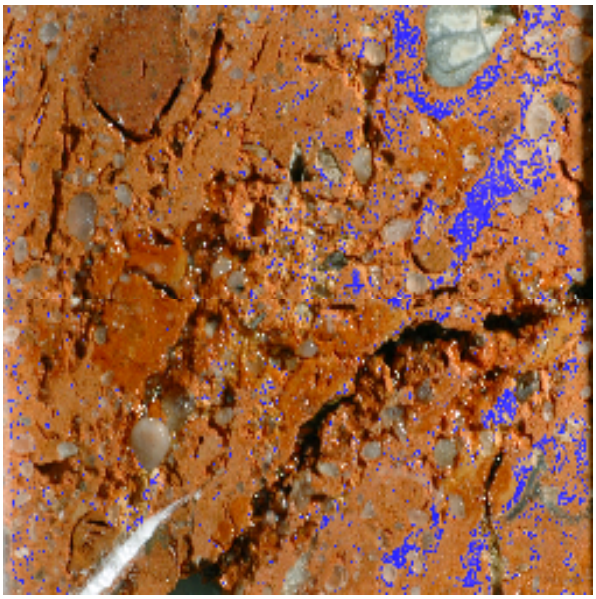

Fig 9.d.2 Digitally enhanced photomicrograph of sample 294-17 (slice 4)

Sample 294-17 consists of a fine, visually uniform matrix containing a number of (apparently) well distributed crystalline and opaque mineral inclusions. There is

some evidence of the presence of a second matrix phase which is slightly lighter in appearance compared to the major, continuous phase; the minor phase can be clearly identified in the enhanced image (blue colouration) where digital colour sampling and substitution techniques have been used to highlight this region.

There is no apparent correlation between phase type and inclusion content as seen in previous examples (e.g. 321-1, case study A); the extent to which the minor phase is present may indicate small scale heterogeneity in the raw clay materials rather than the presence of an admixture of more than one different, raw material. The size and distribution of included materials is indicative of either efficient mixing of tempering agents (in this case the addition of coarse sand sized granular material) or the presence of this component as a natural consequence of the mineralogy and the sedimentation processes by which the clay was formed.

9.d.2 Staining techniques

The chemical staining techniques described in Chapter 6 (section 6.1.3) were applied to the sample surface. After initial inspection, it was decided that the use of subsequent eosin staining was not required.

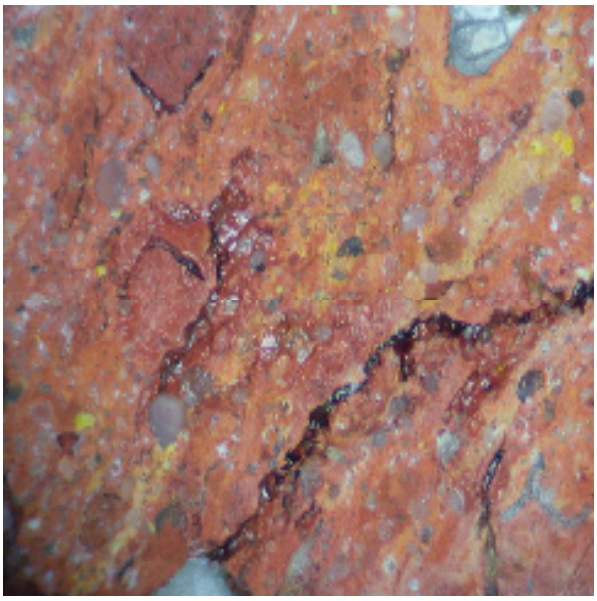

Fig 9.d.3 Digital photomicrograph of sample 294-17 (slice 4) after staining

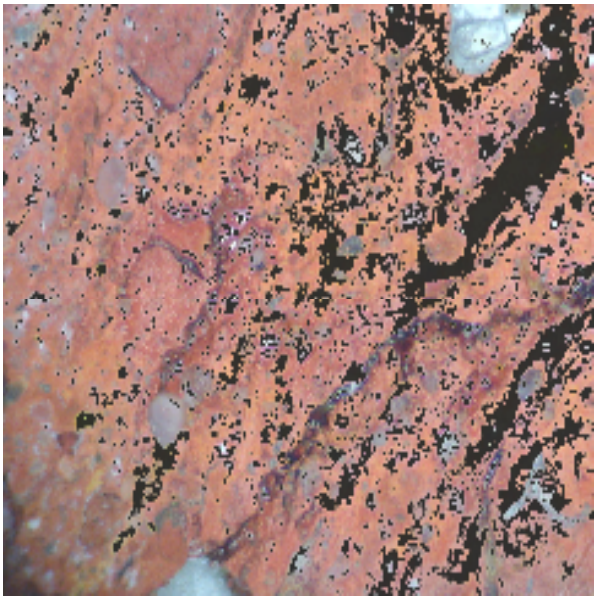

Fig 9.d.4 Digitally enhanced version of photomicrograph (Fig 9.d.3)

The application of staining techniques has revealed an increased concentration of potassium bearing minerals in the minor phase (Fig 9.d.3) previously identified visually (Fig 9.d.1) and by digital enhancement (Fig 9.d.2). The correlation between visually different mineral phases and differing potassium concentrations was identified for sample 321-1 slice 1; whilst less extreme in nature than the previous example, it is still important to recognise the existence of this situation. Digital enhancement techniques were applied to the photomicrograph of the stained section to facilitate the identification of the regions that developed a positive stain (Fig 9.d.4). The majority of included grains remained largely unchanged with respect to opacity and the development of a positive stain and are thus likely to be quartz. Some of the included grains were identified as potassium rich minerals but these were present in very small numbers, and well distributed.

9.d.3 Alpha autoradiography

Autoradiographs were produced using the procedures described earlier (section 9.a.3).

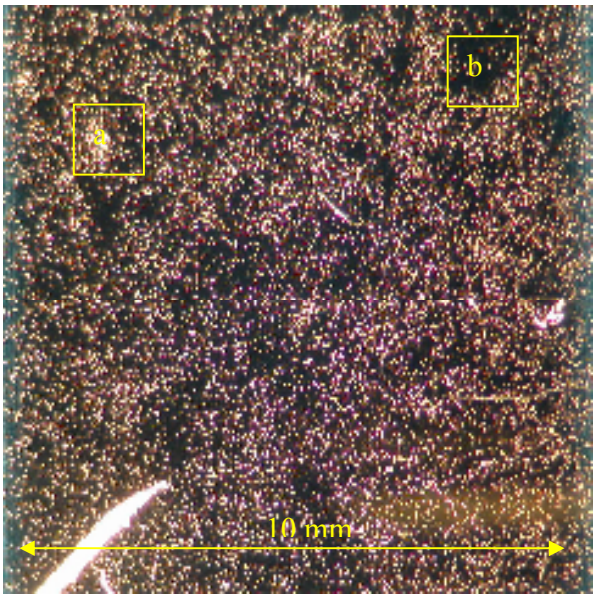

Fig. 9.d.5 Macro alpha autoradiograph produced following a sample-detector contact period of 12 months. The distribution of alpha emitters appears to be generally uniform in nature, with the exception of a small number of slightly increased (a) and reduced (b) areas of localised activity.

Discussion – macro alpha autoradiography

There is some visual correlation between the larger inclusion located towards the top right hand corner of the image (Fig. 9.d.1) and the area of lower activity seen in Fig. 9.d.5 There is no apparent difference in observed alpha activity associated with the presence of the minor phase component identified by the use of staining

techniques; this indicates that whilst the concentration of potassium varies between the two composite phases, the uranium and thorium concentrations are similar.

A further interesting feature revealed by macro alpha autoradiography is the absence of a significant reduction in observed alpha activity at the area of the autoradiograph that corresponds to the fracture in the matrix located towards the lower LHS of the sample. One possible explanation for this feature is the emanation of radon from the fracture, resulting in the deposition of daughter species on the surface of the detector. A second, and perhaps more likely explanation, is due to the shallow depth of the fracture and relatively close proximity to the detector; the alpha particles emitted from the sides and base of the fracture may still have sufficient energy (after passing through <0.5 mm of air) to result in the production of a latent alpha track.

Semi-quantitative alpha autoradiography

134	100	103	109	115
109	102	77	108	121
109	117	127	114	98
102	106	112	121	112
131	88	104	93	106

Fig 9.d.6 Grid showing tracks per counting area

Calculations

Total tracks counted	= 2718
Mean track density	= 108.6 tracks / 2.56 mm^2.
Variance (of mean)	= 6.07 %
Adjusted track density	= 4242 tracks cm^{-2}
Mean sample activity	= 516 $Bqkg^{-1}$
Uranium concentration	= 2.47 ppm
Thorium concentration	= 10.54 ppm

9.d.4 Quantitative analysis – AAS

During the final stages of experimental work, the ICP-MS used for the quantitative determination of uranium and thorium was out of service due to failure of the turbo molecular vacuum pump. Attempts were made to out source this work, but due to time and financial constraints, this was not possible. As the distribution of uranium and thorium appears to be uniform across the surface of sample 294-17, and as validation of the semi-quantitative values for uranium and thorium concentration by alpha autoradiography has been made in previous case studies, the decision was made to perform quantitative analyses on the areas of interest, with respect to potassium concentration only. In the presence of a homogeneous distribution of alpha emitters, the primary source of dose-rate heterogeneity is likely to be derived from this component.

Micro-sampling was performed at the areas highlighted in Fig. 9.d.8

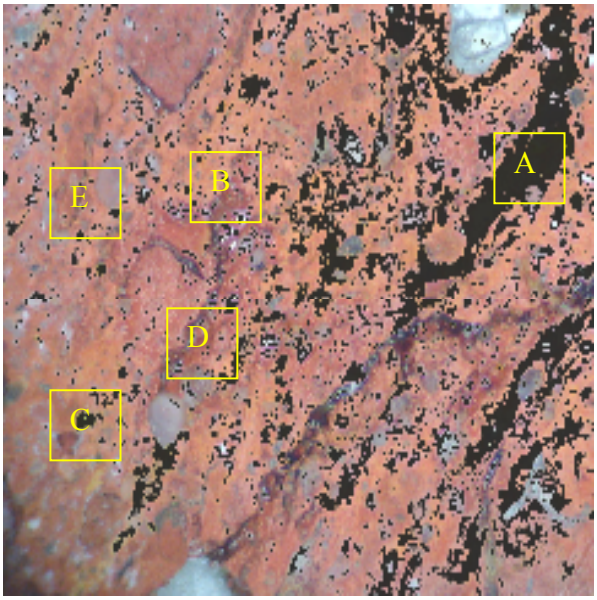

Fig 9.d.8 Enhanced digital photomicrograph of sample 294-17 (S4) showing AAS sampling locations. Samples A and C were taken from areas that developed a positive reaction to sodium hexanitrocobaltate (III) staining, whilst samples B, D and E were combined to investigate the mean matrix potassium concentration.

Results AAS

Sample Ref	[K] %
A	1.79
C	2.25
B,D,E	1.79

Discussion AAS

As with previous examples, quantitative analyses were performed to characterise the differing matrix components highlighted by initial testing. In this case, it is interesting to note that the mean matrix potassium concentration (combined

B,D,E) is identical to the determined value for sample A, which had previously been highlighted, by staining methods, as an area of higher potassium concentration. The initial photomicrograph (not enhanced) of the stained section shows that the colour developed in this area (A) is much less intense than in other areas (C) where potassium rich inclusions were clearly identified. This indicates that the area of increased potassium concentration was either superficial (with respect to the 1 mm micro-sampling depth), or, had developed colour to due to the staining process, possibly to the same extent as other areas of the sample matrix, but appeared more obvious because of the slightly lighter initial matrix colouration in this area .

The concentration of potassium in sample C is slightly higher than the mean matrix value, although not at the same levels seen in other K-rich inclusions determined in other examples.

9.d.5 Discussion of analytical results and summary of material characteristics

Digital analysis and staining techniques revealed a generally uniform matrix consistency, with few areas of increased local potassium concentration. These results were confirmed by quantitative analysis. A generally uniform distribution of alpha emitters was revealed by the use of alpha autoradiography, indicating homogeneity in the dispersion of alpha emitters throughout the matrix.

With regard to the suitability of this material for luminescence dating, the matrix characteristics provide a uniform environment with respect to the dose rate applicable to composite mineral inclusions. Spatially resolved luminescence

measurements indicate the presence of a number of brighter inclusions and highlight the strong OSL signal from the prominent grain located towards the lower left hand corner (Clearly visible in Fig 9.d.1, and seen as red in Fig 9.d.9), which, given the overall homogeneity of the material, may be considered not to significantly affect the integrity of the mean aliquot luminescence measurements made using disaggregated grain techniques.

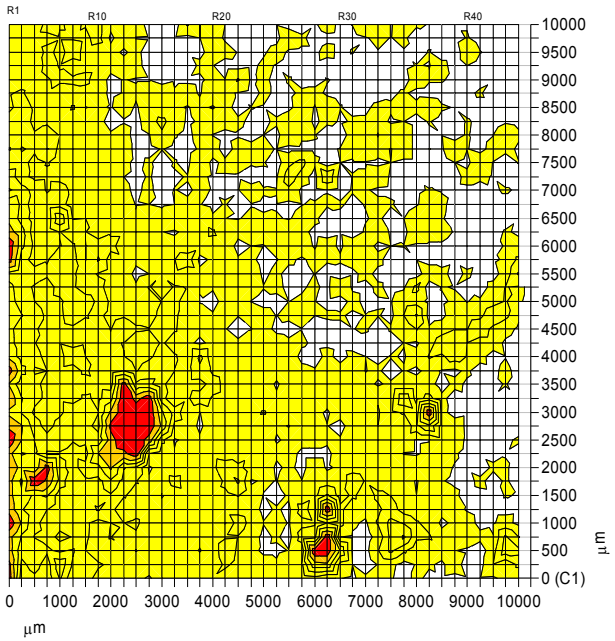

Fig 9.d.9 Map of natural luminescence intensity, measured across the surface of sample 294-17 (S4) Areas shaded red represent the highest levels of luminescence emission, whilst areas shaded yellow represent luminescence emission at levels that are substantially (2X or more) above sample background levels.

Case study E - Sample 304-1

Introduction

Sample 304 is an example of late medieval brick that was taken from Hallstead Hall, Lincolnshire as part of a research project that aimed to apply luminescence dating to buildings in that region (Bailiff, 2008). The luminescence characteristics of the sample enabled the production of a luminescence date of A.D. 1555 ±27. It was decided that there was insufficient independent dating evidence to include this sample in the subsequent publication. However, this sample was chosen for inclusion within this project because the material displays a relatively high degree of visual homogeneity, making it potentially useful in comparison to samples such as laboratory reference 321-1 (case study A), where visual heterogeneity is evident. The matrix material is fine textured, with a small number of localised areas of slightly differing colour. The distribution of included minerals appears to be uniform and of a well defined grain size range (Fig 9.e.1).

9.e.1 Digital analysis and photomicrography

1 mm x 1 cm x 1 cm slices were prepared from a small sub-sample of material for use in scanning experiments to measure the distribution of luminescent species across the surface of the sample. After all spatially-resolved OSL measurements were made, digital photographs of the slice were taken using a Nikon Coolpix digital camera, coupled to the eye piece of a binocular microscope using appropriate magnification (10x) to provide the best resolution across the surface

area of the sample (Fig 9.e.1). Adobe Photoshop ™ was then used, as described in Chapter 6 (Section 6.2) to highlight subtle differences in matrix colour and texture in order to reveal the presence of multiple matrix component phases and / or effects caused by poor mixing during manufacture or heterogeneity of parent clay materials (Fig 9.e.2).

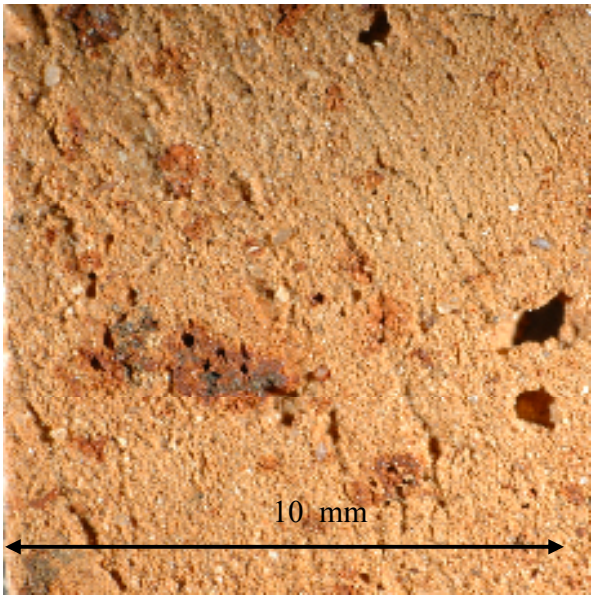

Fig 9.e.1 Digital photomicrograph of sample 304 (slice 3)

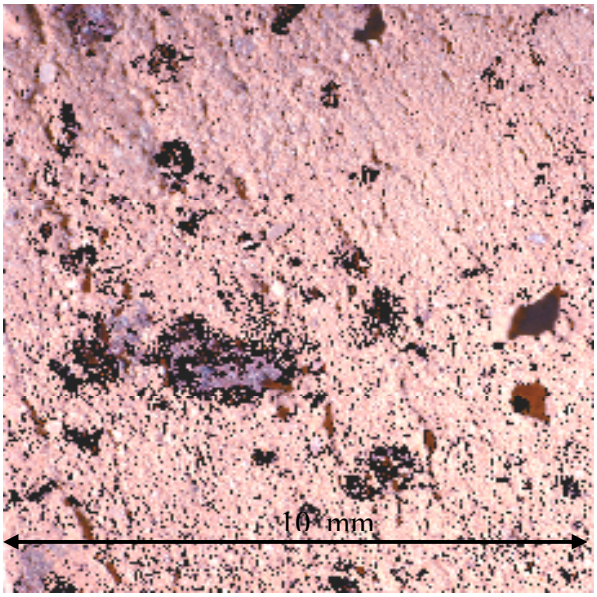

Fig 9.e.2 Digitally enhanced photomicrograph of sample 304 (slice 3)

The matrix appears to be generally homogeneous with the exception of the presence of several voids, and a number of small areas with differing colour characteristics. In this case, the use of digital enhancement techniques does not reveal any subtle or "hidden" features that were not previously seen without enhancement.

9.e.2 Staining techniques

The chemical staining techniques described previously (Section 6.1.3) were applied to the sample surface. After initial inspection, it was decided that the use of subsequent eosin staining was not required.

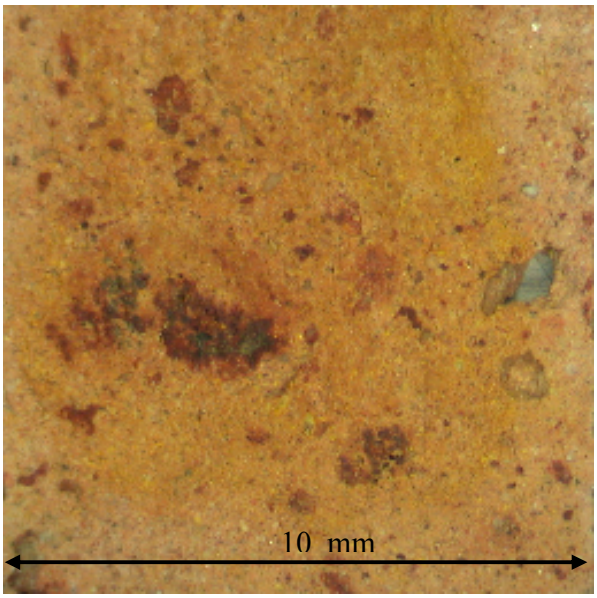

Fig 9.e.3 Digital photomicrograph of sample 304 (slice 3) after staining

Apart from a slight smoothing of the sample surface due to the HF vapour etching procedure sample 304 (slice 3) has remained effectively unchanged after the application of staining chemicals.

The application of K- staining techniques did not give rise to the appearance of any brightly coloured inclusions that are visible to the naked eye or under low magnification (Fig 9.e.3); the areas that appear to be visually darker than the continuous matrix have also remained unaltered, indicating an absence of localised areas of increased potassium concentration. The absence of a noticeable colour change associated within the continuous matrix phase indicates that the concentration of potassium throughout this phase is either uniform, and present below the levels of detection associated with the staining techniques

used or, is present in the form of small areas of increased localised potassium concentration that are too small to be detected under normal levels of magnification.

9.e.3 Alpha autoradiography

Results – macro alpha autoradiography

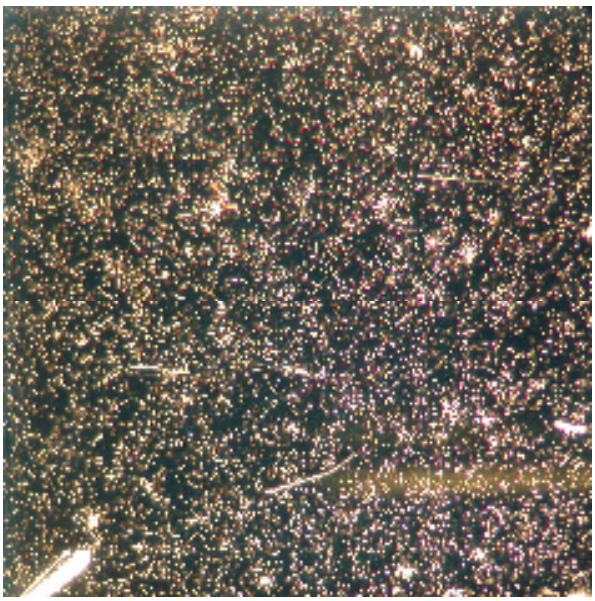

Fig 9.e.4 Alpha autoradiograph of sample 304 (slice 3) 12 month contact time.

The presence of a number of uniformly distributed areas of localised, increased alpha activity can be seen as lighter areas on the autoradiograph. A number of small scratches are also present due to mechanical damage while handling the material.

The presence of numerous areas of localised, increased alpha activity is highlighted, despite the uniform nature of the ceramic matrix (Fig 9.e.4). There is no apparent visual correlation between either the small areas of differing colour characteristics or crystalline inclusions, and the areas of increased alpha activity. It is reasonable to conclude in this

case, that the areas of increased activity are associated with the continuous fine matrix material; from a geochemical perspective, it is possible that resistant, heavier minerals such as zircon may survive the weathering and mechanical processes to a greater extent than other, less resilient species that represent the major compositional phases of the clay materials used in the production of ceramics. In visually homogenous materials, the existence of "invisible" micro inclusions of heavier minerals, particularly zircons (because of the associated increase in uranium concentration discussed in Chapter 1) may result in the areas of increased alpha activity seen above. If these mineral grains are distributed uniformly throughout the matrix (as seems to be the case with sample 304), there may be no significant effect on the matrix dose rate heterogeneity derived from beta radiation, although the ability to detect the presence of these grains is important with respect to the overall characterisation of the material The use of SEM / EDX or cathodoluminescence techniques offer the ability to characterise micro deviations in the mineralogical composition of ceramics, (as seen for sample 321-1, case study A). However, the resources available within the scope of this work were insufficient to provide this level of analysis for all samples.

Semi-quantitative alpha autoradiography

74	78	67	72	75
89	72	62	79	94

79	58	64	82	104
76	75	93	77	80
82	72	65	73	95

Fig 9.e.6 Grid showing number of tracks per counting area

Calculations

Total tracks counted	= 1937
Mean track density	= 77.5 tracks / 2.56 mm^2.
Variance (of mean)	= 6.2%
Adjusted track density	= 3027 tracks cm^{-2}
Mean sample alpha activity is	= 373 $Bqkg^{-1}$
Uranium concentration	= 1.8 ppm
Thorium concentration	= 7.6 ppm

9.e.4 Quantitative analysis – AAS

As with sample 294-17(case study D) , the final stages of experimental work for this sample were also disrupted by the inability to perform ICP-MS analyses to determine uranium and thorium concentrations. For completeness within this current work, the quantitative determination of these elements would have been useful, however, with regard to the routine application of the techniques developed within this project, to the characterisation of luminescence dating samples (radionuclide distribution patterns), it is unlikely that ICP-MS, and indeed AAS analyses would be performed, due to the established homogeneity of

the material. As instrumental time had been made available, it was decided to continue with a limited number of samples for the determination of mean matrix potassium concentration for this sample.Micro-sampling was performed at the areas highlighted in fig 9.e.7.

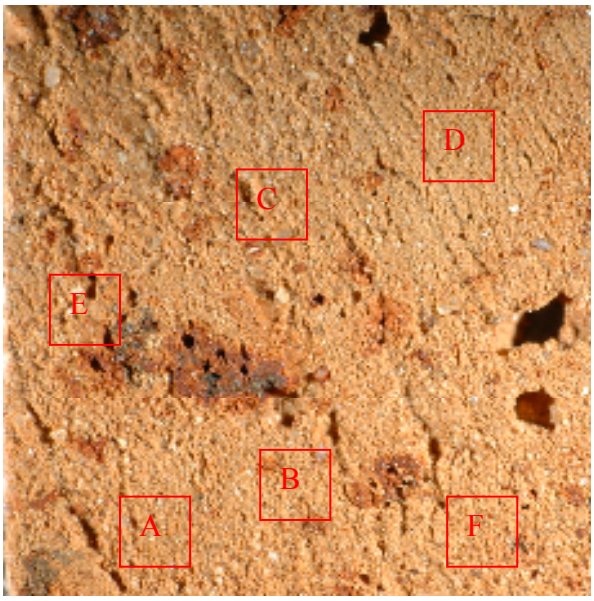

Fig 9.e.7 Sample 304 (S3) AAS - sampling locations.

Samples A and B were physically combined to provide a mean value for K concentration. Samples C and D, and E and F were also combined to give a total of three mean matrix values. Due to the limited availability of resources, combined samples were used to minimise the number of individual aliquots presented for analysis.

Results - AAS

Sample Ref	[K] %
A,B	1.62
C,D	1.60
E,F	1.48

Discussion - AAS

As predicted by the application of staining techniques, there appears to be little variation in potassium concentration across the surface of the sample. The mean matrix concentration value of 1.57% K is slightly lower than seen in other samples, but is not atypical.

9.e.5 Discussion of analytical results and summary of material characteristics

This sample was included in this work because of the absence of visual heterogeneity across the surface of the sample. Digital enhancement techniques did not reveal the presence of any additional matrix components and the sample remained generally unchanged after the application of sodium hexanitrocobaltate(III) staining solution, indicating an absence of localised regions of elevated potassium concentration (visible to the naked eye).

Macro alpha autoradiography revealed the presence of a uniform distribution of regions of higher alpha activity associated with the presence of micro-inclusions of Th or U rich minerals, whilst semi-quantitative alpha autoradiography revealed that the presence of these minerals did not substantially affect the uniformity of the alpha activity across the surface of the sample.

With regard to the suitability of this material for use in luminescence dating, the uniformity of both the alpha emitting species and potassium bearing component indicates uniformity in the dose-rate across the surface of the sample. Spatially resolved measurements of the natural luminescence signal measured across the surface of the sample (Fig 9.e.8) appear to indicate a uniform distribution of emitting species, displaying similar levels of luminescence sensitivity.

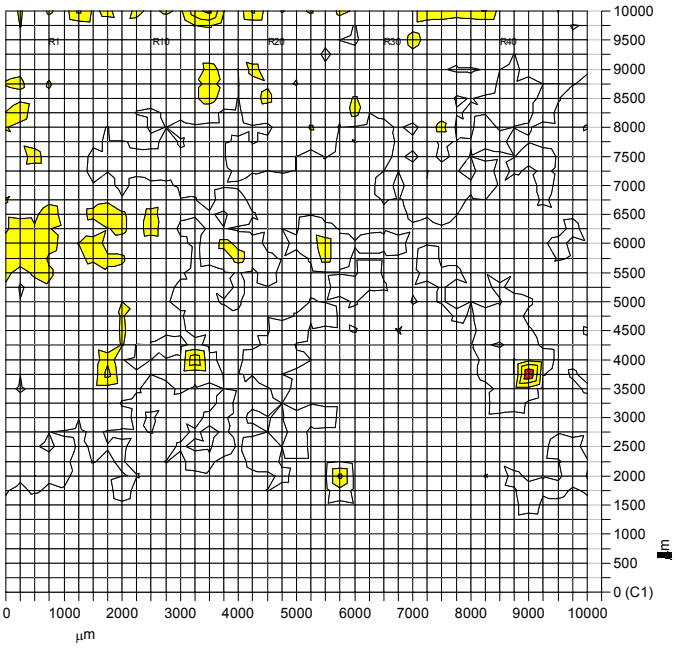

Fig 9.e.8 Map of natural luminescence intensity, measured across the surface of sample 304-1.

Areas shaded red represent the highest levels of luminescence emission, whilst areas shaded yellow represent luminescence emission at levels that are substantially (2X or more) above sample background levels.

The combination of a uniform dispersion of emitting species of comparable luminescence sensitivity throughout a generally uniform matrix represents an optimal situation with respect to phosphor characteristics and dose-rate environment for luminescence dating.

The luminescence date produced for this sample was A.D. 1555 ±27, where the second value denotes a type B overall error (which includes both random and systematic errors). The error associated with the production of this date is particularly low, and it is likely that this is as a direct consequence of the near ideal sample characteristics with regard to luminescence and dose-rate homogeneity.

Chapter 10 Conclusion and discussion

The application of the analytical techniques developed throughout this work, to samples of archaeological interest has proved successful in the characterisation of the mm and sub-mm scale distribution patterns of uranium, thorium and potassium (as an indicator of ^{40}K).

10.1 Visual appraisal and digital enhancement techniques

The extent to which digital enhancement techniques are useful depends upon the physical characteristics of an individual sample; in some cases, where matrix heterogeneity is clearly apparent (e.g. sample 294-1, case study C), digital enhancement may offer little additional information. In other cases, where colour and textural differences are subtle, the use of these techniques may provide a useful means of determining the presence of more than one matrix phase or component.

In the case of sample 321-1(case study A), where there was clear evidence of matrix heterogeneity due to the presence of a number of mineral inclusions of varying sizes, digital enhancement revealed the presence of a second matrix phase that was not apparent on initial visual inspection. The application of subsequent techniques in this case, highlighted a clear correlation between differing visual and textural properties and the presence of potassium at elevated concentrations, with respect to the other major phase.

For sample 294-1 a clear correlation was also made between visual and textural properties and the presence of potassium at locally elevated levels, together with a subsequently determined difference in the distribution characteristics and concentrations of uranium and thorium.

Although based on a limited number of examples, it is apparent that the presence of more than one discrete material phase, identified by differences in visual characteristics (and resulting from poor mixing of raw materials, raw material heterogeneity etc.), displays the potential to disrupt the uniformity of the distribution of radionuclides across the sample, on both a macro and micro (mm and sub-mm) scale. Hence, the initial stages of routine investigation when considering the suitability of a sample for luminescence dating should include a detailed visual analysis of the material composition, with the use of digital enhancement where appropriate.

10.2 Staining techniques

The development and application of qualitative staining techniques to reveal the presence of areas of (increased) potassium concentration have revealed a number of interesting features, both from a methodological and material perspective.

The presence of potassium in the continuous fine/clay rich matrix in bricks is not routinely revealed by staining with sodium hexanitrocobaltate(III); staining does take place, but where potassium is distributed throughout the fine matrix phase, in the form of micro inclusions or as a continuous phase component, there may be insufficient visual contrast to detect staining without the use of microscopic techniques. This effect may also be valid for clay rich sediments, such as sample 316-2 (case study B), where the presence of a uniform distribution of K-rich micro-inclusions was only identified by subsequent photomicrography, and was not apparent on initial visual examination after staining. In this case, the combination of both staining techniques and photomicrography displayed comparable efficacy to the use of SEM-EDX analysis with regard to the identification and characterisation of the size and distribution characteristics of this K-rich mineral component.

Additionally, with regard to fine grain/clay rich matrix components care must be taken when interpreting results obtained from staining, where there is a substantial difference in the initial base colours of the materials (e.g. sample 294-1, case study C). When considering the comparison of two clay types, for example, where both contain similar concentrations of potassium, but one is lighter in colour (due perhaps to the absence of iron rich species, or the presence of calcium and other carbonates), the lighter colour may appear to produce a positive stain after the application of sodium hexanitrocobaltate (III), whilst the other does not. In this case, the use of quantitative techniques would be required to determine any real difference in potassium concentrations between the two materials.

The application of staining techniques to identify K-rich mineral inclusions is not subject to matrix interference, and a number of such species were readiliy identified and subsequently used in quantitative determinations of potassium concentration (eg. Sample 321-1, case study A). K concentrations of between 3% and 8% were found, which are typical of those present naturally in alkali feldspars (although lower than true K-Feldspars).

When applied to sample 321-1, staining techniques revealed the presence of a K-rich inclusion closely associated with (almost within) a larger quartz inclusion, which agreed with the results found previously from SEM-EDX analysis of this sample.

Staining with sodium hexanitrocobaltate(III) solution provides a quick and inexpensive method of assessing the distribution characteristics of potassium bearing minerals (which of course relates to the dose-rate distribution arising from ^{40}K beta radiation) throughout a ceramic or sediment sample and should form part of the routine investigations used when considering the suitability of a sample for luminescence dating.

10.3 Alpha autoradiography

The use of alpha autoradiographic techniques was explored initially to provide a qualitative, visual assessment of the spatial distribution patterns of alpha emitters across the surface of a number of archaeological samples. Initial results based on long-term exposures using CR-39 SSNTD detectors provided excellent results with respect to the identification of areas of increased localised alpha activity (associated with U/Th rich mineral inclusions), seen as intense clusters of tracks on the CR-39 detector. When illuminating the detector from the side, it was noticed that areas of high track density became visible from directly above the surface, which enabled the production of photomicrographs of the full 1 cm x 1 cm detector area. Such techniques have been referred to in the text as "macro alpha autoradiography", where the distribution patterns of the surface alpha emitters (subsequent tracks) can be clearly seen across the entire surface, and the visual correlation between alpha activity and sample features (such as large quartz grains in the case of sample 321-1, case study A) can be made.

The presence of heavy mineral grains (such as zircon), detected by track clustering due to higher alpha activity appears to be very common, with these features appearing frequently in four of the five samples tested, with the exception of sample 294-17, case study D). Alpha autoradiography also revealed the presence of such mineral inclusions actually sited within a number of larger quartz crystals (sample 321-1, case study A) and this finding was later confirmed by SEM-EDX analysis.

In an attempt to characterise the detection parameters associated with macro alpha autoradiography, and in particular, the ability to differentiate between effects such as natural random track clustering and actual heterogeneity in the alpha emitter distributions, a number of computer based simulations were performed. several different sample

conditions were simulated; the most important finding was that visually, it is difficult to differentiate between random track clustering and areas of real high alpha activity until the ration between local and background activity approaches 20 (based on a simulated distribution of 1000 counts across a simulated detector surface of $1mm^2$).

CR-39 and a number of other SSNTD materials are used primarily in the quantitative detection of environmental radon. The application of this particular use of CR-39 was explored to establish a technique to actually quantify alpha emitter concentrations across the surface of the sample, to provide a mean cross sectional alpha activity value, and additionally in small localised areas of high alpha activity.

The limitations of this technique include the inability to differentiate between U and Th series members (equal activity must be assumed), the assumption of similar material Z values for intercomparisons between sample and standard data, and the production of localised alpha activity values must be regarded as *minimum* values in the case of heavy mineral inclusions. That said, initial results were very encouraging, and the production of an initial detector efficiency value (to take into account particle energy and detector geometry effects) was validated by long term exposure tests, using standard reference materials, and where calculated activity and subsequent concentrations of both uranium and thorium agreed very well with certified values.

Despite the apparent accuracy of this technique when verified with standard materials, it must still be regarded as semi-quantitative due to the various assumptions mentioned above, and additionally, the variable material compositions of the materials of interest to this work.

10.4 Micro-sampling and quantitative techniques

Sub-samples of matrix material were taken by the use of a 1 mm diameter dental burr coupled to a standard craft drill. A standard binocular microscope was used to ensure sampling precision at each area of interest, and material was harvested by shaking off the surface drill debris and collecting in a suitable container. Spatial resolution, at the level required during this work was efficiently achieved using this equipment, although in certain cases (for example sample 321-1), access to micro-drilling equipment to sub-sample from within larger quartz inclusions would have been useful. In this particular case, the use of laser ablation techniques (LA-ICP-MS) might have proved interesting, and the application of this technique to the determination of internal uranium and thorium concentrations in quartz may form the basis of future research.

The analytical capabilities of both the ICP-MS and AAS techniques were validated by the use of standard materials and were assessed to meet expected requirements. Routinely, analyses were performed for U and Th concentrations only, due to operator and instrument time constraints, however the addition of zirconium as a routine analyte was introduced in later measurements to provide information about the possible mineralogical origins of uranium (i.e., the presence of zircons). Future work in this area should also include the simultaneous analysis of cerium (to indicate the presence of monazites, to account for increased thorium concentration) and a number of other trace and ultra-trace elements; in this case, the use of elemental ratios, rather than definitive concentration values may prove to reduce the problems associated with the use of encapsulating resins, and provide additional information about the elemental composition of archaeological samples for use in material characterisation and provenance investigations.

10.5 Conclusion

The development of these techniques has enabled the introduction of a series of initial routine tests to determine the suitability of a material for use in luminescence dating.

A short commentary based on the application of these methodologies to the samples used as case studies was included at the end of each section, and assessments were made regarding the overall suitability (with regard to material dose-rate heterogeneity) of these samples for dating. Interestingly, the samples that displayed good material characteristics with respect to phosphor and dose-rate homogeneity, were dated successfully (e.g. Sample 294-17, case study D) whilst others (particularly 321-1, case study A) as predicted by the data produced during this work, were extremely problematic.

The factors involved in maintaining the integrity of data associated with luminescence dating techniques are both complex and numerous, however, the techniques developed and applied during this work may be used to identify and potentially minimise at least one of the potential sources of error.

References

Adamiec G. and Aitken M.J. (1998) Dose rate conversion factors: update. Ancient TL, 16, 37-50.

Aitken M.J. (1985) Thermoluminescence Dating. Academic Press, London.

Attix F.H., (1986). Introduction to Radiological Physics and Radiation Dosimetry. Wiley-Interscience, New York

Azkour K. , Nourreddine A. , Adloff J. C. and Pape A. (1998) α-Particle radioactivity from LR 115 by two methods of analysis. Radiation Measurements 31, 223-226.

Bailiff I.K. and Mikhailik V.B. (2003) Spatially-resolved measurement of optically stimulated luminescence and time-resolved luminescence. Radiation Measurements 37, 151-159.

Bailiff I.K. (2006) Development of single grain OSL dating of ceramic materials: Spatially resolved measurement of absorbed dose. Radiation Measurements 41, 7-8, 744-749.

Bailiff I.K. (2008) Methodological developments in the luminescence dating of brick from English late-medieval and post- medieval Buildings. Archaeometry 49, 827-851.

Baily R.M., Stokes S. and Bray H. (2003) Inductively coupled plasma mass spectrometry (ICP-MS) for dose rate determination: some guidelines for sample preparation and analysis

Barillon R., Fromm M. and Chambaudet A. (1995) Variation of the critical registration angle of alpha particles in CR39; implications for radon dosimetry. Radiation Measurements 25, 631-634.

Berger G.W., Sadovsky T.F. and Davis D.A. (1996) A simple staining method for K-feldspars before sample preparation for IR-OSL dating. Ancient TL 14, 9-11.

Bloodworth A. and Highley D. (2005) Brick Clay - Geological Survey Fact Sheet for the Office of the Deputy Prime Minister. Crown Publishing. London.

Borden D. and Giese R.F. (2001) Baseline studies of The Clay Minerals Society source clays : Cation exchange capacity measurements by the ammonia-electrode method. Clays and Clay Minerals 49, 444-445.

Brennan B.J. (2003) Beta doses to spherical grains. Radiation Measurements 37, 299-303.

Catalano J.E. and Brown G.E (2005) Uranyl adsorption onto montmorillonite: Evaluation of binding sites and carbonate complexation. Geochimica et Cosmochimica Acta. 69, 2995–3005.

Chambaudet A., Barillon R., Grivet M., Fromm M., Rebetez M., Klein D. and Khalil A. (1995) Applications of nuclear tracks in geoscience. Radiation Measurements 5, 487-494.

Chattopadhyay P. (1995) Direct flame atomic absorption spectrophotometric determination of alkalis in geochemical samples, Talanta 42, 1965-1971.

Cho S.H., Reece W.D. and Kim C.H. (2004) Validity of two simple rescaling methods for electron/beta dose point kernels in heterogeneous source-target geometry. Radiation Physics and Chemistry 69, 265-272.

Clark R.J. and Bailiff I.K. Fast time-resolved luminescence emission spectroscopy in some feldspars. Radiation Measurements *29*, 553–560.

Clifton-Taylor A. (1962) The Pattern of English Building. B.T. Batsford Ltd. London.

Cochran J.K., Carey A.E., Sholkovitz E.R. and Surprenant L.D. (1986) The geochemistry of uranium and thorium in coastal marine sediments and sediment pore waters. Geochimica et Cosmochimica Acta 50, 663-680

Cohen D.D., Duerden P., Clayton E. and Wall T. (1980) The use of PIXE for the measurement of thorium and uranium at $\mu g\ g^{-1}$ levels in thick ore samples. Nuclear Instruments and Methods 168, 523-528.

Daskalova N. and Boevski I. (1999) Spectral interferences in the determination of trace elements in environmental materials by inductively coupled plasma atomic emission spectrometry. Spectrochimica Acta partB 54, 1099-1122.

Duller G.A.T. and Murray A.S. (2000) Luminescence dating of sediments using individual mineral grains. Geologos 5, 88-106.

Elan 6000 ICP-MS Training course CD-ROM (Reference L020-0080) Perkin – Elmer Training, Perkin-Elmer Ltd - Sales, Service & Support, Analytical Instruments Division Buckinghamshire, England.

El-Hawary M.M., Mansy M., Hussein A., Ammar A.A and El-Serby A.R. (1999). Alpha particle absorption and inclined incidence track parameters evaluation in plastic detectors. Radiation Physics and Chemistry 54, 547-550.

Fitzpatrick E.A. (1986) An Introduction to Soil Science. Second Edition, Longman Scientific and Technical. Essex.

Fujino O., Umetani S., Uenoa E., Shigeta K. and Matsuda T (2000) Determination of uranium and thorium in apatite minerals by inductively coupled plasma atomic emission spectrometry with solvent extraction separation into diisobutyl ketone. Analytica Chimica Acta 420, 65–71.

Gore D.J. and Jenner T.J. (1980) Alpha and fission fragment autoradiography with superimposed tissue images in CR-39 plastic. Phys. Med. Biol. 25 1095-1104.

Grun R. And Fenton C. (1990) Internal dose rates of quartz grains separated from fault gouge. Ancient TL 8, 26-28.

Greenwood N.N. and Earnshaw A. (1997) Chemistry of the Elements. Second Edition Butterworth and Heinemann. Oxford.

Hadler J. C., Iunes P. J. and Paulo S. R. (1995) A possibility of monitoring indoor radon daughters by using CR-39 as an alpha-spectrometer. Radiation Measurements 25, 1-4, 609-610.

Haustein M., Roewer G., Krbetschek M.R. and Pernicka, E. (2003) Dating archaeometallurgical slags using thermoluminescence. Archaeometry 45, 3, 519–530.

Hayes J.R. and Klugman M.A. (1959) Feldspar Staining methods. Journal of Sedimentary Petrology 39, 2, 227-232.

Heinrich E.Wm. (1958) Mineralogy and geology of radioactive raw materials. McGraw Hill Book Company inc. New York.

Henshaw D. L. (1982) Applications of CR-39 nuclear track detector in medicine and technology. Physics in Technology 13, 266-72.

Hermsdorf D., Hunger M., Starke S. and Weikert F. (2007) Measurement of bulk etch rates for poly-allyl-diglycol carbonate (PADC) and cellulose nitrate in a broad range of concentration and temperature of NaOH etching solution. Radiation Measurements 42, 1-7.

Hou X. and Roos P. (2008) Critical comparison of radiometric and mass spectrometric methods for the determination of radionuclides in environmental, biological and nuclear waste samples. Analytica Chimica Acta 608 105–139.

Huntley D.J. and Baril M.R (1997) The K content of thr K-Feldspars being measured in optical dating or in thermoluminescence dating. Ancient TL 15, 11-13.

Huntley D.J., Hutton J.T. and Prescot J.R. (1993) Optical dating using inclusions within quartz grains. Geology 21, 1087-1090.

Jagam P. and Simpson J.J. (1993) Measurements of Th, U and K concentrations in a variety of materials. Nuclear Instruments and Methods in Physics Research A324, 389-398.

Katz J.J., Seaborg G.T. and Morss L.R.(1986) The Chemistry of the Actinide Elements. Second Edition, Volume 1. Chapman and Hall, New York.

Kazunori S. and Mitsuru E. (1997) Precise determination of rare earth elements, thorium and uranium in chondritic meteorites by inductively coupled plasma mass spectrometry - a comparative study with radiochemical neutron activation analysis. Analytica Chimica Acta 338 237-246.

Keeling P.S. (1963) The Geology and Mineralogy of Brick Clays. Brick Development Association Ltd., Windsor.

Khan H.A. and Qureshi I. E. (1999) SSNTD applications in science and technology - a brief review. Radiation Measurements 31, 1-6, 25-36.

Klein D., Barillon R., Demongeot S., Tomasella E., Chambaudet A. (1995) Investigative techniques for radon level characterization. Radiation Measurements 25, 553-556.

Krepelova A., Sachs S. and Bernhard G. (2006) Uranium(VI) sorption onto kaolinite in the presence and absence of humic acid. Radiochimica Acta 94, 825-833.

May T.W. and Wiedmeyer R.H. (1998) A Table of Polyatomic Interferences in ICP-MS. Atomic Spectroscopy 19, 150-155.

Mayya Y.S., Morthekai P., Murari M.K. and Singhvi A.K. (2006) Towards quantifying beta microdosimetric effects in single-grain quartz dose distribution. Radiation Measurements 41, 1032-1039.

McCoy D. G., Prescott J. R. and Nation R. J. (2000) Some aspects of single grain luminescence dating. Radiation Measurements 32, 859-864.

Mejdahl V. (1979) Thermoluminescence dating: Beta dose attenuation in quartz grains. Archaeometry 21, 61–72.
Mejdahl V. (1987) Internal radioactivity in quartz and feldspar grains. Ancient TL 5, 10-17.

Merroun M.L., Raff J., Rossberg A., Hennig C., Reich T. and Selenska-Pobell S. (2005) Complexation of uranium by cells and s-layer sheets of Bacillus sphericus JG-A12, Applied and Environmental Microbiology 71, 5532-5543.

Murray A.S. and Roberts R.G. (1997) Determining the burial time of single grains of quartz using optically stimulated luminescence. Earth and Planetary Science Letters 152, 163-180.

Nikezic D. and Yu K.N. (2003) Calculations of track parameters and plots of track openings and wall profiles in CR39 detector. Radiation Measurements 37, 595-601.

Ottley, C.J., Pearson, D.G. and Irvine, G.J. (2003) A routine method for the dissolution of geological samples for the analysis of REE and trace elements via ICP-MS. In: Holland, J.G., Tanner, S.D. (Eds.), Plasma Source Mass Spectrometry: Applications and Emerging Technologies. Royal Society of Chemistry, Cambridge, 221–230.

Pankrath R., Perney B., Eberhardt P., Ramseyer K. and Mullis J. (1992) Microdistribution of Al, Li, and Na in α quartz: Possible causes and correlation with short-lived cathodoluminescence. American Mineralogist 77, 534-544.

Pöllänen R., Siiskonen T. and Vesterbacka P. High-resolution alpha spectrometry from thick sources (2005) Radiation Measurements 39, 565-568.

Preusser f> and Casper H.U. (2001) Comparison of dose rate determination using high-resolution gamma spectrometry and inductively coupled plasma –mass spectrometry. Ancient TL 19, 19-23.

Pollard A.M. and Heron C. (1996) Archaeological Chemistry. RSC Paperbacks, Cambridge.

Potts P.J. (1987) A handbook of silicate rock analysis. Blackie, New York

Rao T.P., Metilda P. and Gladis J.M. (2006) Preconcentration techniques for uranium(VI) and thorium(IV) prior to analytical determination—an overview. Talanta 68 1047–1064

Renfrew C. and Bahn P. (2000) Archaeology : Theories Methods and Practice. Thames and Hudson (Third Edition), London.

Rice T.D. (1997) Comparison of dissolution methods for the determination of potassium in rocks and minerals by atomic absorption spectrometry Analytica Chimica Acta 91, 221-228.

Rubinson K.A. and Rubinson J.F. (2000) Contemporary Instrumental Analysis. Prentice Hall, New Jersey.

Sanzelle S., Fain J. and Mailler D. (1986) Theoretical and experimental study of alpha counting efficiency using LR-115 Kodak SSTND applied to dosimetry in the field of thermoluminescence dating. International Journal of Radiation Applications and Instrumentation. Part D. Nuclear Tracks and Radiation Measurements 12, 913-916.

Schueler J.E. and Thomas R.P. (1933) Determination of potassium by sodium cobaltinitrite. Industrial and Engineering Chemistry, Analytical Edition 5, 163-165.

Donghuai Sun, Bloemendal J., Rea D. K., VandenbergheV, Fuchu Jiang , Zhisheng An and Ruixia Su (2002) Grain-size distribution function of polymodal sediments in hydraulic and aeolian environments, and numerical partitioning of the sedimentary components. Sedimentary Geology 152, 263-277.

Takeuchi T. and Suzuki M. (1964) The determination of sodium, potassium, magnesium, manganese and calcium in cement by atomic-absorption spectrophotometry. Talanta 11, 1391-1397.

Temperli A.T. and Misteli H. (1969) Determination of potassium in soil extracts by atomic absorption spectrophotometry. Analytical Biochemistry 27, 2, 361-363.

Tsunashima A., Brindley G.W. and Bastovanov M. (1981) Adsorption of uranium from solutions by montmorillonite; Compositions and properties of uranyl montmorillonites. Clays and Clay Minerals 29, 10-16.

Vince A. (2005) Ceramic Petrology and the Study of Anglo-Saxon and Later Medieval Ceramics. Medieval Archaeology 49, 219-245.

Wagner G.A., Glasmacher U.A. and Greilich s. (2005) Spatially resolved dose-rate determination in rocks and ceramics by neutron-induced fission tracks : fundamentals. Radiation Measurements 40, 26-31.

Wintle A.G. (2008) Fifty years of luminescence dating. Archaeometry 50, 276-312.

Appendix

Validation of initial CR39 detector efficiency values.

A.1 Experimental

Approximately 2g of standard sediment (XXXXXX) was mixed thoroughly with a small amount of PVA based binding solution before being pelletized (using laboratory equipment used routinely to produce samples for EDXRF analysis) to produce a solid, homogenous material with similar matrix characteristics to an archaeological ceramic, but with known concentrations of U and Th and where secular equilibrium has been verified by the use of gamma spectrometry. CR39 detectors were placed in contact with this material (as used with thin slices of archaeological material discussed in later chapters) and left undisturbed for a measured period of time before being etched using the standard procedures detailed in Chapter 5, Section 5.4.1.

A.2 Results

136	121	134	125	136
126	131	127	129	125
132	127	129	124	134
128	138	128	130	127
138	126	131	125	132

Fig A.1 Grid showing tracks per counting area

A.3 Calculations

The sample - CR39 detector contact time was 90.0 days. The counting area per individual grid section (using 40x magnification) is effectively reduced by the grid scribing process in which a surface channel of 0.5mm thickness is removed per scribed gridline. Each effective countable area measures 1.6mm x 1.6mm (2.56mm^2).

Results based upon 25 equivalent measurements made across the detector surface -

Mean track density = 129.6 tracks / 2.56 mm^{-2}.

Total number of tracks counted = 3143

Standard deviation = 3.51 %

Adjusted track density = 5063 tracks cm^{-2}

%Error associated with counting = (N)^0.5/(N)*100 = 1.78 ~2%

Using a mean alpha range of 25 μm, a CR39 detector area of 1cm^2, and an arbitrary material density of 2.6gcm^{-3} (which is reasonable for the pelletized standard sediment), the volume of matrix material from which alpha particles can reach the detector is 0.0025 cm^3, resulting in a contributing material mass of 6.5 mg (derivation given in Chapter 4, section 4.3.2).

The calculated total number of alpha emissions (per 6.5mg of sample) is ((5063 x 4) / 0.65) = 31157

Rate of emission = (31157 / (90*86400) = 4.01 x10-3 emissions per second.

Converting to standard units, (and still assuming a contributing mass of 6.5mg) the mean sample activity is 616 $BqKg^{-1}$

Using the previous assumptions of equal activity for thorium and uranium, with no disruption to secular equilibrium (confirmed by gamma spectrometry) it is possible to calculate the estimated concentrations of both species.

Estimated uranium concentration

308 / 104.4 = 2.95ppm uranium (where 104.4 refers to complete decay series alpha activity of ^{238} U and ^{235} U at typical levels of abundance).

Estimated thorium concentration

308 / 24.48 = 12.58ppm thorium (where 24.48 refers to complete decay series alpha activity).

Standard certified values of uranium and thorium

Th	12.4 ± 1.2 mg/kg
U	3.0 ± 0.4 mg/kg

Discussion

The estimated concentrations of uranium and thorium in standard sediment, derived by alpha autoradiography, and calculated using the initial 65% detector efficiency factor agree very well with the standard certified values (differing by <2%).

This result is extremely encouraging as the data validate not only the initial detector efficiency factors calculated using high activity materials, but also the use of this technique to quantify the localized concentrations of uranium and thorium (assuming equal activity) in the materials of interest. The difference in effective z values (and hence alpha particle range values) between the matrices of the SiO2 based NBL standards, and the

aluminosilicate based sediment standards has clearly had only a negligible effect on the accuracy of this technique; this is also very encouraging as it is reasonable to assume that deviations in z value due to material heterogeneity in the archaeological materials tested are also unlikely affect the integrity of the technique.

The results from this technique also compare very favourably with those derived from the ICPMS determinations performed on small aliquots of standard material.

Inter sample comparison

Assuming minimal effects due to differences in elemental composition (relating to mean Z and A values of major compositional species), the use of an arbitrary contributing mass of 6.5 mg and a material density of 2.6 gcm-3 in the calculation of theoretical counts and bulk material activity, is appropriate due to the linear relationship between alpha range and material density (in similar materials).

For ex ample, if the average of range (R_ϱ) of an alpha particle is 58μgmm^{-2}, the calculated range would be (58/2.6) 22.3 μm.

The evaluation of (range x detector area x density) would produce a contributing material mass of 5.8mg.

Conversely, for a lower effective density, if the average of range (R_ϱ) of an alpha particle is 58μgmm-2, the calculated range would be (58/1.8) 32.2 μm.

The evaluation of (range x detector area x density) would still produce a contributing material mass of 5.8mg.